Reorientation Dynamics in Condensed Phases

Phineus R L Markwick

A thesis submitted in fulfilment of the requirements
for the degree of Doctor of Philosophy
to the
University of Edinburgh
2000

Abstract

Using Raman lineshape analysis and dielectric relaxation techniques, the reorientation dynamics of single molecules in partially disordered phases is studied. Reorientational correlation functions for a prototypical isotropic liquid CS_2 are presented over a broad temperature range. Calculated values of the integrated correlation time, rms intermolecular torque and collision frequency suggest the onset of substantial local structuring in the liquid phase on cooling to below $220K$. An *ab initio* DFT computer simulation shows that the intermolecular torque arises from a strong dipole moment interaction created by the intra-molecular vibration. A solvation dynamics study of CS_2 in cyclohexane provides the first observation of the free-volume effect occuring at the isotropic-plastic crystal phase transition.

Reorientation correlation functions are presented for various members of the nCB [4-n-Alkyl-4'-Cyanobiphenyl] homologous series in the isotropic phase. Two distinct relaxation processes are observed, a very fast intra-molecular relaxation mechanism assigned to the flexibility of the anisotropic molecules, and a slow exponentially-decaying rotational-translational relaxation process with a complex temperature dependence. The results of dielectric relaxation studies under high pressure of two liquid crystals (6PCH [4-trans-4-n-Hexyl-Cyclohexyl-Benzonitrile] and 8CB) are presented. The extraction of reorientational activation parameters in the isotropic, nematic and smectic A phases allows the formulation of a reorientational model, in which steric effects play the predominant role.

Single molecule reorientation dynamics is determined by a complex hierachy of relaxation processes. The extraction of realistic correlation functions allows for the identification and separation of different relaxation processes occurring on different timescales, and of different intermolecular interactions occurring over varying distance scales. The single molecule dynamics in a partially disordered system is highly dependent on the degree of local structuring. However, in a synergetic manner, it is apparent that the physical characteristics of the constituent

Declaration

This thesis has been composed by myself and it has not been submitted in any previous application for a degree. The work reported within was executed by me, unless otherwise stated.

For my parents, of course

Chapter 1

Introduction

Molecular dynamics of condensed phases has been the subject of intense theoretical and experimental research in the past fifty years. Not only do the details of molecular motion govern some of the most important physical properties of such systems, including phase stability, diffusion, viscocity and response to applied fields, they determine the complex and diverse variety of condensed phases. All condensed phases resemble each other in the property of cohesion; they maintain a boundary surface. In a molecular crystal, the cohesive forces are strong enough to prevent either translational or reorientational movements of the individual molecules, which vibrate about equilibrium positions located on a three-dimensional periodic lattice. In direct contrast, the molecules in an isotropic liquid possess enough kinetic energy to overcome the cohesive forces exerted by their neighbouring molecules, and the liquid state exhibits translational and orientational disorder.

There are, at present, two other groups of well-defined thermodynamic states in which the extent of molecular ordering lies between that of a solid, and that of an isotropic liquid. These so-called mesophases are known as plastic crystals and liquid crystals. Plastic crystals [1] are composed of globular molecules, for which the barriers of rotation are small relative to the lattice energy. Given enough thermal energy, the molecules are capable of overcoming the these rotational energy barriers, but are not sufficiently energetic to break up the lattice. The resulting phases exhibit substantial orientational disorder, but retain long-range translational order.

Liquid crystalline mesophases [2] are generally composed of either elongated rod-like (calamatic) or disk-like (discotic) molecules. Despite the fact that these

mesophases are fluid, that is to say that the molecules are not constrained to a lattice, they possess long-range orientational order due to the preferential alignment of the molecules parallel to some common axis, labelled by a unit vector (or director). Numerous liquid-crystalline phases have been identified, many of which possess partial translational order. Calamatic liquid crystals are divided into two broad classes: nematic and smectic. The nematic phase is the simplest of these orientationally ordered fluid phases as there is no long range correlation of the molecular centre of mass positions. The smectic mesophases have one degree of translational ordering, resulting in layered structures and as such can be regarded as quasi-one-dimensional solids, or quasi-two-dimensional liquids. There exists a large variety of smectic mesophases depending on the orientation of the director relative to the molecular layers and the ordering of the constituent molecules within the layers. Discotic liquid crystals are two-dimensionally ordered systems. They can be described as a two-dimensional array of liquid tubes and are called columnar phases.

The particular condensed phases described above are depicted schematically in Figs. 1a and 1b. There are far too many mesophases to discuss here, and the reader is referred to the references for more information. It is however clear from the above examples, that there exist numerous complex disordered and partially disordered systems. Indeed the structure of a liquid or mesophase on a molecular scale is considerably more difficult to visualise than the complete disorder which occurs in a gas, or the regular arrangement that is found in a crystal. Furthermore, it is apparent that there is an inextricable link between "structure" and dynamics in cohesive phases. Additionally, it appears that the molecular structure also plays an important role. Indeed, with the exception of some polymorphous smectics, there are no known substances that exhibit both plastic- and liquid-crystalline phases.

These observations can best be understood by considering the energetics of the system in question. In any condensed phase, a molecule experiences a potential energy field due to the molecular interaction between itself and its environment. The extent to which this intermolecular potential controls the dynamics of the molecules depends on the kinetic energy of the molecules. At low temperatures the kinetic energy of the molecule is not great enough to overcome the intermolecular interaction, resulting in an ordered solid. At the other extreme, when the kinetic energy of the molecules is much greater than the mean interaction potential energy, the molecular motions are uncorrelated, which is the case of

a disordered gas. In a liquid or liquid crystal, for example, there is a delicate equilibrium: the kinetic energy of the molecules is not great enough to overcome the immediate local intermolecular interaction and the high packing density determines the extent of local structure, but the kinetic energy is large enough to prevent long-range translational ordering. The nature of the local structure is determined by the form of the intermolecular interaction potential for the particular molecule. The shape, size and even chemical make-up of the individual constituent molecules could therefore affect the structure and macroscopic properties of the system. On this basis, the study of molecular motion liberates valuable information about the intermolecular interaction, the local molecular structure and consequently macroscopic properties of condensed phases.

Unfortunately the study of molecular motion and structure in partially disordered phases is confronted with two substantial obstacles. The first is that of understanding the nature of molecular interactions. There exists considerable uncertainty over the validity and transferability of interaction potentials used to model soft condensed phases which are exacerbated by the coexistance of a wide variety of heirarchical interactions and highly directional forces. Generally speaking these forces are considered to be repulsive for small molecular separations and become attractive at larger separations. However, the exact nature of intermolecular forces in a given system is most certainly specifically defined by the physical characteristics of the consituent molecules, their anisotropy, flexibility and electronic charge distribution. The second fundamental problem is that of relating the bulk or macroscopic properties of a system to the microscopic or molecular properties. All experimentally determined properties are bulk properties which represent a combination or averaging of molecular properties. This unavoidable situation faced in all experimental measurements is particularly problematic when trying to determine the potential energy function which describes the way in which an isolated pair of molecules interacts.

Molecular motion in partially disordered phases is the result of a complex interaction of numerous underlying dynamic processes occuring across a broad range of time-scales. Each of these dynamic processes can therefore be associated with a characteristic relaxation time. In order to probe these dynamical properties a statistical description of the transport and other temporal phenomena is required. Central to this approach is the formulation of time correlation functions, the integrals of which over time describe the transport and dynamics of the ensemble. These functions provide a concise method of expressing the degree to which

two dynamical properties are correlated as a function of time. In other words, they describe quantitatively how long some property of the system persists until it is averaged out by thermal molecular motion. Whilst the determination of thermodynamic parameters and the analysis of x-ray diffraction and neutron scattering data provide an insight into the structural properties, it is spectroscopic techniques which yield information about the dynamics of soft condensed matter phases. All spectroscopic techniques use as a probe an external field which is weakly coupled to the system, and study the response of the system to that probe. The weak nature of the coupling ensures that the probe does not influence or obscure the dynamical behaviour of the ensemble. The response is described in terms of the time correlation functions of the dynamic properties. This process is commonly referred to as the action of atomism. The probing external field perturbs the system, which proceeds to relax on characteristic time-scales associated with the dynamic properties of the ensemble. Spectroscopic experiments are generally made in the frequency domain. The spectrum of frequencies, commonly known as lineshape is then transformed into the appropriate time correlation function.

All spectroscopic techniques (both absorption and scattering) are associated with a their own particular correlation function. Indeed it is clear that no single approach could explain more than a small part of the entire picture of molecular motion, for a particular method observes accurately only those dynamical phenomena which occur on the same time-scale of the measurements. This apparently obvious statement is nevertheless of immense importance. For example, the prediction of momentary relative orientations between weakly interacting molecules cannot be obtained by the extrapolation of chemical shift data, as the time-scale of the orientational motion is approximately $10^{-8}-10^{-12}sec$, whilst the time-scale of the measurements is of the order of fractions of seconds. For a full clarification of the complex molecular motion of the system it is therefore neccessary to combine the results of several different types of experiment. Table 1. indicates the variety of both absorption and scattering techniques frequently employed and the associated dynamical phenomena studied.

In several cases the spectroscopic technique yields only the integrated correlation time, such as is the case for NMR studies of rotational-translational motions of molecules. This leads to the obvious disadvantage that the measurement is not sensitive to the detailed characteristics of the molecular motion. Additionally, some experimental measurements cannot isolate an individual dynamic process.

For example, in infra-red spectroscopy the time correlation function for the dipole moment describes how a vibrating dipole orientated in a certain direction at time $t = 0$ reorientates until as t approaches infinity, the correlation function tends to zero, signifying that there is no longer any correlation between the present and original dipolar positions. However, the molecule has not only undergone reorientational relaxation, but also vibrational relaxation, so-called vibrational-dephasing. The correlation function in infra-red spectroscopy does not separate these two dynamical processes, and therefore represents the combined roto-vibrational relaxation of the dipole. In the present study, we are interested in the dynamical properties of single molecules in partially disordered condensed phases. The most suitable experimental technique for this purpose is Raman spectroscopy, which allows the separation and extraction of both reorientational and vibrational correlation functions.

A knowledge of the functional form of the correlation function is of immense importance. Whilst correlation times are characteristic of the time-scale of the relaxation process, they only give physically meaningful dynamic parameters when used in conjunction with a suitable reorientational model. Despite the fact that correlation functions occupy the realms of classical mechanics, their functional form is indicative of the type of reorientational diffusion proccess of the single molecules, which are subject to the laws of quantisation of angular momentum. In formulating a theoretical model, a plausible physical description of the dynamics of the system is produced, and the respective correlation function is computed, which in turn is compared to the experimental data. An explicit correlation function not only reveals the time-scale, but also the very nature of the dynamic proccess.

In this study, we look at the the complex reorientational molecular motion of several partially disordered condensed phases. Chapter 2 contains the main theoretical discussion of reorientational correlation functions. In particular, the relationship between the experimental Raman band the the correlation function is discussed. Within the mathematical formalism described in appendix A, the various reorientational models are presented, with their computed correlation functions.

Raman spectroscopy, as with any other experimental technique used to determine the molecular dynamics of a system, is faced with one major draw-back. Such experimental techniques all study an entire system comprised of N component molecules, and all parameters obtained are time and orientation averages over all

of these N constituent molecules. It is not possible to extract information about the exact reorientational dynamics of a single molecule as a function of time using experimental techniques alone. It is for this reason that computer simulation has developed so rapidly in the last forty years. A combination of computer simulation and experimental results liberates a great deal more information about the dynamics of the system. In order to make the simulation as exact as possible on a molecular scale, it is necessary to resort to solving the exact poly-electronic quantum mechanical equations for the system, a so-called *ab initio* approach. Chapter 3 contains a discussion of the theory behind *ab initio* density functional computer simulation and its application to studying the orientational dynamics and interactions in partially disordered phases.

Combining the theory developed in chapters 2 and 3, chapter 4 presents the results, both experimental and from computer simulation, of the study of a prototypical isotropic liquid: carbon disulphide. This study includes an analysis of the correlation times as a function of temperature, an investigation of the collision frequency and the nature of the intermolecular torques between the component molecules. In Chapter 5, carbon disulphide is used as a dopant to study the dynamics of a typical plastic crystal, cyclohexane. The results and discussion presented in chapter 5 include the direct observation of the free volume effect occurring at an isotropic-plastic crystal phase transition.

Carbon disulphide is a small rigid linear molecule. Chapter 6 presents the work carried out to investigate the effect of internal degrees of molecular reorientation freedom (flexibility) on the molecular dynamics of a system. The study concentrates on the lower members of the liquid crystalline nCB homologous series in the isotropic phase. The results presented also reveal the reorientational dynamics of single anisotropic molecules in the pre-transitional phase.

Another experimental technique commonly employed to analyse reorientation dynamics in partially disordered systems is dielectric relaxation. This technique involves placing a system comprised of polar molecules in an alternating electric field and measuring the variation in the dielectric constant, expressed as a complex permitivity, as a function of the field frequency. Chapter 7 provides an outline of the theory behind dielectric relaxation measurements, including a discussion of the relationship between the dielectric relaxation results and thermodynamic properties of the system of interest. Results of dielectric relaxation measurements for two liquid crystalline systems are presented in chapter 8. The results cover isotropic, nematic and smectic liquid crystalline phases and the single-molecule

reorientational dynamics is discussed in view of the degree of orientational order of the system using experimentally calculated thermodynamic parameters. Finally, there is a summary including conclusions and the discussion of future research in the field of reorientation dynamics.

Fig. 1a Condensed Matter Phases

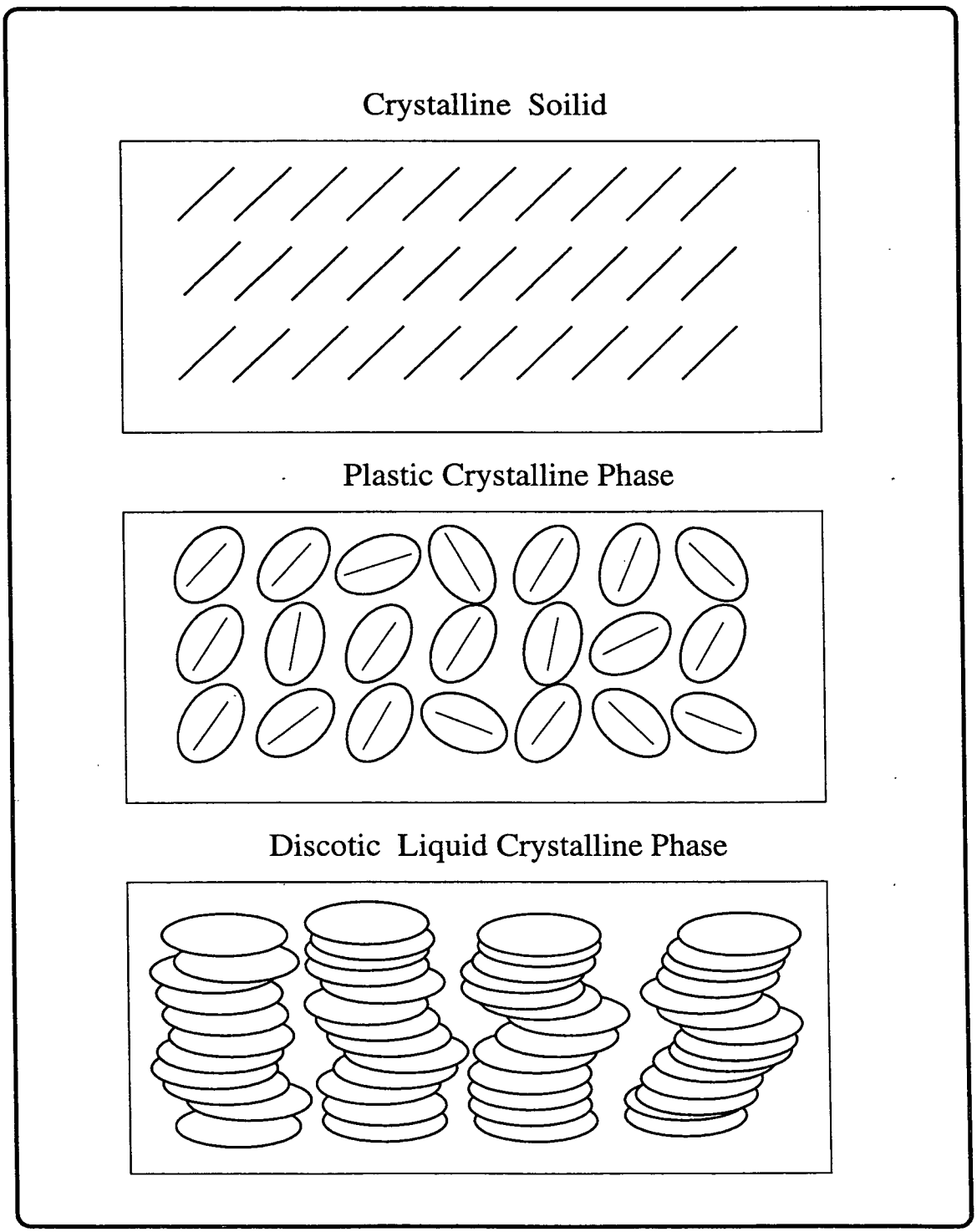

Fig. 1b Condensed Matter Phases Cont.

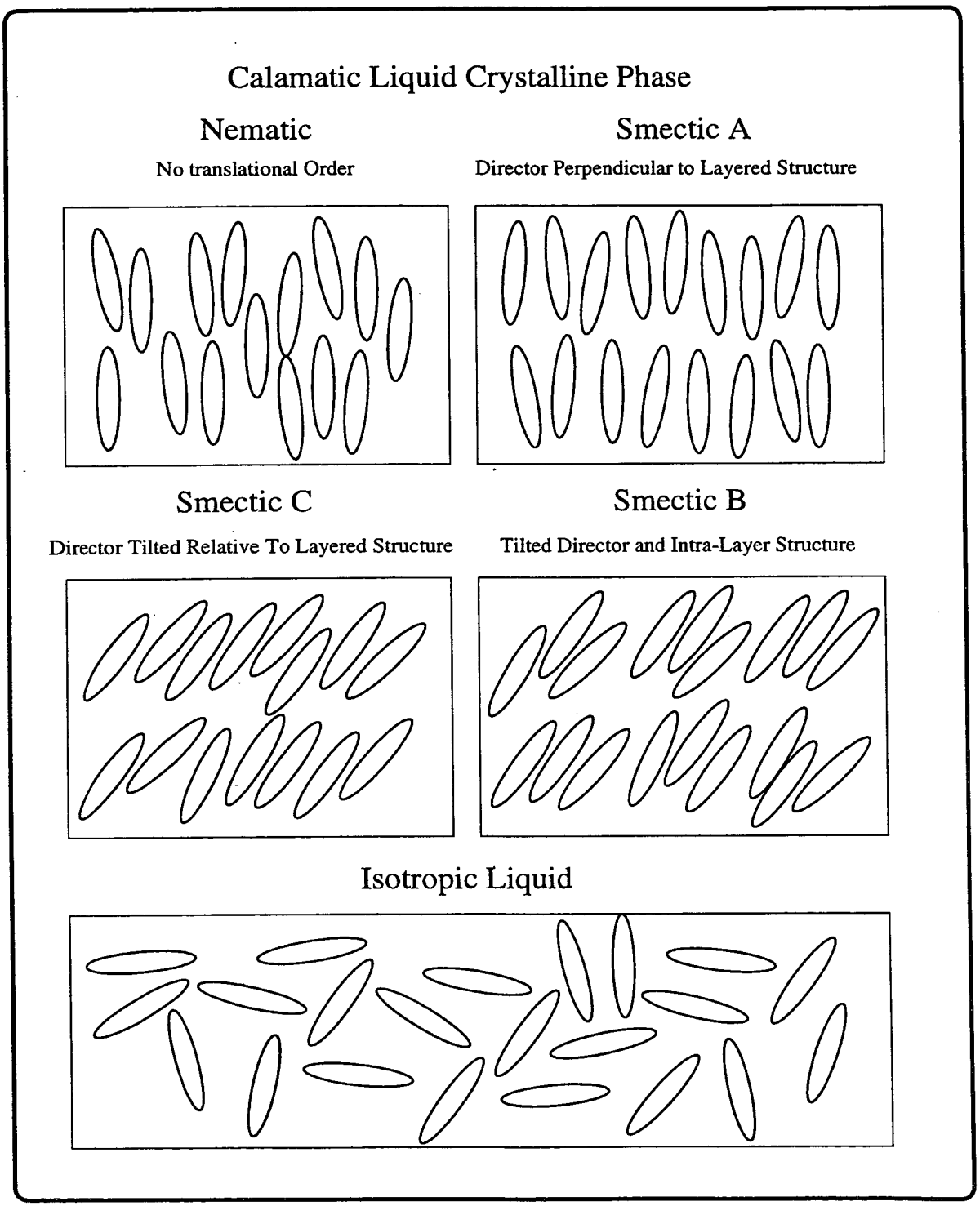

Table 1 Spectroscopic Technics for Dynamical Processes

	Absorption Technique	Process		Scattering Technique
		Non-peopagating Density Fluctuations		Rayleigh
Intermolecular	[Ultrasonic / Hypersonic]	Propagating Density Fluctuations (Sound Waves)		Brillouin (Doppler Effect)
Translational	a.c. Methods	Uncorrelated, Random Orientation		Depolarised Rayleigh (Rotational Raman)
Rotational	Audio, Radiofrequency and Microwave (Debye) Dielectric Relaxation	Dipole Monent Orientation	Polarisability Change	
Processes		Correlated Orientation (Libration)		Depolarised Rayleigh "collisional wings"
	Far Infra-Red (Poley) Absorption	Rotation of Dipole (permanent or collision induced dipole moment)	Polarisability Change	
		Vibration / Reorientation		Vibrational Raman
Intramolecular	Infra-Red	Dipole Moment Change	Polarisability Change	
Quantised	Visible and Ultra-Violet	Electronic Transtions		
Processes	X-ray	Electronic Transitions (X-ray > bonding energy)		
	Gamma-Ray	Moessbauer		

Chapter 2

The Reorientational Correlation Function

2.1 Introduction

In this chapter we discuss the formulation of the reorientational correlation function. This chapter contains the body of the theory and includes all the formulae and models used in later chapters. All the mathematical foundations used here, such as the small Wigner rotation matrices and irreducible tensor notation are discussed in more detail in Appendix A, which provides an overall view of the basic concepts of quantisation of angular momentum.

In general, the reorientational correlation function can be expressed mathematically as [3]

$$C(t) \equiv C^{LL'}_{NN'MM'}(t) = \langle D^{L}_{NM}(\Omega(0)) D^{*L'}_{N'M'}(\Omega(t)) \rangle - \langle D^{L}_{NM} \rangle \langle D^{*L'}_{N'M'} \rangle \qquad (2.1)$$

where the brackets $\langle ... \rangle$ denote an average over all molecular orientations, and $\Omega \equiv \alpha\beta\gamma$, the Euler angles which relate the laboratory fixed frame to the body fixed frame. As discussed in the appendix, the elements of the Wigner D-matrices in the above equation are used to express any orientation-dependent molecular property. First we will discuss how to obtain such a correlation function from a vibrational Raman band (or lineshape). This alone does not give an insight into the orientational motion of the individual molecules in a partially disordered system. To this end we next formulate several hypothetical models of reorientational dynamics and look at the functional form of their respective correlation functions.

We then show how to combine the experimentally extracted correlation functions with a suitable theoretical model and discuss how statistical mechanics is used to obtain classical dissipative parameters such as rotation diffusion coefficients from time-dependent microscopic fluctuations of the constituent particles of the system. Finally, we show how the functional form of the correlation functions provides an insight into intermolecular interaction and allows the calculation of intermolecular torques.

2.2 Obtaining Correlation Functions from Raman Lineshapes

Following the approach of Bartoli and Litovitz [4,5,6], using a semi-classical expression for the expansion of the electronic polarisability in terms of the normal coordinates of vibration, the expression for the intensity of scattered radiation as a function of frequency, ω for a single isolated molecule is given by [7]:

$$I(\omega) = A(\omega_i - \omega_v)^4 \sum_i \rho_i \sum_f \mid \langle f \mid \varepsilon^f \cdot \mathbf{R}^v \cdot \varepsilon^i \mid i \rangle \mid^2 \delta(\omega + \omega_f - \omega_i) \qquad (2.2)$$

where ω_v,ω_i and ω_f denote the frequencies of the v^{th} normal vibrational mode, the incident photon and the scattered photon respectively and $\omega = \omega_f - \omega_i + \omega_v$, and ε^i and ε^f are the polarisation vectors for incident and scattered light respectively, A is a constant of proportionality and ρ_i is a Boltzmann factor governing the population of initial translational-rotational states $\mid i\rangle$ which are assumed to form a complete set governed by the rotational-vibrational Hamiltonian. Notice that in this general expression, there is a summation over all initial and final ,$\mid f\rangle$, roto-vibrational states. $\mathbf{R}^v$ is the Raman tensor for an isolated molecule whose symmetry axes correspond to the laboratory axes. For convenience the Raman tensor can be expressed in terms of the electronic polarisability tensor, α^v, and the vibrational coordinate Q^v. Defining $\mid \phi_a^v\rangle$ and $\mid \phi_b^v\rangle$ as the eigenkets of the initial and final pure vibrational groundstate wavefunctions and using the subscripts j and k to define the polarisation directions of the incident and scattered photons:

$$R_{jk}^v = \alpha_{jk}^v \langle \phi_b^v \mid Q^v \mid \phi_a^v \rangle \qquad (2.3)$$

Using the above expression, equation 2 can be expanded as follows

$$I(\omega) = A(\omega_i - \omega_v)^4 \sum_a \rho_a \sum_b \sum_i \rho_i \sum_f | \langle f | \varepsilon^f \cdot \alpha^v \cdot \varepsilon^i | i \rangle \langle \phi_b^v | Q^v | \phi_a^v \rangle |^2 \delta(\omega + \omega_f - \omega_i) \tag{2.4}$$

where a hot band summation over the initial vibrational states has been included.

The vibrational and rotational line-broadening effects are separated by introducing an additional term, $\mathbf{V}^v$ into the Hamiltonian of the system which operates on the vibrational wavefunctions, thereby perturbing the original vibrational energy levels, but does not operate on the electronic wavefunctions and so does not alter the electronic polarisability. The following expression is obtained after converting from the Schroedinger picture to the Heisenberg picture [8],

$$\begin{aligned} I(\omega) = A(\omega_i - \omega_v)^4 (2\pi)^{-1} \int_{-\infty}^{+\infty} \textstyle\sum_i \rho_i \langle i | [\varepsilon^f \cdot \alpha^v(0) \cdot \varepsilon^i][\varepsilon^i \cdot \alpha^v(t) \cdot \varepsilon^1] | i \rangle \\ \times \textstyle\sum_a \rho_a \langle \phi_a^v | Q^v(0) Q^v(t) | \phi_a^v \rangle \exp(i\omega t) dt \, . \end{aligned} \tag{2.5}$$

The operators $\alpha^v(t)$ and $Q^v(t)$ are now time dependent and are expressed as

$$\alpha^v(t) = \exp(iH^{tr}t/\hbar)\alpha^v \exp(-iH^{tr}t/\hbar) \tag{2.6}$$

and

$$Q^v(t) = \exp(i\mathbf{V}^v t/\hbar) Q^v \exp(-i\mathbf{V}^v t/\hbar) \, . \tag{2.7}$$

As the operator $\mathbf{V}^v$ is a stochastic variable which is at least partially dependent on the molecular environment, the time dependent normal mode vibration coordinate is averaged over the molecular ensemble.

As a light scattering experiment, Raman spectroscopy possesses two polarisation components, which result in different Raman lineshapes. The incident and scattered radiation can be polarised either parallel or perpendicular to one-another (see Fig. 2). To simplify the situation, it is assumed that there occurs no red-shifting due to hot bands. The two spectral lineshapes for the two polarisation components are now:

$$\begin{aligned} I_{||}(\omega) = A(\omega_i - \omega_v)^4 (2\pi)^{-1} \int_{-\infty}^{+\infty} \langle \tfrac{1}{15} \textstyle\sum_{jk} [2\alpha_{jk}^v(0)\alpha_{jk}^v(t) + \alpha_{jj}^v(0)\alpha_{kk}^v(t)] \rangle \\ \times \langle Q^v(0) Q^v(t) \rangle \exp(i\omega t) \end{aligned} \tag{2.8}$$

$$I_{\perp}(\omega) = A(\omega_i - \omega_v)^4(2\pi)^{-1} \int_{-\infty}^{+\infty}\langle\tfrac{1}{30}\textstyle\sum_{jk}[3\alpha_{jk}^v(0)\alpha_{jk}^v(t) - \alpha_{jj}^v(0)\alpha_{kk}^v(t)]\rangle \times\langle Q^v(0)Q^v(t)\rangle \exp(i\omega t)\ . \tag{2.9}$$

In the above equations, the indices of the polarisability tensor represent the molecular axes, and averaging over all orientations is performed (represented by the brackets $\langle ...\rangle$ assuming that the molecules are orientated randomly with respect to the polarised incident and scattered radiation. The polarisability tensor is then separated into its spherical and non-spherical parts,

$$\alpha_{jk}^v(t) = \alpha^v\delta_{jk} + \beta_{jk}(t)\ . \tag{2.10}$$

The spherical part is orientationally independent and the trace of $\beta^v(t)$ is zero:

$$I_{\parallel}(\omega) = A(\omega_1-\omega_v)^4(2\pi)^{-1}\int_{-\infty}^{+\infty}\langle(\alpha^v)^2+\frac{2}{15}Tr[\beta^v(0)\cdot\beta^v(t)]\rangle\times\langle Q^v(0)Q^v(t)\rangle\exp(i\omega t) \tag{2.11}$$

$$I_{\perp}(\omega) = A(\omega_1 - \omega_v)^4(2\pi)^{-1}\int_{-\infty}^{+\infty}\langle\frac{1}{10}Tr[\beta^v(0)\cdot\beta^v(t)]\rangle\times\langle Q^v(0)Q^v(t)\rangle\exp(i\omega t)\ . \tag{2.12}$$

The author points out that $I_{\parallel}(\omega)$ is now the intensity of the scattered radiation as a function of frequency for the case that the incident and scattered radiation are polarised parallel to one another, a spectrum referred to later as a VV spectrum. Similarly $I_{\perp}(\omega)$ refers to the case where the incident and scattered radiation are polarised at ninety degrees to one another, which shall be called the VH spectrum. The separation of the translational-rotational and vibrational motion is achieved by invoking an isotropic spectral band as follows:

$$I_{iso}(\omega) = I_{\parallel} - \frac{4}{3}I_{\perp}(\omega) = A(\omega_1 - \omega_v)^4(2\pi)^{-1}(\alpha^v)^2\int_{-\infty}^{+\infty}\langle Q^v(0)Q^v(t)\rangle\exp(i\omega t)\ . \tag{2.13}$$

The perpendicular and isotropic spectra are normalised ($I_{\perp,norm}(\omega) = I_{\perp}(\omega)/\int_{-\infty}^{+\infty} I_{\perp}(\omega)d\omega$) and the correlation functions for pure vibrational relaxation, total rotational and vibrational relaxation and pure reorientational relaxation of the system are obtained by Fourier transformation.

$$C_{vib}(t) = \langle Q_{norm}^v(0)Q_{norm}^v(t)\rangle = \int_{-\infty}^{+\infty} I_{iso,norm}(\omega)\exp(-i\omega t)d\omega \tag{2.14}$$

$$C_{tot}(t) = \langle Tr[\beta^v_{norm}(0)\cdot\beta^v_{norm}(t)]\rangle\langle Q^v_{norm}(0)Q^v_{norm}(t)\rangle = \int_{-\infty}^{+\infty} I_{\perp,norm}(\omega)\exp(-i\omega t)d\omega \tag{2.15}$$

$$C_{rot}(t) = \langle Tr[\beta^v_{norm}(0)\cdot\beta^v_{norm}(t)]\rangle = \frac{\int_{-\infty}^{+\infty} I_{\perp,norm}(\omega)\exp(-i\omega t)d\omega}{\int_{-\infty}^{+\infty} I_{iso,norm}(\omega)\exp(-i\omega t)d\omega}\ . \tag{2.16}$$

The above derivation is given in a generalised form to express the relationship between the Raman lineshape and the correlation function *via* a Fourier transform. It also serves to show how reorientational and vibrational dephasing can be separated by use of the different polarisability components in Raman spectroscopy. However, to extract useful information about the reorientational motion of the individual molecules it is necessary to analyse the reorientational correlation function more closely.

2.3 Orientational Motion and the Selection of Raman Bands

The lineshape of a Raman band is sensitive to the reorientational motion of the molecular system *via* the anisotropic part of the polarisability tensor β^v. For a system with no optical rotatory power, this tensor is symmetric and has only five independent components. In the molecular frame (MF), β^v_{jk} are constants characteristic of the structure of the molecule. In spherical notation they are given by [9]:

$$\beta^v_0 = [6^{1/2}/2]\beta^v_{zz} \tag{2.17}$$

$$\beta^v_{\pm1} = 1/2(\mp\beta^v_{xz} - i\beta^v_{yz}) \tag{2.18}$$

$$\beta^v_{\pm2} = 1/2(\beta^v_{xx} - \beta^v_{yy} \pm i\beta^v_{yz})\ . \tag{2.19}$$

If the molecular frame is turned through an Euler angle Ω to coincide with the laboratory frame, the β^v_m components transform according to:

$$\beta^v_n(\Omega) = \sum_{m=-2}^{2} D^{l=2}_{nm}(\Omega)\beta^v_m(MF), \tag{2.20}$$

where $D^{l=2}_{nm}$ are the rotational D matrices and $\beta^v_m(MF)$ are the spherical polarisability elements in the molecular frame.

A spectrum (VV, VH, HV or HH) selects a single element of the polarisability

tensor $\beta^v_{ij}(\Omega)$ in the laboratory frame. For example:

$$\beta^v_{yz}(\Omega) = i[\beta^v_{+1}(\Omega) + \beta^v_{-1}(\Omega)], \tag{2.21}$$

as $2\beta^v_{+1} = (-\beta^v_{xz} - i\beta^v_{yz})$ and $2\beta^v_{-1} = (\beta^v_{xz} - i\beta^v_{yz})$. Now

$$\beta^v_{yz}(\Omega) = i[D^2_{1m}(\Omega) + D^2_{-1m}(\Omega)]\beta^v_m(MF)\ . \tag{2.22}$$

It follows that the reorientational correlation function becomes:

$$\langle \beta^{*v}_{yz}(\Omega')\beta^v_{yz}(\Omega)\rangle = \sum_{mm'} \langle [D^{*2}_{1m'}(\Omega) + D^2_{-1m}(\Omega')] \times [D^2_{1m}(\Omega) + D^2_{-1m}(\Omega)]\beta^{*v}_{m'}(MF)\beta^v_m(MF)\rangle\ . \tag{2.23}$$

All that remains is to evaluate the ensemble average, requiring the use of the single particle orientational probability density $P(\Delta\Omega, t)$, which is the probability density that at a time t a molecule will have turned through an angle between $\Delta\Omega$ and $\Delta\Omega + \delta\Delta\Omega$, from its initial orientation Ω. Integrating over Ω and $\Delta\Omega$ and applying orthogonality conditions for the D matrices, the final expression for the reorientational correlation function is:

$$\langle \beta^v_{yz}(\Omega')\beta^v_{yz}(\Omega)\rangle = C_0 \sum_{m=-2}^{m=+2} \mid \beta^v_m(MF) \mid^2 f^{l=2}_m(t)\ . \tag{2.24}$$

In the above equation, the spherical harmonic index has been fixed with $l = 2$ as we are dealing with a Raman transition, and m can take integer values between $-l$ and $+l$. C_0 is simply a constant arising from the integration over all molecular orientations. The functions $f^l_m(t)$ describe different aspects of reorientational motion. Light scattering experiments probe the $l = 2$ component of $P(\Delta\Omega, t)$ and the functions $f^l_m(t)$ describe a specific m component of the $l = 2$ correlation function. As an example, let us consider a symmetric top molecule (such that $f^2_m(t) = f^2_{-m}(t)$) with the major symmetry axis being the z-axis in the MF. Now $f^2_0(t)$ describes the 'tumbling' motion of the molecular symmetry axis only, whilst the functions $f^2_1(t)$ and $f^2_2(t)$ will involve some combination of the tumbling motion and 'spinning' motion about the major axis of symmetry. In order to determine the combination of these two motions it is neccessary to resort to a reorientational model.

The $\mid \beta^v_m(MF) \mid^2$ are coupling coefficients of the correlation function to each

$f_m^2(t)$. By choosing a vibration for which only one of these coefficients is non-zero, it is possible to study each $f_m^2(t)$ separately. The symmetry of the molecule allows us to do this as the form of the polarisability tensor $\beta^v(MF)$ is completely determined by the symmetry of the vibration [10]. The functional form of each $f_m^2(t)$ allows us to analyse how the molecule undergoes reorientational motion (be it only tumbling or some combination of tumbling and spinning). The theoretical formulation of $f_m^2(t)$ requires the use of a reorientational model, which is the subject of the next section.

2.4 Models of Reorientational Motion

In the previous section it was apparent that it is possible to separate various modes of reorientation dynamics by analysing the polarisation components of Raman bands for a given molecular and vibrational symmetry. The functional forms of the resulting correlation functions gives an insight into the reorientation process of these different modes of reorientation dynamics. In an attempt to better understand these processes, it is necessary to formulate a series of models for molecular reorientational motion and predict the functional form of the corresponding correlation function. It is obvious that single molecule reorientation plays an important role and in the following subsections various reorientational models formulated to represent the rotation of a single molecule in the potential energy field of its neighbours will be presented. This is not to presume that correlated rotations do not occur, but the complexity of such correlated rotational motion has caused limited progress to be made in this particular field. In general the models can be divided into two distinctive groups: the inertial models, and the stochastic models. The stochastic models are based on the assumption that the reorientation occurs as a series of thermally activated jumps over a potential energy barrier. These models are special cases of Markov chains and involve many concepts originating from the ideas of classical probability theory operating in a limit where the time to make a jump is negligible to the time between jumps, which is similar to the theory used for the ideal gas. All stochastic models predict exponentially decaying reorientational correlation functions which are only concerned with the time dependence of orientations on a given intermolecular potential energy surface.The inertial models consider the temporal fluctuations of the angular momentum or combinations of the angular momentum and orientation. These models are explicitly dependent on the symmetry of the molecular

system. The calculation of inertial models of reorientation is based on the solution to the well known equations of motion [11]:

$$\dot{L}_x = (\frac{1}{I_{zz}} - \frac{1}{I_{yy}})L_y L_z + N_x \tag{2.25}$$

$$\dot{L}_y = (\frac{1}{I_{xx}} - \frac{1}{I_{zz}})L_z L_x + N_y \tag{2.26}$$

$$\dot{L}_z = (\frac{1}{I_{yy}} - \frac{1}{I_{xx}})L_x L_y + N_z, \tag{2.27}$$

where **L** is the angular momentum in the body fixed frame, **N** is the torque on the molecule and **I** is the moment of inertia. The simplest of the inertial models is that of the free rotor that considers the reorientation of an isolated non-interacting single molecule. This model can then be extended to account for intermolecular collisions and torques.

2.4.1 The Free Rotor

The dynamics of an ensemble of rigid non-interacting molecules of a particular symmetry is most practically solved by the use of the Liouville equation [12]:

$$\frac{\partial W}{\partial t} = -i\hat{\mathcal{L}}W \tag{2.28}$$

where $W(\Gamma(t), t, \Gamma(0))$ is the conditional probability density that a molecule will have rotational phase space variables $\Gamma(t)$ at time t if it was known to have variables $\Gamma(0)$ at time $t = 0$, and $\hat{\mathcal{L}}$ is the Liouville operator. The specific form of the Liouville operator depends on the choice of phase-space variables. There is no formal solution to the classical equations of motion for an antisymmetric top experiencing no intermolecular torques, so we concentrate here on the solutions for the symmetric top and linear molecule. In the case of a symmetric top $I_{xx} = I_{yy} = I$. Choosing the phase-space variables to be the Euler angles and the body-fixed angular momentum, and working in a frame that precesses with respect to the body-fixed frame with angular velocity $\omega_p = (I_{zz}^{-1} - I^{-1})L_z$, the explicit form of the Liouville operator is [12]:

$$\hat{\mathcal{L}} = \frac{1}{I}\sum_{\mu=-1}^{1} L_\mu l_\mu \tag{2.29}$$

where L_μ is the spherical component of L in the precessing frame and l_μ is the body-fixed component of the quantum mechanical angular momentum operator. The formal solution for $W(\Gamma(t),t,\Gamma(0))$ is:

$$W(\Gamma(t),t,\Gamma(0)) = \sum_{J=0}^{\infty}\sum_{R,R'=-J}^{J} \frac{2J+1}{8\pi^2} D^J_{RR'}(\delta\Omega) f^J_{RR'}(\mathbf{L}(t),t;\mathbf{L}(0)) \qquad (2.30)$$

where

$$\begin{aligned} f^J_{RR'}(\mathbf{L}(t),t;\mathbf{L}(0)) &= \exp(-iR'b\times L(0)t/I)\exp(i(R-R')\phi_L(0))\times \\ &\quad \textstyle\sum_{M=-J}^{J}\exp(iML(0)t/I)d^J_{RM}(\theta_L(0))d^J_{R'M}(\theta_L(0)) \\ &\quad \times \textstyle\prod_{\mu=-1}^{1}\delta(L_\mu(t)-L_\mu(0)\exp(i\mu b\times L(0)t/I))\ . \end{aligned} \qquad (2.31)$$

In the above equation $\phi_L(0),\theta_L(0),L(0)$ are the spherical polar coordinates of the body-fixed $\mathbf{L}$ at $t=0$ and $b=(I-I_{zz})/I$.

In a similar way, the Liouville operator can be expressed explicitly for a linear molecule [12]. In this case, it is mathematically more convenient to use the space-fixed angular velocity, rather than the body-fixed angular velocity. The phase space variables are the magnitude and azimuthal orientation angle of the angular velocity $\omega(t)$ at time t, $\omega(t)$ and $\phi_\omega(t)$ respectively and $\delta\alpha$, $\delta\beta$, the azimuthal and polar displacements of the molecule. The conditional distribution function is found to be

$$W(\Gamma(t),t;\Gamma(0)) = \sum_{R}^{J}\frac{2J+1}{4\pi}D^J_{R,0}(\delta\alpha,\delta\beta,0)f^J_R(\omega(t),t;\omega(0)) \qquad (2.32)$$

where

$$f^J_R(\omega(t),t;\omega(0)) = \sum_M \exp(iM\omega(0)t)d^J_{0M}(\tfrac{\pi}{2})d^J_{RM}(\tfrac{\pi}{2})\times\exp[-iR\phi_\omega(0)]\delta(\omega(t)-\omega(0))\ . \qquad (2.33)$$

Such conditional distribution functions can be used to formulate correlation functions with the general equation being [13]:

$$C_{rot}(t) \equiv \langle D^{*J}_{RR'}(\delta\Omega)\rangle = \int D^{*J}_{RR'}(\delta\Omega)W(\Gamma(t),t;\Gamma(0))d\Gamma(t)W^0(\Gamma(0))d\Gamma(0) \qquad (2.34)$$

where $W^0(\Gamma(0))$ is the probability density for $\Gamma(0)$ at $t=0$. The relevant initial probability distributions for the cases of the symmetric top and linear molecule

are Maxwellian distributions for angular momentum and angular velocity respectively:

$$f^0(\mathbf{L}(0))d\mathbf{L}(0) = \frac{1}{(2\pi kT)^{3/2}II_{zz}^{1/2}} \exp[-\frac{L^2(0)}{2IkT}(1 + b\cos^2\theta_L(0))] \times d\phi_L(0)\sin\theta_L(0)d\theta_L(0)L^2(0)dL(0) \quad (2.35)$$

$$f^0(\omega(0))d\omega(0) = \frac{I}{2\pi kT}\exp[-\frac{I\omega^2(0)}{2kT}]d\phi_\omega(0)\omega(0)d\omega(0)\ . \quad (2.36)$$

The above expressions are integrated over the phase space variables $\Gamma(t)$. Notice that as the angular momentum and angular velocity are vectors the integration is performed over both the magnitude and the orientation angle. The resulting correlation functions are

$$\langle D^{*J}_{RR'}(\delta\Omega)\rangle = \int \langle f^J_{RR'}(\mathbf{L}(t), t; \mathbf{L}(0))\rangle_{\mathbf{L}(t)} f^0(\mathbf{L}(0))d\mathbf{L}(0) \quad (2.37)$$

for the symmetric top, and

$$\langle D^{*J}_{RR'}(\delta\Omega)\rangle = \frac{\delta_{R',0}\delta_{R,0}I}{kT}\int d^J_{00}(\omega(0)t)\exp[-\frac{I\omega^2(0)}{2kT}]\omega(0)d\omega(0) \quad (2.38)$$

in the case of the linear molecule. For the special case of a spherical top the correlation function has the form:

$$\langle D^{*J}_{RR'}(\delta\Omega)\rangle = \frac{\delta_{RR'}}{2J+1}\sum_{M=-J}^{J}(1 - M^2t^{*2})\exp[-M^2t^{*2}/2] \quad (2.39)$$

where t^* is the time in reduced units, given by $t^* = t(kT/I)^{1/2}$. In the case of the dipole moment correlation function, the function becomes negative for a period of time, which is representative of the fact that the linear molecule has on average undergone a rotation through 180° [14].

2.4.2 Collisions in Condensed Phases

There are two obvious deficiencies in the free-rotor model discussed above. First, the model takes no account of intermolecular torques. This problem alone is not of great significance, as even in dense phases, the torque will tend to zero as the intermolecular interaction potential approaches spherical symmetry. In the case of non-spherical molecules, the torque about any given high-symmetry axis is usually small enough as to have no major effect on the functional form of the correlation functions. The second deficiency is, however, of far greater concern: the free-rotor

model ignores all possible collisions between the constituent particles of a system. It is for this reason that, whilst the free-rotor model has been used with great success to analyse reorientational correlation functions in gases [12], it breaks down badly when applied to condensed phases.

From the free-rotor models it is apparent that the representative motion of a molecule as a function of time is completely expressed by the given components of the small Wigner rotation matrices. In the case of the linear molecule, the only component of interest is $d^J_{00}(\omega t)$, which represents pure tumbling motion. If we consider the case for dipole moment correlation functions (the first spherical harmonic index) $d^1_{00}(\omega t) = \cos(\omega t) = \cos(\theta)$ where θ is the angle between the unit dipole moment vector $\mathbf{m}(0)$ at time $t = 0$ and $\mathbf{m}(t)$ at time $t = t$. In this way, the dot product relationship (direction cosine) is immediately apparent. In the case of the fluctuations of a second rank tensor, $d^2_{00}(\omega t) = \frac{1}{2}[\cos^2(\omega t) - 1]$. The free-rotor correlation function is then obtained using a Boltzmann distribution and integration over the angular velocity. Following the work of Gordon [15], it is possible to formulate a hypothetical correlation function based on a model of successive reorientational steps each terminated by a collision. In the second harmonic index for a linear molecule, the first rotation step is given by $d^2_{00}(\omega_1 t_1)$. Assuming that the collision which ended the first diffusion step occured at t_1, the contribution to the correlation function from a molecule that has made two angular diffusion steps is:

$$F_2(t) = t^{-1} \int_0^t d^2_{00}(\omega_1[t - t_1]) - d^2_{00}(\omega_1 t_1) dt_1 \ . \tag{2.40}$$

As the collision which terminated the first diffusion step could have occurred at any time between 0 and t it is neccessary to perform the integration over t_1. The rate of the rotational diffusion is determined by the collision frequency, β, which is given by a Poisson distribution [16]. The number of molecules at a time t which are in their $(n+1)$th diffusion step is then $1/n!(\beta t)^n \exp(-\beta t)$. Extending the theory to account for molecules in the first, second,... $(n+1)$th diffusion step the total correlation function is given by:

$$F(t) = \exp(-t\beta) \sum_{n=0}^{\infty} \beta^n [\int_0^t dt_n d^2_{00}(\omega_{(n+1)}[t - t_n]) \times \int_0^{t_n} dt_{n-1} d^2_{00}(\omega_n[t_n - t_{n-1}]) \ldots$$
$$\int_0^{t_3} dt_2 d^2_{00}(\omega_3[t_3 - t_2]) \times \int_0^{t_2} dt_1 d^2_{00}(\omega_2[t_2 - t_1]) d^2_{00}(\omega_1 t_1) \ . \tag{2.41}$$

The above equation is the general diffusion formula for an ensemble of molecules

undergoing successive collisions of negligible duration compared to the time between collisions. The molecular motion between collisions is that of free rotation and, whilst the direction of the angular momentum vector is randomised after each collision, the molecular orientations upon entering and exiting a collision are unchanged. The exact definition of a collision is extremely tenuous, as it really refers to a change in the angular momentum, and not specifically to an event where two or more molecules actually collide with one-another. The generalised diffusion equation is not as yet complete as it still remains to define the angular velocity distribution function and to perform the necessary integration. Gordon [15] defined two limiting cases: in addition to randomising the direction of the angular momentum vector at each collision, the magnitude of **L** can also be randomised (J-diffusion) or can remain unchanged (M-diffusion). However, it is already apparent from the multiple integrations that appear in the generalised equation, that a more tractable form is required if we are to formulate such models.

2.4.3 The M-Diffusion Model

In the M-diffusion limit, it is considered that $\omega_0 = \omega_1 = \omega_2 ... = \omega_n$ in the generalised equation. Each collision therefore randomises the direction of the molecular angular momentum in the plane perpendicular to the axis of the linear molecule, though the magnitude remains constant. Averaging over a Boltzmann distribution of rotation velocities, the specific formula in reduced units is given by:

$$\begin{aligned} F_M(t) = \int_0^\infty \omega \exp(-\tfrac{1}{2}\omega^2) \times \exp(-t\beta) \sum_{n=0}^\infty \beta^n \int_0^t dt_n d_{00}^2(\omega[t-t_n]) \\ \times \int_0^{t_n} dt_{n-1} d_{00}^2(\omega[t_n - t_{n-1}]) ... \int_0^{t_3} dt_2 d_{00}^2(\omega[t_3 - t_2]) \\ \times \int_0^{t_2} dt_1 d_{00}^2(\omega[t_2 - t_1]) d_{00}^2(\omega t_1) \ . \end{aligned} \tag{2.42}$$

As $d_{00}^2(x)$ is the second Legendre polynomial with argument $cosx$, the above multiple integral expression can be expressed, and solved using Kummer's confluent hypergeometric function [17]. Using the free-rotor expression for $F_0(t)$,

$$F_0(t) = \int_0^\infty \cos(\omega t)\omega \exp(-\frac{1}{2}\omega^2) d\omega, \tag{2.43}$$

all higher terms $F_k(t)$ are found by the recursion relationship

$$F_k(t) = -t^{-2}[F_{k-1}(t) - 2^{(k-1)}(k-1)!/(2k-2)!], \tag{2.44}$$

and used in the series

$$F_M(t) = \exp[-t\beta] \sum_{n=0}^{\infty}(n+1)(t\beta/2)^n \times \sum_{k=0}^{[(n+1)]/2} F_k(t)/2^k k!(n+1-2k)! \ . \tag{2.45}$$

2.4.4 The J-Diffusion Model

The explicit expression for the J-diffusion model is the multiple integral of the free-rotor over given time steps weighted by a Poisson distribution of the collision frequency, β. The magnitude of angular momentum is randomised at each step:

$$F_J(t) = \exp(-t\beta) \textstyle\sum_{n=0}^{\infty} \beta^n [\int_0^t dt_n F_0(t-t_n) \times \int_0^{t_n} dt_{n-1} F_0(t_n - t_{n-1}) \ldots$$
$$\times \int_0^{t_3} dt_2 F_0(t_3 - t_2) \times \int_0^{t_2} dt_1 F_0(t_2 - t_1) F_0(t_1)] \ . \tag{2.46}$$

Numerical calculation of the J-diffusion model can be achieved using a trapizoidal integration approach [18]. The required formula is:

$$F_J(t) = \sum_{n=0}^{\infty} \exp(-\beta t)\beta^n F(n+1, t) \ . \tag{2.47}$$

$F(1,t)$ is the expression for the free-rotor for a linear molecule. Invoking a time-step, Δ, and regarding v as an integer variable:

$$F(1, \Delta v) = \int_0^{\infty} d\omega \frac{1}{2}[\cos^2(\omega \Delta v) - 1]\omega \exp(-\omega^2/2) \ . \tag{2.48}$$

Using a recursion relationship it is then possible to generate all F(n,t) as follows:

$$F(n, \Delta u) = \sum_{v=0}^{u} d_v F(n-1, \Delta v) F(1, \Delta u - \Delta v) \tag{2.49}$$

where u is also an integer variable, and d_v has the value $\Delta/2$ for $v = 0$ and $v = u$, otherwise $d_v = \Delta$.

Obviously such extended diffusion models can be calculated in any spherical harmonic index, for any given molecular symmetry [19,20,21], as long as a numerical or analytical solution to the free-rotor for that system exists. We have concentrated here on the solutions in the second harmonic index for a rigid linear

molecule such as CS_2, which will be discussed in Chapter 4.

2.4.5 The Stochastic Models: Small Step Rotation Diffusion

The extended diffusion models provide a much more accurate representation of reorientational diffusion in condensed phases than the free-rotor model. The extent to which the reorientational motion is hindered is determined by a single parameter, the collision frequency, β. However, molecular reorientation in dense phases can be approached from a different perspective. In the case of highly hindered motion, we can regard reorientation to occur as a series of thermally activated jumps over given potential energy barriers. The molecules are now permanently experiencing each other's presence, and therefore it is only neccessary to consider the time dependence of the molecular orientations rather than the angular momentum. Using the ideas of classical probability theory, these models can be regarded as Markov chains. Furthermore the process can be simplified by assuming that the stochastic process is stationary. This means that the orientational probability distribution is time independent and that the conditional probability distribution, defined earlier as $W(\Gamma(t), t, \Gamma(t'))$, depends on the difference $t - t' = \tau$ alone. It is therefore not neccessary to work with phase-space distribution functions, as a calculation of the partially averaged conditional probability density for reorientation $W(\delta\Omega)$ suffices. $W(\delta\Omega)$ can be regarded as the probability density for a reorientation $\delta\Omega$ in time t. A quasicontinuous set of orientation sites exists such that $\delta\Omega$ can be regarded as being made up of a set of infinitessimal increments in angle in Hilbert space. Within this representation, we can solve $W(\delta\Omega)$ using the transition density $\Psi(\delta\Omega; \delta\Omega')$ that gives the probability of a change from $\delta\Omega'$ to $\delta\Omega$ in unit time:

$$\frac{\partial W(\delta\Omega)}{\partial t} = \int \Psi(\delta\Omega; \delta\Omega') W(\delta\Omega') d\delta\Omega' \; . \tag{2.50}$$

Asssuming that the reorientational steps are small, $W(\delta\Omega')$ can be expanded in a Taylor series around $W(\delta\Omega)$.

$$W(\delta\Omega') = W(\delta\Omega) + \sum_{i=x,y,z} \Delta\psi_i \frac{\partial W}{\partial \psi_i}_{\partial\Omega} + \frac{1}{2} \sum_{i,j=x,y,z} \Delta\psi_i \Delta\psi_j \frac{\partial^2 W}{\partial\psi_i \partial\psi_j}_{\partial\Omega} + \ldots \tag{2.51}$$

where $\Delta\psi_i$ denotes a small rotation about the ith molecule-fixed axis. We formulate the small step rotation diffusion model by stating that:

$$\int \Delta\psi_i \Psi(\delta\Omega;\delta\Omega')d\delta\Omega' = 0 \tag{2.52}$$

and

$$\frac{1}{2}\Delta\psi_i\Delta\psi_j\Psi(\delta\Omega;\delta\Omega')d\delta\Omega' = \mathcal{R}_{ij} \tag{2.53}$$

where $\mathcal{R}_{ij}$ is an element of the rotation diffusion tensor. Choosing the molecular fixed axes such that $\mathbf{R}$ is diagonalised, the general equation becomes [22,23]:

$$\frac{\partial W}{\partial t} = \sum_{i=x,y,z} \mathcal{R}_{ii}\frac{\partial^2 W}{\partial\psi_i^2} \; . \tag{2.54}$$

The solutions to this second-order differential equation can be expanded as a complete set of functions

$$W(\delta\Omega) = \sum_J \sum_{R,R'=-J}^{J} f^J_{RR'} D^J_{RR'}(\delta\Omega) \tag{2.55}$$

where the expressions for the coefficients $f^J_{RR'}$ depend on the nature of the rotation diffusion tensor. For the case when the rotational diffusion tensor is diagonal with principle elements $\mathcal{R}_\perp, \mathcal{R}_\perp, \mathcal{R}_\parallel$ we obtain the well-known expression [24]:

$$f^J_{RR'} = \delta_{RR'} \exp[-(J(J+1)\mathcal{R}_\perp + R^2(\mathcal{R}_\parallel - \mathcal{R}_\perp)t] \; . \tag{2.56}$$

This is not the only derivation of the small-step rotation diffusion model. Indeed, Debye [25] produced the same result by finding the conditional probability distribution as a solution of the diffusion equation:

$$\frac{\partial W}{\partial t} = -\mathbf{L}\cdot\mathbf{R}\cdot[\mathbf{L} + (\mathbf{L}k_B U(\Omega))]W \tag{2.57}$$

where $\mathbf{L}$ is formally equivalent to the quantum mechanical angular momentum operator, a vector operator which generates infinitessimal rotations. k_B is the Boltzmann constant and $U(\Omega)$ is the orientational energy of a molecule as a function of the Euler angles. Obviously there are an infinite number of solutions to this equation depending on the symmetry of $\mathbf{R}$ and the choice of the potential function U. For the isotropic case $U = 0$. In this form, it is immediately apparent that the symmetry of the molecule is no longer important compared to the

symmetry of the potential, in comparison to the inertial models.

The small step rotation diffusion model is the most common of the stochastic models used. As with all stochastic models, it gives exponential correlation functions with a time exponent τ related to the elements of the rotation diffusion tensor. The coefficients $f^J_{RR'}$ are directly comparable to those coefficients in equation 2.24 when $J = 2$ and $R = R' = m$.

2.5 Time and Distance

The free-rotor and small-step rotation diffusion model are extreme limiting cases for the description of reorientational motion in condensed phases. As will be seen later, experimental correlation functions are neither perfect free-rotors nor exponentials. The extended diffusion models can be regarded as intermediates, but even these models possess two extreme limiting cases (J and M). Realistic correlation functions are likely to show aspects of all these models; in the very short time limit (less than $0.1ps$), the molecule behaves as a free-rotor, as the damping of reorientational motion due to intermolecular interaction is insignificantly small in this time limit. Over the next few tenths of picoseconds, the effect of the intermolecular torques increases, slowing the reorientational relaxation. In condensed phases the molecule is likely to physically interact with other molecules situated around it, by means of collisions. The nature of the correlation function in the first few picoseconds therefore is determined by the local structuring and environment in the system. At longer time-scales, the so-called hydrodynamic regime, the form of the correlation function depends on a hierachy of complex many-body long range interactions. Such a complex system cannot be modelled exactly. Using statistical mechanics the time-reversible microscopic orientational fluctuations of the single molecule can be related to macroscopic dissipative rotation diffusion coefficients. This is known as Kubo's fluctuation dissipation theorem [26]. At long time-scales the correlation functions decay exponentially. It is a commonly misunderstood concept that this exponential decay is indicative of small-step reorientation diffusion. All correlation functions in soft-condensed phases will eventually exhibit exponential decay by virtue of the fact that all partially disordered systems are isotropic over large distance scales [27]. In this way correlation functions provide an inextricable link between time and distance.

2.6 Intermolecular Torques

All models discussed in this chapter do not account for molecular flexibility, nor for the presence of intermolecular torques. Indeed attempts were made to include the effect of the intermolecular torque in the stochastic models. This was achieved by solving the rotational Langevin equation, which included an expression for the intermolecular torque as a function of the friction constant tensor. Two limiting cases were then invoked to calculate this friction constant tensor. In the 'stick' boundary condition [28,29], the friction constant tensor is estimated from the solutions of the Stokes-Einstein equation for the hydrodynamic drag of a body rotating in a viscous medium. Not surprisingly this model breaks down as it involves the use of the shear viscocity, a macroscopic hydrodynamic property, which cannot be used when considering the dynamics of a molecule. In the 'slip' boundary condition [30,31], the rotational resistance is considered entirely due to the fact that a non-spherical body must displace a certain amount of viscous fluid during rotation. Neither model proved successful and the reader is referred to the references [28-31] for further details.

Although models involving the intermolecular torque have not proven to be successful, it is possible to calculate the root mean square torque given a rotational correlation function [32,33,34]. The classical reorientational correlation function is a real, even function of time. As such it may be approximated at short time by an even power series in time. In the case of a Raman spectrum:

$$\langle \alpha(0).\alpha(t) \rangle = \sum_{n=0}^{\infty} \frac{t^n}{n!} [\frac{d^n}{dt^n} \langle \alpha(0).\alpha(t) \rangle_{t=0}] \tag{2.58}$$

where α is the transition polarisability. The coefficients in this time series may be identified with the frequency moments of the spectrum, $M(k)$, which are the time derivatives of $C(t)$ evaluated at $t = 0$. In the second harmonic, the moments expansion of a Raman spectrum for a classical linear molecule is given by:

$$\begin{aligned} C_{rot}(t) &= \sum_{k=0}^{\infty} \frac{(it)^k}{k!} M(k)(-i)^k [\frac{d^k C(t)}{dt^k}]_{t=0} \\ &= 1 - (\frac{3kT}{I})t^2 + [4(\frac{kT}{I})^2 + \frac{1}{8I^2}\langle (OV)^2 \rangle]t^4 + ... \end{aligned} \tag{2.59}$$

where $\langle (OV)^2 \rangle$ represents the equilibrium average of the mean square torque. Noticeably, the second moment is independent of intermolecular torques, which first appear in the t^4 term and have the effect of damping the decay of $C_{rot}(t)$

with time.

2.7 Summary

In this chapter we have discussed the relationship between Raman lineshapes and correlation functions. We have seen how the functional form of the correlation function is dependent on reorientational motion and looked at the various standard models for reorientational relaxation. Additionally we have seen how it is possible to calculate intermolecular torques and rotation diffusion constants. All the theories discussed here will be used later in obtaining and analysing rotational correlation functions in partially disordered systems.

Fig. 2 Raman Lineshape Analysis

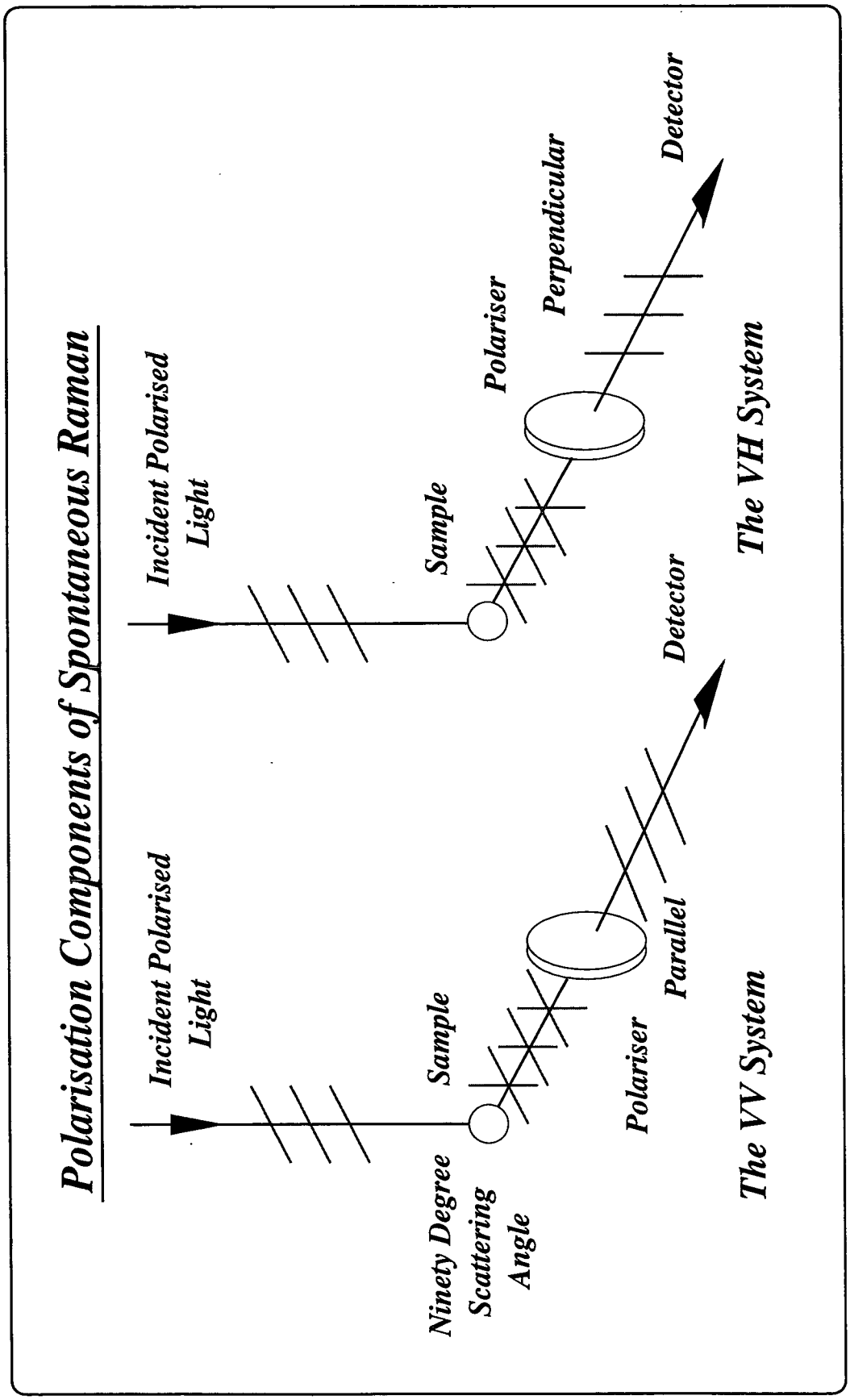

Chapter 3

Ab Initio DFT Molecular Dynamics Simulation

3.1 Introduction

In the previous chapter we discussed the formulation of the reorientational correlation function and how such correlation functions can be extracted from Raman lineshape analysis. In particular, it was shown that the specific functional form of the correlation function is dependent on the molecular reorientational relaxation process. It is clear from the previous discussion that reorientational correlation functions are inherently classical, and are formulated as an average over all molecular orientations. There is to date no available experimental technique which allows us to specify an individual molecule in a macroscopic system and follow its reorientational motion as a function of time. The last forty years has seen a rapid development in the field of molecular dynamics computer simulation techniques. Computer simulations generate at a suitable time interval the position coordinates of the constituent particles in a macroscopic system, and the forces acting on the particles. Computer simulation techniques are extremely useful when combined with experimental techniques to probe the dynamics of condensed matter systems.

The most important aspect of any computer simulation technique is the definition of the interaction potential energy function. It is the accuracy with which we define the interaction potential that determines how realistic the simulation is. Let us consider classical MD simulation techniques, which are nowadays readily

available [35]. In classical MD simulations, the constituent molecules in a system are considered to be rigid bodies with a simplistic symmetry, such as spheres or sphero-cylinders. A semi-empirical interaction function is then defined. There are a hierachy of semi-empirical interaction potentials available. For an isotropic liquid, the most common interaction potential is the Lennard Jones potential, which has the general form [36]:

$$V = 4\varepsilon[(\sigma/R)^{12} - (\sigma/R)^{6}] \tag{3.1}$$

where R is the inter-particle distance, and ε and σ are parameters defining the depth of the potential energy well and the inter-particle distance at $V = 0$ respectively. For a given molecular system the parameters are determined from experimentally obtained average values. The potential is static: it does not account for molecular flexibility or changes in molecular conformation and vibrations which will act to break the symmetry of the molecular system. Having defined the specfic interaction potential and a given ensemble (that is to say, a given set of physical constraints, such as pressure, temperature and volume), the constituent particles are arranged randomly, yet realistically in an imaginary (periodically repeating) box. Using the interaction potential, the forces on the constituent particles are calculated. The classical equations of motion are then solved and the particles are allowed to move for a short period of time. Once the new position coordinates of the particles have been determined, the new forces are calculed and the procedure is repeated. In general, classical MD simulations deal with systems containing at least 150,000 constituent particles.

As the name suggests, classical MD allows the accurate computational analysis of classical dynamics, in particular dissipation parameters, such as translational and rotational diffusion constants in the hydrodynamic regime (i.e. dynamics at long timescales). However, due to the fact that the interaction potential completely ignores intra-molecular dynamics occuring at ultra-fast timescales, such as molecular vibrations and changes in the geometric molecular conformation, any information about the ultra-fast relaxation processes in condensed systems is lost. A higher level of computer simulation is required, which incorporates intra-molecular motion. The constituent molecules are no longer regarded as rigid bodies, but rather as a group of ions in an electron cloud. For a given set of ionic position coordinates, the polyelectronic wavefunction (which is parametrically dependent on the position of the nuclear ions) is calculated. From the resulting potential energy surface it is then possible to calculate the forces acting

on the ions, and to formulate a Lagrangian which defines the dynamics of the ions and the electrons in the system. The intra- and inter-molecular interactions are therefore calculated simultaneously. This type of computer simulation is called *ab initio* as it involves the first principles calulation of the quantum mechanical electronic structure, rather than using an analytic interaction potential defined by experimentally obtained averaged parameters.

There are two types of *ab initio* computer simulation techniques: Hartree Fock (HF) and Density Functional Theory (DFT), which are in many ways comparable, as they both attempt to solve exactly the same problem. In Chapter 4, results are presented for the study of the prototypical isotropic liquid CS_2 using Raman lineshape analysis and *ab initio* DFT computer simulation. In particular the ultra-fast relaxation processes are investigated including the calculation of the intermolecular torque as a function of temperature. It is the purpose of this chapter to provide a general discussion of the *ab initio* DFT simulation technique used. It is not possible here to provide an exact in-depth discussion of all the aspects involved in the computer simulation and the author strongly refers the reader to the references provided for a more detailed discussion. The author makes particular reference to the paper by M.C. Payne *et al.* [37] which is concerned with the plane wave total energy pseudo-potential method, which is that used in the Cambridge-Edinburgh-Total-Energy-Package (CETEP) program employed in the simulation of CS_2 in Chapter 4.

3.2 An Overview of *ab initio* DFT Molecular Dynamics Simulation

In this section the author provides an overview of the DFT simulation technique. In principle, all knowledge about a system can be obtained from the quantum mechanical wavefunction. This is obtained (non-relativistically) by solving the Schroedinger equation of the complete many electron system. However, in practice solving such an N-body problem proves to be impossible. Density Functional theory (DFT) was developed by Kohn and Sham based on the theory of Hohenberg and Kohn which is an exact ground state theory. As the name suggests, the fundamental function in DFT is the electron density rather than the electronic wavefunctions. In this formalism, the N-electron problem is expressed as

N one-electron equations (the Kohn-Sham equations), where each electron interacts with all other electrons *via* an effective exchange correlation potential. These interactions are then calculated using the local density approximation (LDA) to exchange and correlation. Plane wave basis sets and the total energy pseudopotential techniques are then used to solve the Kohn-Sham one-electron equations. The Hellmann-Feynman theorem is then used to calculate the forces required to integrate the ionic equations of motion within the Car-Parrinello molecular dynamics simulation [56]. The valence electron wavefunctions are expanded in a plane wave basis set and the electronic structure calculation proceeds *via* a preconditioned conjugate gradients energy minimisation algorithm using the plane wave coefficients as variational parameters. After optimisation of the polyelectronic wavefunction, the system is given a kinetic energy equivalent appropriate to the required temperature and the classical equations of motion are then integrated with a timestep of $1.0fs$, which ensures conservation of energy.

In the remaining sections of this chapter we will discuss in more detail the exchange-correlation interaction between electrons, the solution to the poly-electronic problem: the Kohn-Sham equations and self-consistent field theory. We will also discuss the formulation of the poly-electronic wavefunctions, the local density approximation and the pseudopotential approximation, the Car-Parrinello Lagrangian and the Hellmann-Feynman theorem.

3.3 Poly-electronic Interactions: The Exchange Correlation

There are three types of electron-electron interaction. The coulombic repulsive interaction is intuitively obvious and has a classical analogue. However there are two other quantum mechanical interactions between electrons which do not have a classical analogue, these are the exchange interaction and electron correlation. It is the purpose of this section to show explicitly what exchange correlation is.

Let us consider a system containing two electrons. The antisymmetry principle (also known as the Pauli exclusion principle) does not distinguish between identical electrons and requires that the electronic wavefunctions be antisymmetric with respect to interchange of space and spin coordinates of any two electrons. For the two-electron system we can express correctly antisymmetrised wavefunctions

in the form of the well-known Slater Determinant:

$$\Psi(\mathbf{x}_1, \mathbf{x}_2) = 2^{-1/2}(\psi_i(\mathbf{x}_1)\psi_j(\mathbf{x}_2) - \psi_j(\mathbf{x}_1)\psi_i(\mathbf{x}_2)) \tag{3.2}$$

where ψ_i represents a single-electron spin orbital and the coordinate $\mathbf{x}_n$ defines both the position and spin of electron n. Notice that the minus sign ensures that the wavefunction is antisymmetric with respect to interchange of the coordinates of electrons one and two. Let us now see how the antisymmetrisation affects the wavefunction. Let us assume that the electrons have opposite spins and occupy different spatial orbitals:

$$\psi_1(\mathbf{x}_1) = \phi_1(\mathbf{r}_1)\alpha(\omega_1) \tag{3.3}$$

$$\psi_2(\mathbf{x}_2) = \phi_2(\mathbf{r}_2)\beta(\omega_2)\ . \tag{3.4}$$

Let $P(\mathbf{r}_1, \mathbf{r}_2)d\mathbf{r}_1 d\mathbf{r}_2$ be the probability of finding electron-one in $d\mathbf{r}_1$ and simultaneously electron-two in $d\mathbf{r}_2$. This probability is obtained by taking the square of the wavefunction and integrating over the spins of the two electrons. The result for a system of two electrons with opposite spins is:

$$\begin{aligned} P(\mathbf{r}_1, \mathbf{r}_2)d\mathbf{r}_1 d\mathbf{r}_2 &= \int d\omega_1 d\omega_2 |\Psi|^2 d\mathbf{r}_1 d\mathbf{r}_2 \\ &= \tfrac{1}{2}[|\phi_1(\mathbf{r}_1)|^2|\phi_2(\mathbf{r}_2)|^2 + |\phi_1(\mathbf{r}_2)|^2|\phi_2(\mathbf{r}_1)|^2]d\mathbf{r}_1 d\mathbf{r}_2\ . \end{aligned} \tag{3.5}$$

The first term is the product of the probability of finding electron one in $d\mathbf{r}_1$ at $\mathbf{r}_1$ times the probability of finding electron-two in $d\mathbf{r}_2$ at $\mathbf{r}_2$ *if electron-one occupies spatial orbital-one and electron-two occupies spatial-orbital-two.* The second term has electron-one occupying spatial orbital-two and electron-two occupying spatial-orbital-one. Since the electrons are indistinguishable, the correct probability is the average of the two terms as shown. The electrons are capable of exchanging, as the wavefunction is antisymmetric, however, the electrons are still uncorrelated. This is particularly obvious if spatial orbitals one and two are the same spatial orbital, in which case the probability $P(\mathbf{r}_1, \mathbf{r}_1)$ is not equal to zero. There is a finite probability of finding two electrons with opposite spins at the same point in space at the same moment in time. If the two electrons have the same spin (eg. β), then we obtain:

$$\begin{aligned} P(\mathbf{r}_1, \mathbf{r}_2) &= \tfrac{1}{2}(|\phi_1(\mathbf{r}_1)|^2|\phi_2(\mathbf{r}_2)|^2 + |\phi_1(\mathbf{r}_2)|^2|\phi_2(\mathbf{r}_1)|^2 \\ &-[\phi_1^*(\mathbf{r}_1)\phi_2(\mathbf{r}_1)\phi_2^*(\mathbf{r}_2)\phi_1(\mathbf{r}_2) + \phi_1(\mathbf{r}_1)\phi_2^*(\mathbf{r}_1)\phi_2(\mathbf{r}_2)\phi_1^*(\mathbf{r}_2)]) \end{aligned} \tag{3.6}$$

where we now have an extra cross term that ensures that the electrons are correlated. This is exchange correlation between electrons of parallel spin. As we see, the probability of finding two electrons with parallel spin at the same point in space at the same time is zero. A *Fermi hole* is said to exist around an electron. In the Slater determinant the motion of electrons with parallel spins is correlated, but the motion of electrons with opposite spins is not.

In summary, the antisymmetry of the polyelectronic wavefunction produces spatial separation between electrons that have the same spin function, thus reducing the coulomb energy of the electronic system. This energy reduction due to antisymmetry is called the exchange energy. The calculation of the total electronic energy including the exchange energy is called the Hartree-Fock approximation. However, electrons of opposite spins are not correlated and therefore the exact many-body energy of an electronic system is greater than the energy of the system calculated in the Hartree-Fock approximation. This energy difference is the correlation energy and is extremely difficult to calculate [38].

3.4 The Solution to the Polyelectronic Problem: The Kohn-Sham Equations and Self-Consistent Field Theory

In 1964 Hohenberg and Kohn [39] proved that the total energy of a homogeneous electron gas including exchange and correlation is a unique functional of the electron density. The minimum value of the total energy functional is the ground state energy of the system, and the density that corresponds to this minimum value is the exact single particle ground-state density. From this theory, Kohn and Sham formulated an expression for the total energy functional for a set of doubly occupied electronic states ψ_i in the presence of a set of static nuclei (using the Born-Oppenheimer approximation) [40]:

$$\begin{aligned} E[\psi_i] \quad &= 2\sum_i \int \psi_i[-\tfrac{\hbar^2}{2m}]\nabla^2\psi_i d^3\mathbf{r} + \int V_{ion}(\mathbf{r})n(\mathbf{r})d^3\mathbf{r} \\ &+\tfrac{e^2}{2}\int \tfrac{n(\mathbf{r})n(\mathbf{r}')}{|\mathbf{r}-\mathbf{r}'|}d^3\mathbf{r}d^3\mathbf{r}' + E_{XC}[n(\mathbf{r})] + E_{ion}(\mathbf{R_I}) \; . \end{aligned} \tag{3.7}$$

The first term represents the electron kinetic energy, V_{ion} is the static total electron-ion potential, $n(\mathbf{r})$ is the electron density given by:

$$n(\mathbf{r}) = 2\sum_i \mid \psi_i(\mathbf{r}) \mid^2, \tag{3.8}$$

$E_{XC}[n(\mathbf{r})]$ is the exchange correlation functional and E_{ion} is the Coulomb energy associated with the interactions between the nuclei at positions $\mathbf{R_I}$. The exact calculation of the Coulomb energy of the ionic system is difficult as the Coulomb interaction is long-ranged in both real and reciprocal space. Ewald formulated a mathematical theory which expresses the total ion-ion coulomb interaction for a periodically repeating system of ions as the sum of two finite series. This is known as the Ewald sum [41].

The polyelectronic problem now reduces to finding the set of wavefunctions ψ_i that minimise the Kohn-Sham energy functional, as it is at this minimum value that the Kohn-Sham energy functional is equal to the ground state energy of the system of electrons with the ions in positions $\mathbf{R_I}$. These wavefunctions are given by the self-consistent solutions to the Kohn-Sham equations:

$$[\frac{-\hbar^2}{2m}\nabla^2 + V_{ion}(\mathbf{r}) + V_H(\mathbf{r}) + V_{XC}(\mathbf{r})]\psi_i(\mathbf{r}) = \varepsilon_i\psi_i(\mathbf{r}) \tag{3.9}$$

where ψ_i is the wavefunction of electronic state i, ε_i is the respective Kohn-Sham eigenvalue, and V_H is given by:

$$V_H(\mathbf{r}) = e^2 \int \frac{n(\mathbf{r}')}{\mid \mathbf{r} - \mathbf{r}' \mid} d^3\mathbf{r}' \ . \tag{3.10}$$

The exchange-correlation potential is given by the functional derivative:

$$V_{XC}(\mathbf{r}) = \frac{\delta E_{XC}[n(\mathbf{r})]}{\delta n(\mathbf{r})} \ . \tag{3.11}$$

The Kohn-Sham equations map the interacting many-electron system onto a system of non-interacting electrons moving in an effective potential due to all the other electrons in the system. Due to the presence of the ionic nuclei, the electron density is not homogeneous and an approximate expression for the exchange correlation energy is required. This is the Local Density Approximation. In order to reduce the cpu time, the ion-electron interaction is also approximated by the use of pseudopotentials. LDA and the pseudopotential approximation are discussed in the next section.

The electronic wavefunction is expressed as a plane wave basis set expansion in reciprocal space:

$$\psi_i(\mathbf{r}) = \sum_{j=1}^{N} C_j exp[i\mathbf{k}_j\mathbf{r}] \; . \tag{3.12}$$

In the CETEP program, the calculation is performed for a periodically repeating supercell, and the actual plane wave basis sets used are the product of a cell-periodic function and a wavelike part as defined above [42]. For the exact plane-wave representation of the Kohn-Sham equations the reader is referred to the reference provided [42]. The author draws attention to the fact that there are a finite number of known basis set wavefunctions in reciprocal space. The variation parameters are the basis set coefficients. The electronic wavefunction is represented on a set of grid points in $3D$ k-space. The Kohn-Sham equations are solved self-consistently so that the occupied electronic states generate a charge density that produces the electronic potential that was used to construct the equations. A self-consistent field is achieved and simultaneously, the energy of the system is minimised. The iterative procedure is carried out by moving from reciprocal to real, to reciprocal space by means of a Fourier transform.

3.5 LDA and the Pseudopotential Approximation

In order to make the solutions to the Kohn-Sham equations mathematically tractable, two approximations are used. The simplest way of describing the exchange correlation energy of an electronic system is to use the Local Density Approximation (LDA)[40,43,44,45]. This approximation is almost universally used in total energy calculations. In the LDA, the exchange correlation energy of an electronic system is constructed by assuming that the exchange correlation energy per electron at a point $\mathbf{r}$ in the inhomogeneous electron gas is equal to the exchange correlation energy per electron in a homogeneous electron gas that has the same density as the inhomogeneous electron gas at point $\mathbf{r}$. Mathematically this is expressed as:

$$V_{XC}(\mathbf{r}) = \frac{\delta E_{XC}[n(\mathbf{r})]}{\delta n(\mathbf{r})} = \frac{\partial[n(\mathbf{r})\varepsilon_{XC}(\mathbf{r})]}{\partial n(\mathbf{r})} \tag{3.13}$$

with

$$\varepsilon_{XC}(\mathbf{r}) = \varepsilon_{XC}^{hom}[n(\mathbf{r})] \; . \tag{3.14}$$

As the name suggests, the LDA regards the exchange correlation functional as being purely local.

The pseudopotential approximation (PA)[46,47,48] plays a major role in total energy calculations. Its value is that it greatly reduces cpu time. The cpu time for the total electron calculation is dependent on the number of plane-wave basis sets. The number of basis sets depends on the number of electrons in the system, the size of the system (*i.e.* the size of the periodic supercell). However, as the electronic wavefunctions are formulated in k-space, the required number of basis functions is also very much dependent on the energy of the electrons. In a poly-electronic system, the true valence functions oscillate rapidly in the region occupied by the core electrons due to the strong ionic potential in this region. In the PA, the core electrons and the strong potential are removed and replaced by a weaker pseudopotential that acts on a set of pseudowavefunctions rather than the true valence wavefunctions. The properties of the pseudopotential for the pseudowavefunctions are identical to those of the ion and core electrons for the true valence wavefunctions. Outside the core-region, the pseudopotential and ion-core electron potential are identical, and therefore so are the pseudo- and true valence wavefunctions. At the periphery of the core region, the valence electron has a given potential energy. This is known as the energy cut-off, and explicitly determines the number of basis sets required. A hierachy of pseudopotentials have been developed and the reader is referred to the references [49,50,51,52,53,54,55] for more information. It is important to note that the energy cut-off in the PA is determined by the type of ions in the system.

3.6 Car-Parrinello Molecular Dynamics and the Hellmann-Feynman Theorem

The Car-Parrinello molecular dynamics approach exploits the quantum mechanical adiabatic time-scale separation of fast electronic and slow nuclear motion, by transforming this separation into classical-mechanical adiabatic energy-scale separation in the framework of dynamical systems theory. The two-component quantum/classical problem is mapped onto a two-component purely classical problem with two separate energy scales. In doing this the explicit time-dependence of the quantum subsystem dynamics is lost. The energy of the electronic subsystem evaluated with some polyelectronic wavefunction Ψ_0, as discussed previously, is a

function parametrically dependent on the nuclear position coordinates. However, this energy can also be considered to be a functional of the polyelectronic wavefunction, and therefore also a functional of the set of single-electron orbitals ψ_i, given by the Kohn-Sham equations, used to construct the polyelectronic wavefunction. In classical mechanics, the force on the nuclei is obtained as the derivative of a Lagrangian with respect to the nuclear positions. In a similar manner, a functional derivative with respect to the single electron orbitals, interpreted as classical fields, yields the force on the orbitals, given a suitable Lagrangian. Car-Parinello postulated a Lagrangian of the general form [56]:

$$L_{CP} = \sum_I \frac{1}{2} M_I \dot{\mathbf{R}}_\mathbf{I}^{\,2} + \sum_i \frac{1}{2} \mu_i \langle \dot{\psi}_i \mid \dot{\psi}_i \rangle - E[\psi_i, \mathbf{R}_\mathbf{I}, \alpha_n] + constraints \; . \qquad (3.15)$$

The first two terms represent the kinetic energy of the electrons and the kinetic energy of the nuclei respectively. The third term represents the potential energy of the system, given by the Kohn-Sham energy functional. The constraints are incorporated in the molecular dynamics Lagrangian using the method of Lagrange multipliers and ensure that the electronic wavefunctions remain orthonormal. μ is a fictitious mass associated with the electronic wavefunctions, $\mathbf{R_I}$ is the position of ion I, and α_n define the size and shape of the unit cell. From this Lagrangian the Car-Parinello equations of motion are then found to be of the form:

$$M_I bf \ddot{R}_I(t) = -\frac{\partial E}{\partial \mathbf{R_I}} + \frac{\partial}{\partial \mathbf{R_I}} constraints \qquad (3.16)$$

$$\mu_i \ddot{\psi}_i(t) = -\frac{\delta E}{\delta \psi_i^*} + \frac{\delta}{\delta \psi_i^*} constraints \; . \qquad (3.17)$$

As in all dynamics methods, an efficient means of calculating the forces acting on the nuclei is required. Numerical calculation of the derivative of the total energy of the system with respect to the position of the ion in terms of a finite difference approximation to the total electronic energy is too costly and inaccurate for dynamical simulations. On expanding the total derivative and calculating the gradients analytically, we observe that there are also contributions to the force from variations of the wavefunction. The force is only the partial derivative of the Kohn-Sham energy functional with respect to the position of the ion. If the wavefunction is an exact eigenfunction, or stationary state wavefunction, then the contributions due to variations of the wavefunction vanish. This is known as the Hellmann-Feynman theorem [57,58].

Car-Parrinello molecular dynamics represents a breakthrough in the way in which quantum-mechanical calculations are performed. In combines the advantages of both Ehrenfest and Born-Oppenheimer molecular dynamics. In Ehrenfest molecular dynamics [59], the time-step for integration is dictated by the dynamics of the electrons, which is much faster than the nuclear motion. The largest timestep possible is that which allows the integration of the electronic equations of motion. In Born-Oppenheimer molecular dynamics [60], no electron dynamics are involved, and so the time step for integration is given by the timescale of the nuclear motion. At each molecular dynamics step, the electronic structure problem must be solved self-consistently, a process avoided in Ehrenfest dynamics as the wavefunctions are allowed to propagate by applying the Hamiltonian to an initial wavefunction. For more details, the reader is referred to the references given [59-60]. Car-Parrinello molecular dynamics takes advantage of the smooth time-evolution of the electronic subsystem, and yet integrates the equations of motion over a long timestep determined by the nuclear motion. In the Car-Parinello equations of motion, the nuclei can be considered to evolve in time at a certain instantaneous physical temperature, whilst the electronic degrees of freedom are associated with a fictitious temperature. The electronic subsystem is close to its instantaneous minimum energy, or the exact Born-Oppenheimer surface. The ground-state wavefunction optimised for the initial configuration of the nuclei remains close to its ground state during time-evolution.

3.7 Problems and Errors Associated with *ab initio* DFT Simulation

In addition to the Born-Oppenheimer approximation, the LDA, and the pseudopotential approximation, there are obviously other intrinsic errors in DFT computer simulations. There are errors associated with using a finite plane-wave basis set, and the formulation of the wavefunction on a finite set of FFT grid points in k-space. In addition there are computational rounding errors, and errors occurring in the calculation of the forces using the Hellmann-Feynman theorem. Most of these errors can be considered to be negligible. The main problem with *ab initio* DFT simulation is that, as it is an iterative procedure, it is exceedingly numerically intensive, leading to very large cpu times for even small systems comprising of less than 100 ions. Computer simulations are therefore severely limited in the size of the system that can be considered. For the case

of simulation of crystalline solids, in which the system is a periodically repeating unit cell, this problem is avoided. For the simulation of liquids and other partially disordered systems, the use of a periodically repeating supercell is inaccurate and will lead to problems associated with finite size effects and artifacts due to periodic boundary conditions. For the case of the simulation of CS_2, the useful information is collected for only the first picosecond and on comparing the results for supercells containing different numbers of CS_2 molecules, it appears that the finite size effects are negligible.

Chapter 4

Reorientation Dynamics in a Prototypical Isotropic Liquid

4.1 Case Study of Carbon Disulphide

In this chapter the results and analysis of an investigation into the reorientation dynamics of a prototypical isotropic liquid are presented, along with a comparison to an *ab initio* DFT molecular dynamics simulation. Carbon Disulphide was chosen as the prototypical substance, as it is particularly suited to Raman lineshape analysis. A small rigid linear molecule, CS_2 belongs to a well-defined symmetry group and is also a strong Raman active chromophore. With a freezing point of $-111°C$ and a boiling point at $46°C$, the isotropic liquid phase of CS_2 is easily experimentally accessible. Due to the fact that the molecule is so small, the reorientational relaxation is very fast and therefore the reorientational contribution made to line broadening is considerable. The theory, including specific equations relevant to the case of a linear molecule, has already been discussed in chapter 2. It remains here to describe the details of the experimental set-up and the specific experimental parameters which need to be optimised. Indeed obtaining accurate correlation functions from Raman lineshapes is a difficult business. The mere observation of a Raman band does not suffice to produce accurate correlation functions. In the next section we discuss in general the way to obtain good correlation functions, before proceeding to the specific case for CS_2.

4.2 Obtaining Accurate Correlation Functions

Reorientation dynamics occurs over a timescale of picoseconds. The useful information to be obtained from analysing a Raman line is to be found in the extreme wings of the Raman band. Furthermore, as it is the lineshape that is of importance, the chosen Raman band must not only possess a good signal to noise ratio (S/N), but also be well isolated from all other Raman bands in the spectrum. Combination bands cannot be analysed accurately. Generally, the experimentalist analyses a Stokes-shifted Raman band, rather than its anti-Stokes equivalent, as the Boltzmann distribution over states predicts that the intensity of the Stokes-shifted band will always be greater than that of the anti-Stokes. The experimentalist can also improve the S/N ratio by choosing a high-frequency incident beam, as the Raman signal is proportional to the fourth power of the incident frequency. A Raman band is considered to be completely symmetric, and in order to avoid the problems of apparent line-broadening due to red-shifting of the band, only the high-frequency side of the band needs to be analysed before symmetrisation.

Having found a well-isolated, high intensity Raman band of the correct symmetry, it is necessary to define the spectral baseline (that is the functional form and magnitude of the noise), in order to accurately assess in the very far edges of the band, what is noise and what is the Raman signal. The technique developed by the author is as follows. The baseline is analysed over a spectral range of $300cm^{-1}$ on either side of the Raman band of interest. If found to be a slope, the baseline is immediately levelled. The Raman band of interest is then recorded over a large spectral range from the band centre, using several count times. The count time is the time over which scattered photons are counted by the spectrometer. The S/N ratio shows a square root dependence on the count time. By comparing the relative intensities at different frequency shifts from the centre of the band, for different count times, it is possible to determine whether the frequency shift is in the signal or the noise. Considering a hypothetical high frequency side of a Raman band and pinpointing three different frequency shifts, named A, B and C, let us now consider the relative intensities at A and B for different count times. If the relative intensities remain unchanged at different count times, then either A and B are both in the signal, or both in the noise. If the intensity relationship is found to be a function of the square root of the count time, then A is in the signal, whilst B is in the noise. Let us assume that it was found that the relative intensities of A and B were equal for different count times, but that the

relative intensities for B and C showed a square root dependence on the count time. This is indicative that both A and B are in the signal, whilst C is in the noise. It is apparent then that we need take spectral measurements only as far out as C, in order to be certain of analysing the whole Raman band. Obviously, if the substance fluoresces an accurate baseline correction is not possible. In this case, the experimentalist would have to resort to UV-Raman, and analyse an anti-Stokes band.

It is well-known that the lineshape of an experimentally obtained Raman band is not the actual lineshape of the band, rather a convolution of the band and the instrumental slit function of the spectrometer [61]. By virtue of the fact that the Fourier transform of a function f, which is a convolution of two functions g and h, is just the Fourier transform of g multiplied by the Fourier transform of h [62], it is easy to correct the measured wavefunction, if the slit-function is known. This is only necessary if the slit width is greater than ten times the full-width-half-height (FWHH) of the band. The author used a triangular slit function where appropriate [63].

In order to obtain good correlation functions it is imperative that the S/N ratio for all spectra (VV and VH) be at least 5 : 1, though in many cases it is observed to be greater than 10,000 : 1. The only way of increasing the S/N is to increase the count-time. In the case of CS_2 in particular it was found that the S/N ratio in the VH was very much smaller than in the VV spectrum. This is not problematic in the case of such a small molecule where the reorientational contribution to line broadening is so large compared to the vibrational contribution. In the case where the reorientational contribution is small, errors created due to large differences in the S/N ratios in the VH and VV spectra are much more significant, and a considerable difference in count-times for the VV and VH spectra is required. In such cases the VV and VH spectra are normalised relative to the respective count-times. In a similar manner the frequency step-size is also dependent not only on the absolute values of the FWHH for the spectra, but also on the difference between VV and VH FWHH, in order to achieve accurate separation of the vibrational and reorientational correlation functions.

The above procedures were carried out for all Raman (VV and VH) spectra recorded and presented here. Having determined the baseline, each spectrum was first lowered onto the x-axis (zero-intensity), before formulating the isotropic and anisiotropic components of the Raman data, normalisation and Fourier transformation to give the respective correlation functions (see chapter 2).

4.3 Experimental Procedure for CS_2

Raman spectra were taken of the CS_2 A_{1g} symmetric stretch at $655cm^{-1}$ with the incident and scattered radiation polarised parallel (VV) and perpendicular (VH) using polarisers with a dichroic ratio measured to be 10^3. The incident beam at $647.1nm$ was obtained from a Krypton ion laser with a power of $200mW$. A Coderg T800 triple-grating spectrometer was used in a 90° configuration. The slit size was set to $50\mu m$ allowing a spectral resolution better than $\frac{1}{3}cm^{-1}$. The data was collected in steps of $\frac{1}{8}cm^{-1}$ out to $45cm^{-1}$ from the centre of the band with a count time of $1sec$ for the VV and $20sec$ for the VH respectively. The baseline correction procedure described in the previous section was carried out on the VV and VH spectra and the high frequency side of the band was used to compute correlation functions. Not only does the use of the high frequency side of the band avoid complications arising from a bending mode overtone vibration on the redshifted side of the line, it also removes the artificial linebroadening arising from red-shifting as previously discussed. Correlation functions were obtained over a temperature range from $300K$ to $180K$. The CS_2 was sealed in a $1mm$ diameter capillary tube, which was cooled using a gas-pumped cryostat.

A series of figures is provided to show the fundamental steps in obtaining the correlation functions from the Raman spectra for a given sample of CS_2 at $300K$. The VV and VH spectra (Fig. 3a and 3b) are symmetrised and a baseline correction is performed, and the bands are then shifted onto the origin (Fig. 3c). The isotropic and anisotropic components are then computed and normalisation followed by Fourier transformation gives the reorientational, vibrational and total correlation functions (Fig. 3d).

4.4 Determination of Experimental Errors

The largest source of experimental error in obtaining the correlation functions comes from the accurate determination of the baseline correction. The baseline, which is the functional form and magnitude of the noise, is affected by fluorescence of the substance, weak spectral features, such as satellites and overtone bands, as well as signals from impurities present in the test substance. In the present work, the baseline was fitted to a fourth-order polynomial, the specific fit parameters being optimised using a least-squares regression fit program. The

baseline correction was performed over different spectral regions: the first baseline fit was performed using the background noise only over the first few wavenumbers on either side of the wings of the band. The most long-ranged baseline correction was performed by fitting to the background noise over a spectral region of 150 wavenumbers from the wings of the band. The difference in the correlation times is particularly obvious. To show this, the author gives a specific example: the CS_2 A_{1g} VH spectral band at $300K$ was used initially with a polynomial baseline correction performed by fitting to the background noise over $10cm^{-1}$ in the immediate vicinity of the bands. The resulting reorientational correlation function gives an integrated correlation time of $1.5ps$ [64]. This was an early initial prublication by the author. In the work here, the baseline correction has been performed over $300cm^{-1}$, from $505cm^{-1}$ to $805cm^{-1}$. The calculated reorientational correlation time obtained is then $0.78ps$. Extending the fit for the baseline correction to an even broader spectral region produced no further change in the correlation functions, or correlation times. This example provides a good means of estimating the experimental error in the correlation time. At best, the author concludes that the reorientational correlation time for CS_2 at $300K$ is $1.2ps \pm 0.3ps$.

The estimation of the magnitude of error in the correlation functions themselves is more complicated. The magnitude of error in the correlation functions at fast time-scales (*i.e.* the first $0.4ps$) is small. This is because the information about the fast relaxation is contained in the far wings of the band, in very close proximity to the background noise used to perform the fit for the baseline correction. The uncertainty in the baseline correction is more predominant towards the centre of the Raman band. Furthermore, the correlation functions depend on the *lineshape* of the Raman band and, in particular, on the gradient of the lineshape. When the gradient of the Raman lineshape is steep, small changes in the baseline correction produce large changes in the gradient of the respective correlation function. It is seen that the gradient of the Raman lineshape is steepest towards the middle of the band and shallow in the far wings of the band. On comparing correlation functions obtained using baseline corrections performed over different spectral regions about the band, it was seen that the correlation functions were identical over short time-scales, but showed variations at longer time-scales (greater than $0.5ps$). The magnitude of error increases on going to longer time-scales and can be weighted with respect to the gradient of the Raman lineshape and the freqeuncy difference between the spectral data in the signal and the background noise.

For the purposes of the present work, the author has chosen to publish correlation functions obtained when using a baseline correction fitted over the largest spectral region, $150cm^{-1}$ on both sides from the centre of the Raman band.These correlation functions show the fastest decay and do not change when going to baseline corrections fitted over larger spectral regions. The correlation functions at different temperatures are comparable, because the baseline correction was fitted over the same spectral region in each case. The error bars indicate to what extent the decay of the correlation functions decreases when performing the baseline correction fit over a shorter spectral region. In the case where more than one correlation function is depicted on the same graph, only one set of error bars are shown, as the spectral region for baseline polynomial fit used when comparing correlation functions, and therefore the error estimation, is always the same.

4.5 Results and Analysis

Fig. 4 shows experimentally obtained correlation functions of CS_2 over a temperature range from $180K$ to $300K$. A monotonic temperature dependence at all time-scales is observed. The reorientational motion, and hence relaxation rate, decreases with the lowering of the temperature. However this relationship is not linear. This can best be seen by integrating the correlation functions, to obtain the correlation time τ. Fig. 5 shows the correlation time as a function of temperature. It can be seen that on cooling to below $240K$, the correlation time starts to rise rapidly. Assuming that the motion is that of small step rotation diffusion, the simplest available model (but obviously from the non-exponential correlation functions invalid), the correlation time τ is related to the rotation diffusion constant $D_\perp$ as $\tau = \frac{1}{6D_\perp}$. So a dramatic increase in correlation time at temperatures lower than $240K$ suggests a significant reduction in reorientational freedom of the constituent molecules due to intermolecular interactions and collisions which hinder the reorientational relaxation of the system. The author points out that the correlation time of CS_2 at $300K$ as measured here is $0.78ps$. This is much faster than previously reported values, including an initial publication by the author, which have reported the correlation time to be as slow as $1.5ps$ [65,4]. The author believes that this arises from the fact that previous authors have assumed the Raman band to be a Lorenzian (liberating an exponentially decaying correlation function) and calculated the correlation times from the FWHH, rather than obtaining the realistic correlation function and performing the integration. In

view of the previous section, discussing the sources of error in the experimental correlation functions, it is more reasonable to conclude that the correlation time of CS_2 at $300K$ is $1.2ps \pm 0.3ps$.

The experimentally obtained correlation functions do not decay exponentially, but can be best fitted to the M-diffusion model. Fig. 6 shows the variation in collision frequency as a function of temperature. Once again a non-linear relationship is observed and the collision frequency rises dramatically at temperatures lower than $240K$. As discussed in Chapter 2, the term collision frequency is somewhat ambiguous, as it refers to deflections in angular momentum of the constituent particles which could arise from long or short range intermolecular interactions, as well as physical collisions between molecules. It can easily be envisaged that as the temperature of the system is reduced, the kinetic energy of the molecules decreases, causing the density of the system to increase. On a molecular scale, the constituent particles feel the presence of their immediate environment; that is to say that the extent of intermolecular interaction between neighbouring molecules increases as the temperature decreases, eventually leading to local ordering. There is a cross-over point, when intermolecular interactions are strong enough to overcome the thermal motion of the molecules, which heralds the onset of local structuring in the liquid state. It appears from the data analysed so far that this occurs at about $240K$.

The collision frequency provides us with an abstract, yet quantitative measure of the rate at which deflections in the angular momentum occur, however, it does not indicate the strength of the intermolecular interactions which cause changes in the directionality of the angular momentum vector. To this end a moments analysis was performed on the experimental correlation functions in order to measure the rms torque. Due to the high resolution and good S/N, it is possible to calculate very accurate values of the rms torque as a function of temperature. To the best knowledge of the author, such a thorough investigation into the strength of intermolecular interactions as a function of temperature has never been published before. An example of the fit-functions obtained is shown in Fig. 7 for CS_2 at $240K$. The correlation function coincides with the free-rotor for the first $0.1ps$ before deviating. This is proof that the baseline correction and choice of spectral frequency range are correct. If the spectral frequency range was too short, the correlation function would lie above the free-rotor at all times. The second and fourth moment in the Taylor expansion provides an excellent fit over the first

$0.25ps$, when the correlation function has deviated substantially from the free-rotor model. As previously discussed, the frequency moments expansion is only valid at very short time scales and eventually curves up (due to the t^4 dependence of the fourth moment). Fig. 8 shows the calculated rms torque over the applicable temperature range. A dramatic increase in the rms torque is observed as the temperature is lowered below $250K$, and by $220K$ no moments analysis is possible as even in the first $0.1ps$ the experimental correlation function lies well above the free-rotor. This is best seen by comparing Fig. 7 (at $240K$) and Fig. 9 (at $180K$). This dramatic increase in rms torque cannot be explained solely by the change in density. It would be expected that a radial force would be highly dependent on the density of the system, yet the torque is a tangential force. Such behaviour is indicative of the fact that there is substantial local molecular structuring at temperatures lower than $220K$, and the onset of this structuring begins when cooling to temperatures below $240K$. Several experiments could be performed to confirm that structuring does occur including quadrupolar splitting in ^{13}C NMR and measurements of the specific heat as a function of temperature. At temperatures greater than $260K$ the constituent CS_2 molecules are considerably more rotationally mobile. This has already been confirmed by the fast relaxation times. The rms torque is surprisingly invariant over the higher temperature range, only decreasing from $1.33 \times 10^{-20}J$ at $260K$ to $1.20 \times 10^{-20}J$ at $300K$.

All the experimentally determined results are averages over time and molecular orientation. To increase our understanding of the nature of the intermolecular interactions in liquid CS_2 it is necessary to analyse the temporal motion and forces on a single molecule. Such information cannot be obtained experimentally and we resort to computer simulation techniques. To continue our study of CS_2 we now progress to an *ab initio* computer simulation, which was done in collaboration with Dr. Stewart Clark.

4.6 *Ab Initio* DFT Computer Simulation of CS_2

The theory of DFT computer simulation has been discussed in Chapter 3. It remains here to define the specific parameters used. *Ab initio* molecular dynamics calculations were performed within the generalised gradient approximation for the exchange and correlation interaction to periodic supercells containing 32 CS_2 molecules. Non-local pseudopotentials generated by the Q_c tuning method of Lin *et al.* [66] in Kleinman-Bylander form [67] are used for the electron-ion

interactions. As discussed previously the valence electron wavefunctions are expanded in a plane wave basis set. The kinetic energy cut-off used for the basis set was set at $700eV$, which converges the total energy of the system to better than $0.001eV/atom/mol$. The molecules were placed in a random starting configuration and allowed to come to thermal equilibrium before collecting the data. The electronic structure calculation proceeds *via* a pre-conditioned conjugate gradients energy minimisation algorithm using the plane wave coefficients as variational parameters. The Hellmann-Feynman theorem was used to calculate the forces on the individual atoms. The simulation was run at $300K$ and the system was given the kinetic energy appropriate to this temperature. The classical equations of motion were then integrated with a time-step of $1.0fs$ which is faster than the time-scales of stretching and bending mode vibrations. The timestep was also small enough that the integration procedure conserves the total energy of the system without the need for a thermostat.

In the molecular dynamics simulation, the coordinates of the molecules are known as a function of time. Therefore, the Raman rotational correlation function (i.e. that in the second spherical harmonics index) can be extracted directly from

$$C_{rot}(t) = \langle P_2[\mathbf{r}(0) \cdot \mathbf{r}(t)] \rangle \tag{4.1}$$

where $\mathbf{r}$ is the intramolecular vector linking C and S atoms, the triangular brackets indicate that the ensemble average is taken, and P_2 is the second Legendre polynomial. The experimental and theoretical results displayed in Fig. 10 show excellent agreement. Whilst many attempts have been made in the past to calculate theoretical vibrational correlation functions and interaction-induced dipole correlation functions using classical MD and *ab initio* simulation techniques [68,69,70,71,72], this is the first time that a calculation of the reorientational correlation function has ever been performed using *ab initio* DFT Car-Parrinello molecular dynamics simulation. Performing a Fourier transform on the ionic velocity autocorrelation function, we acquire the vibrational density of states. Despite the fact that the resolution is poor, as the simulation was only performed over half a picosecond, the A_{1g} totally symmetric stretch at $655cm^{-1}$, from which the experimental correlation functions were obtained, is already clearly visible (see Fig. 11).

Of course at each timestep, that is every $1.0fs$, the simulation generates not only the ionic coordinates, but also the forces acting on each ion. It is therefore possible to calculate the torque as a function of time directly for any given molecule of CS_2 in the simulation by calculating the change in the angular momentum as

a function of time. Fig. 12 shows the variation in root mean square torque experienced by a single molecule of CS_2 as a function of time at $300K$. The time-averaged torque given by this method is in excellent agreement with the indirect experimental method.

The magnitude of the torque varies dramatically. Performing a Fourier transform of Fig. 12, there appears to be two timescales of variation of the torque. The slower, on a timescale of $100fs$ produces the largest change in the magnitude of the torque. The smaller change in the magnitude of the torque variess much more rapidly, on a timescale of $10fs$. The author believes that the slow variation is due to the bending mode vibration of the CS_2 molecule which destroys the linear symmetry and results in the creation of a large dipole moment, whilst the fast variation is due to the high frequency anti-symmetric stretch, which also induces a net dipole moment in the molecule. Obviously any neighbouring molecule feels the effect of these transient dipole moments, which in turn cause a redistribution of the electronic cloud of the neighbouring molecules, whilst also inducing angular momentum. The net result is collective librational motion of the constituent molecules in the liquid, which has been experimentally observed by coherent time-resolved pump-probe experiments and found to have a very fast relaxation time [73]. This is the first time that this so-called dipole-induced-dipole (DID) effect has been explicitly observed in dynamics computer simulation. The author considers that these dipolar effects obscure the very much weaker effects of the quadrupolar moment. Despite the presence of DIDs, the computer simulation confirms that at $300K$ there is very little if any local structuring. This can best be seen from the partial and molecular radial distribution functions shown in Fig. 13. None of the radial distribution functions (dotted: C-S, dashed: S-S, full line: CS_2) show any structuring over large intermolecular distances. The S-S distribution function displays a depletion zone, followed by a rise maximising at 3.5 Ås indicating that it is possible for neighbouring CS_2 molecules to come into close proximity in the order of 0.5Å, however the thermal motion of the molecules at $300K$ prevents the formation of local structuring and the system is highly disordered.

Fig. 3a CS_2 Raman Spectrum; VV at 300K

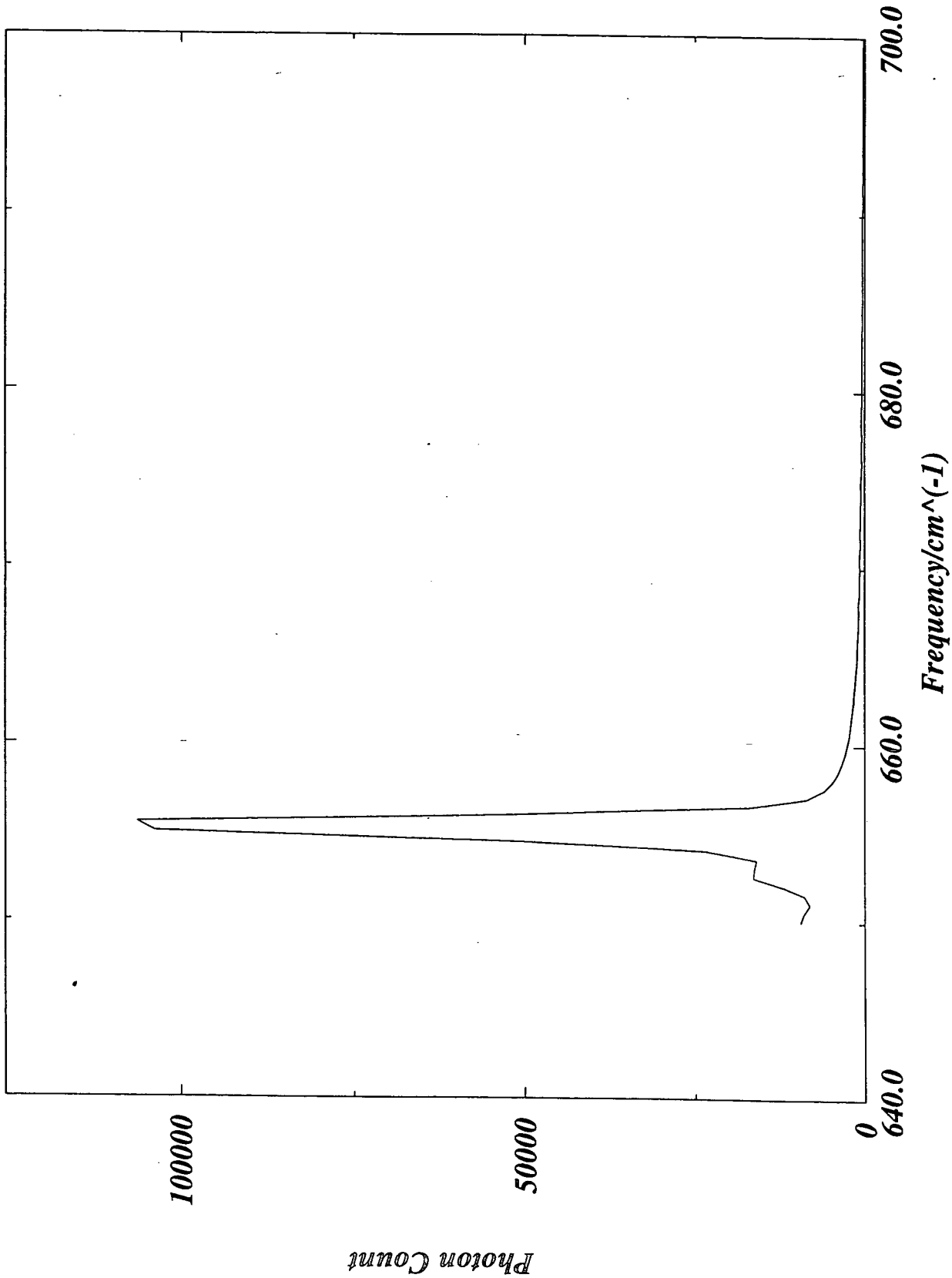

Fig. 3b CS_2 Raman Spectrum; VH at 300K

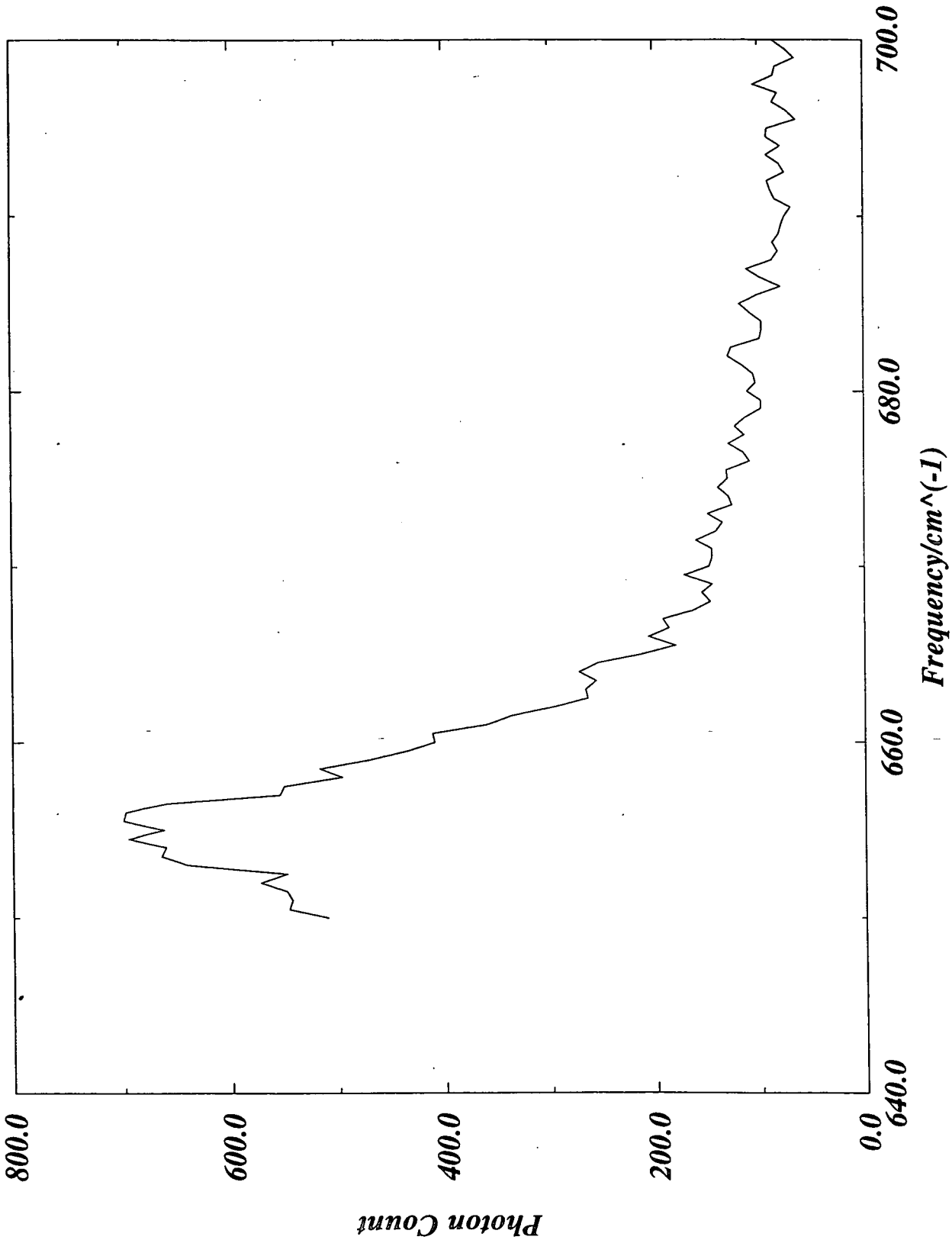

Fig. 3c CS_2 Raman Spectra; VV and VH after Symmetrisation and Baseline Correction

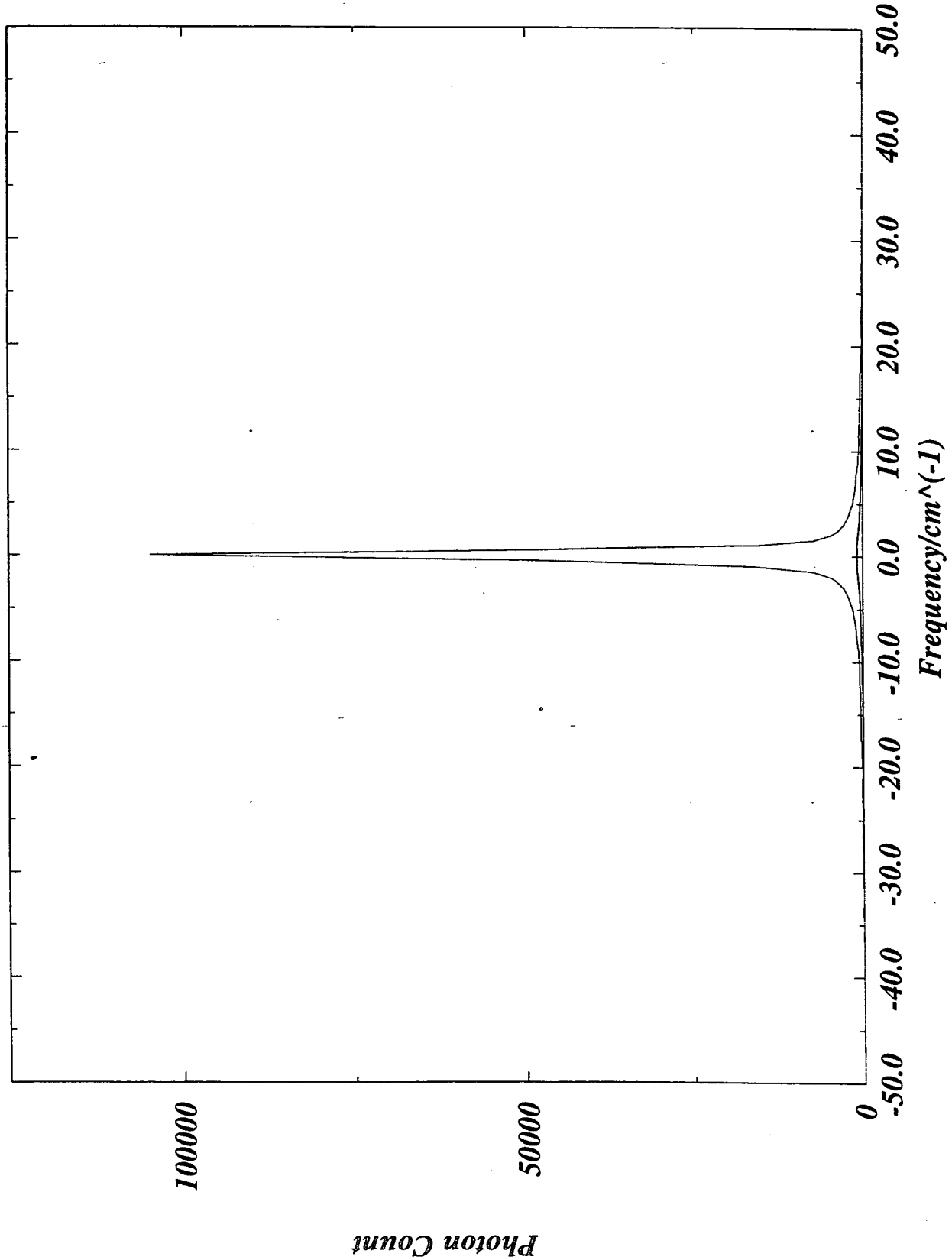

Fig. 3d Correlation Functions of CS_2 at 300K

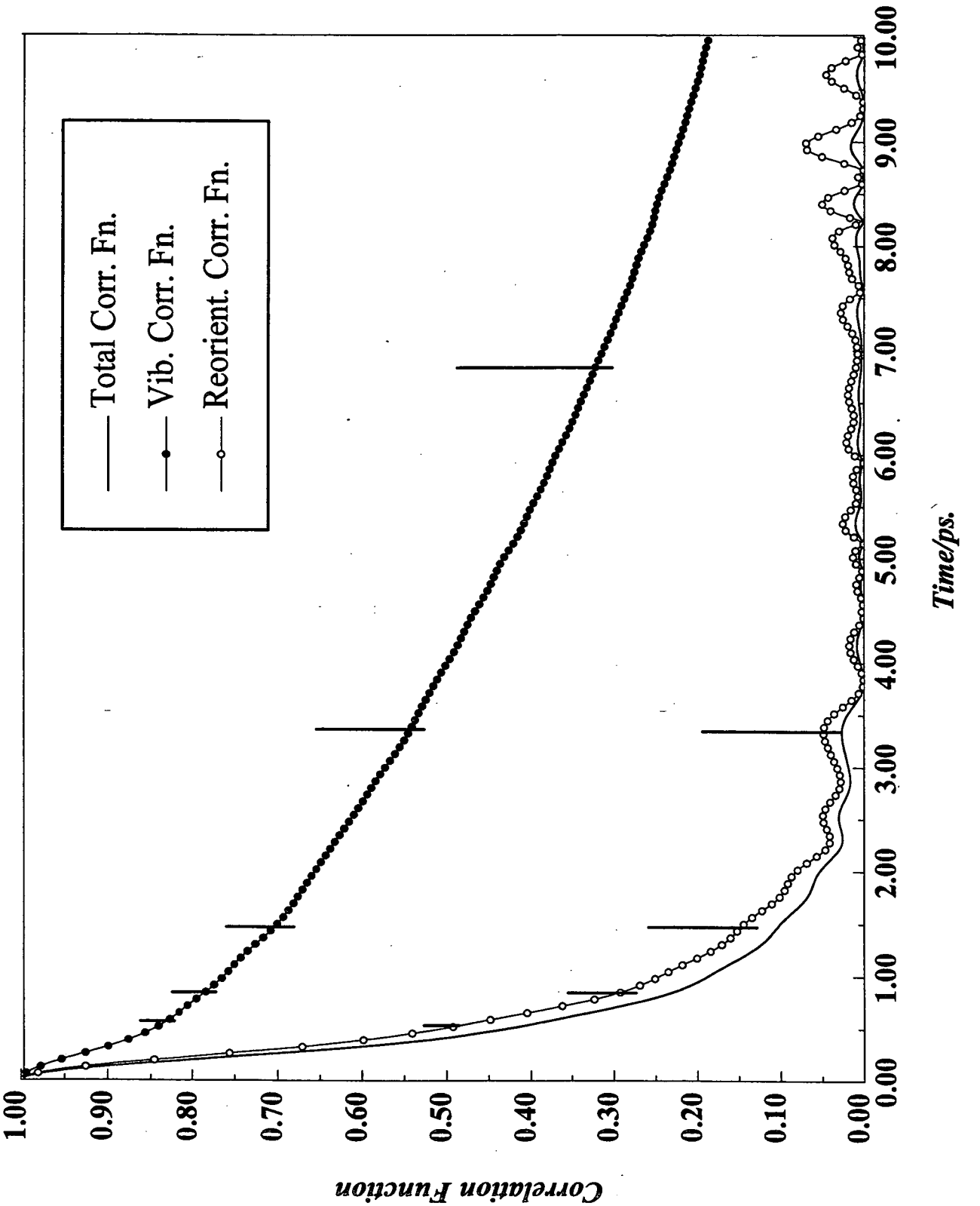

Fig. 4 Rotational Correlation Functions of CS_2 at Various Temperatures

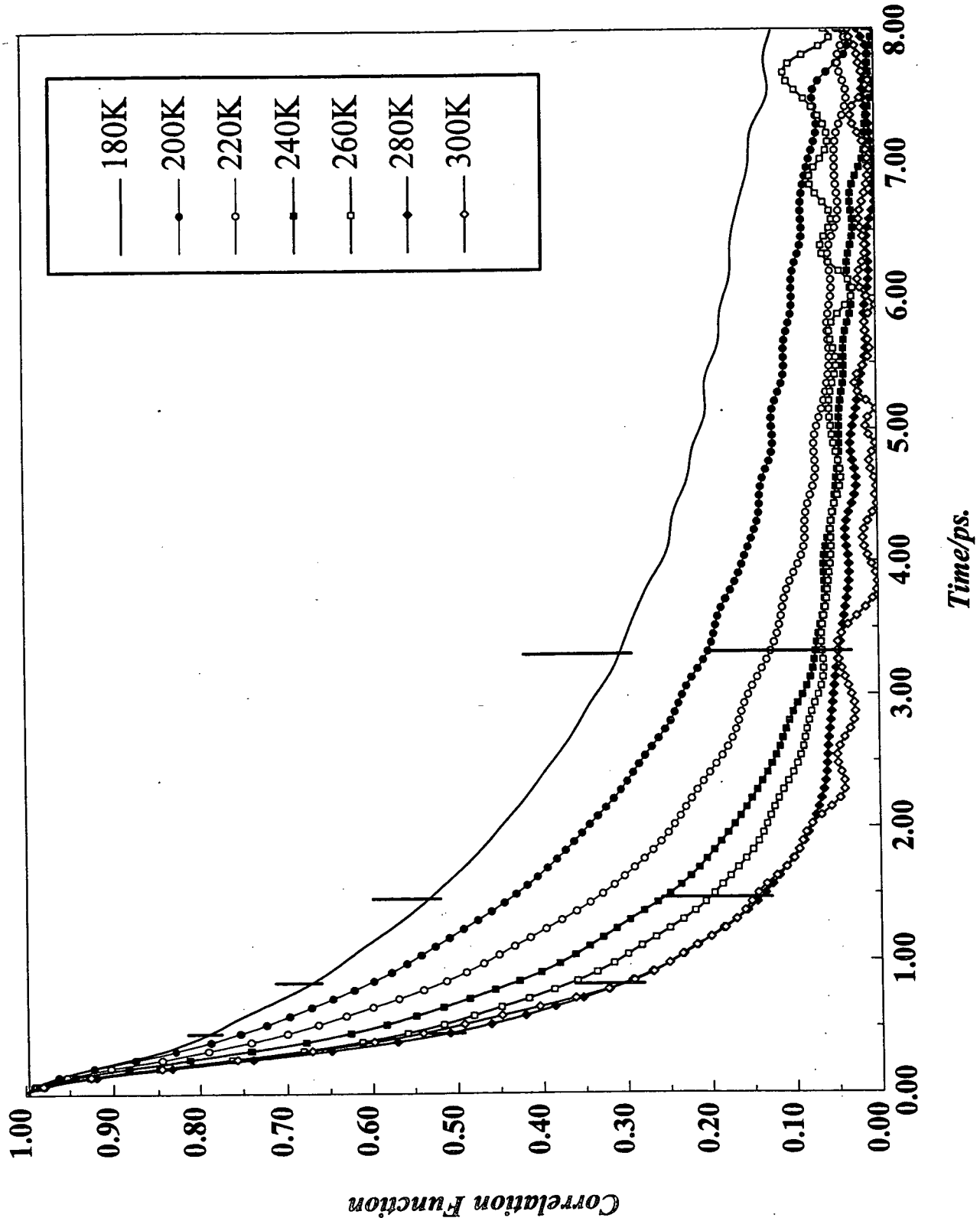

Fig. 5 CS_2 Correlation Times as a Function of Temperature

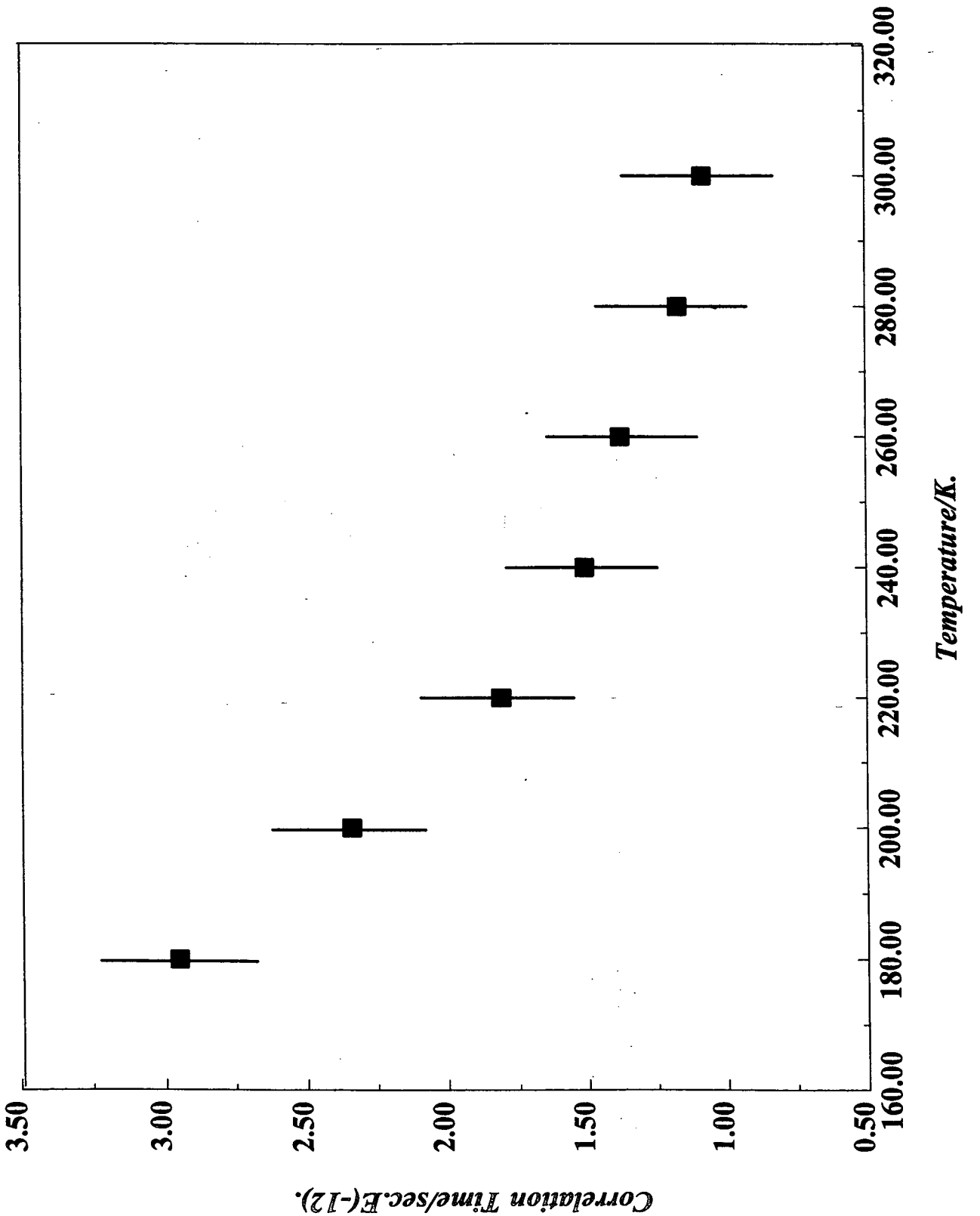

Fig. 6 Temperature Dependence of Collision Frequency in CS_2

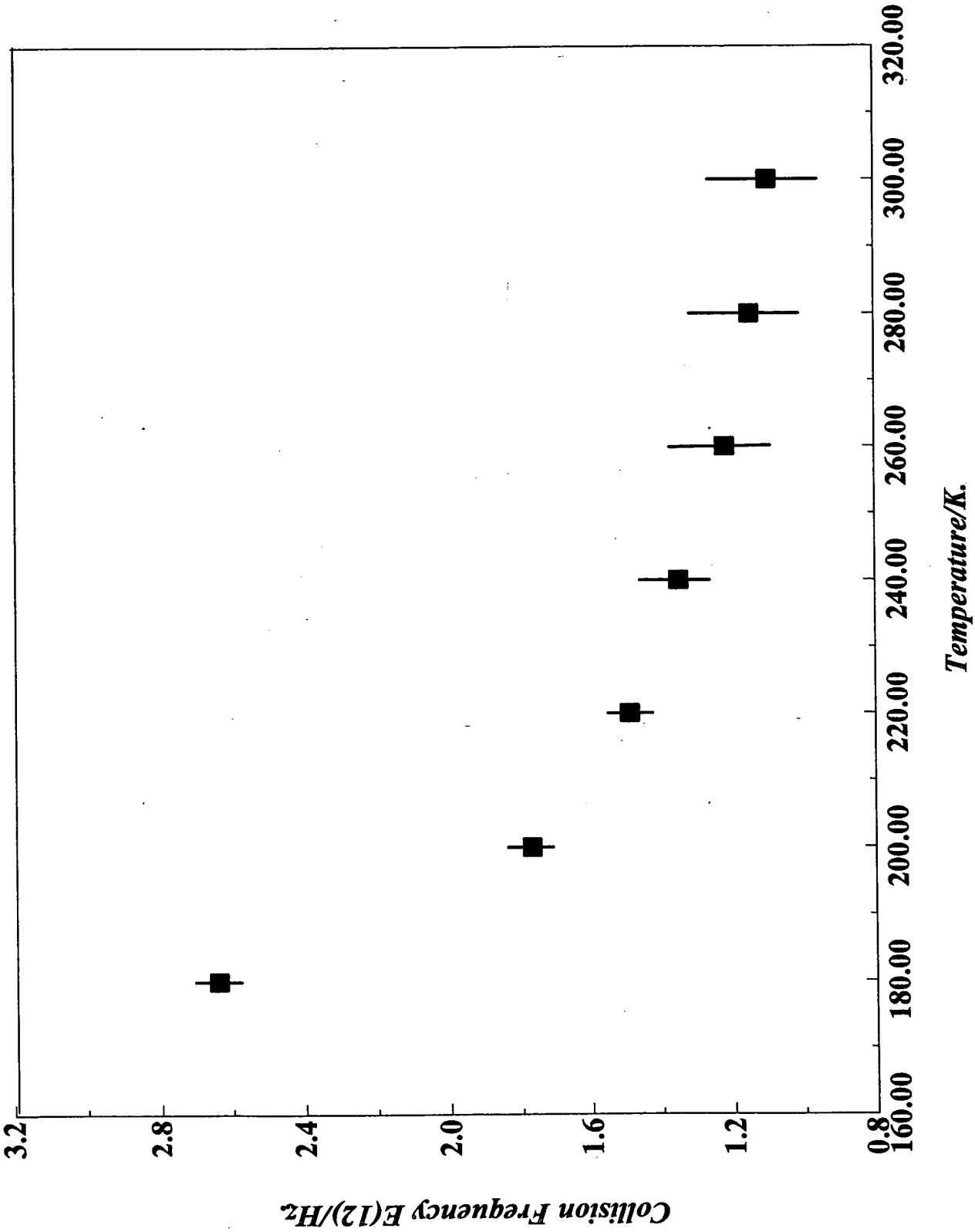

Fig. 7 Moments Analysis at 240K
RMS Torque = 1.994 E(-20) J.

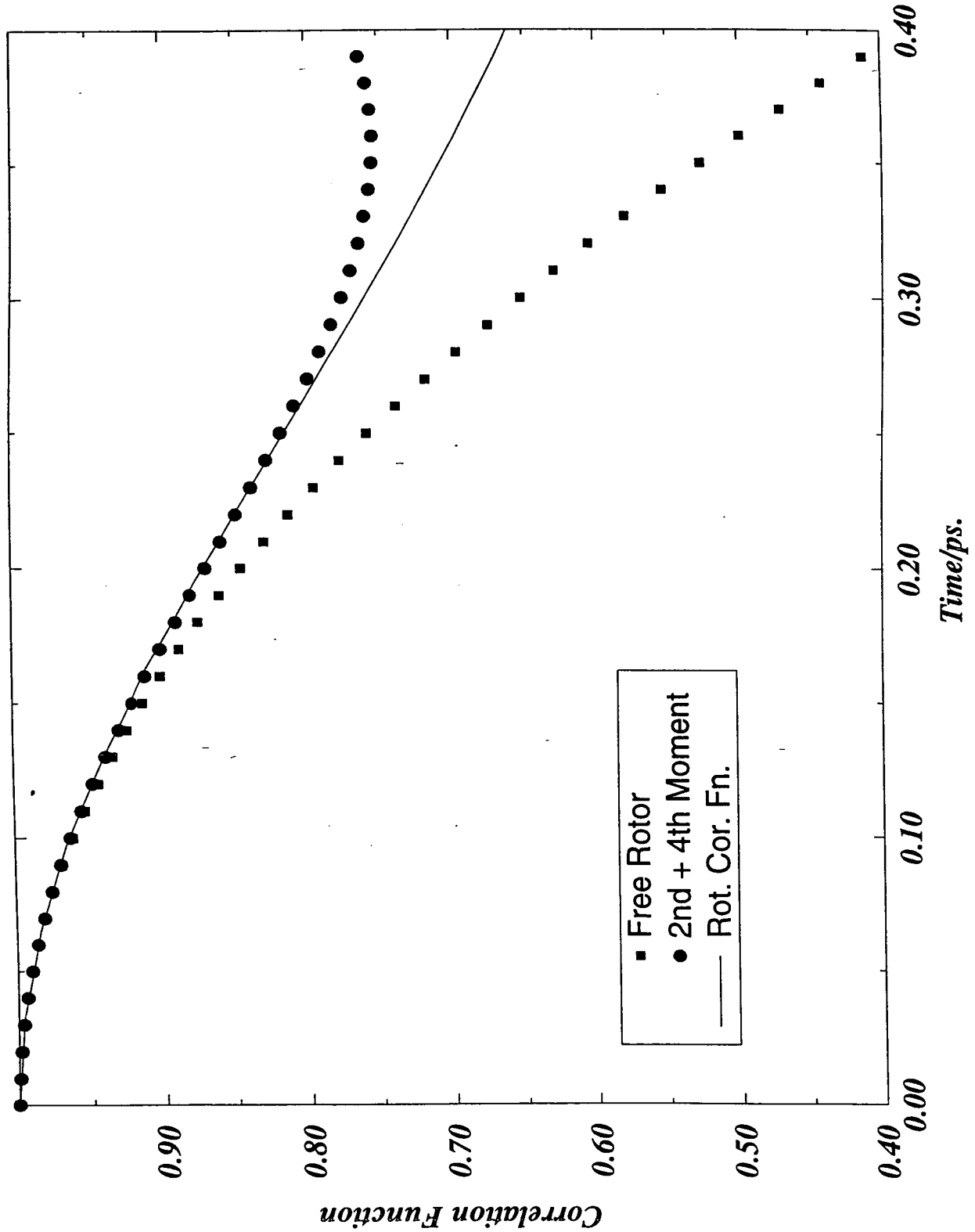

Fig. 8 RMS Torque vs. Temperature for CS_2

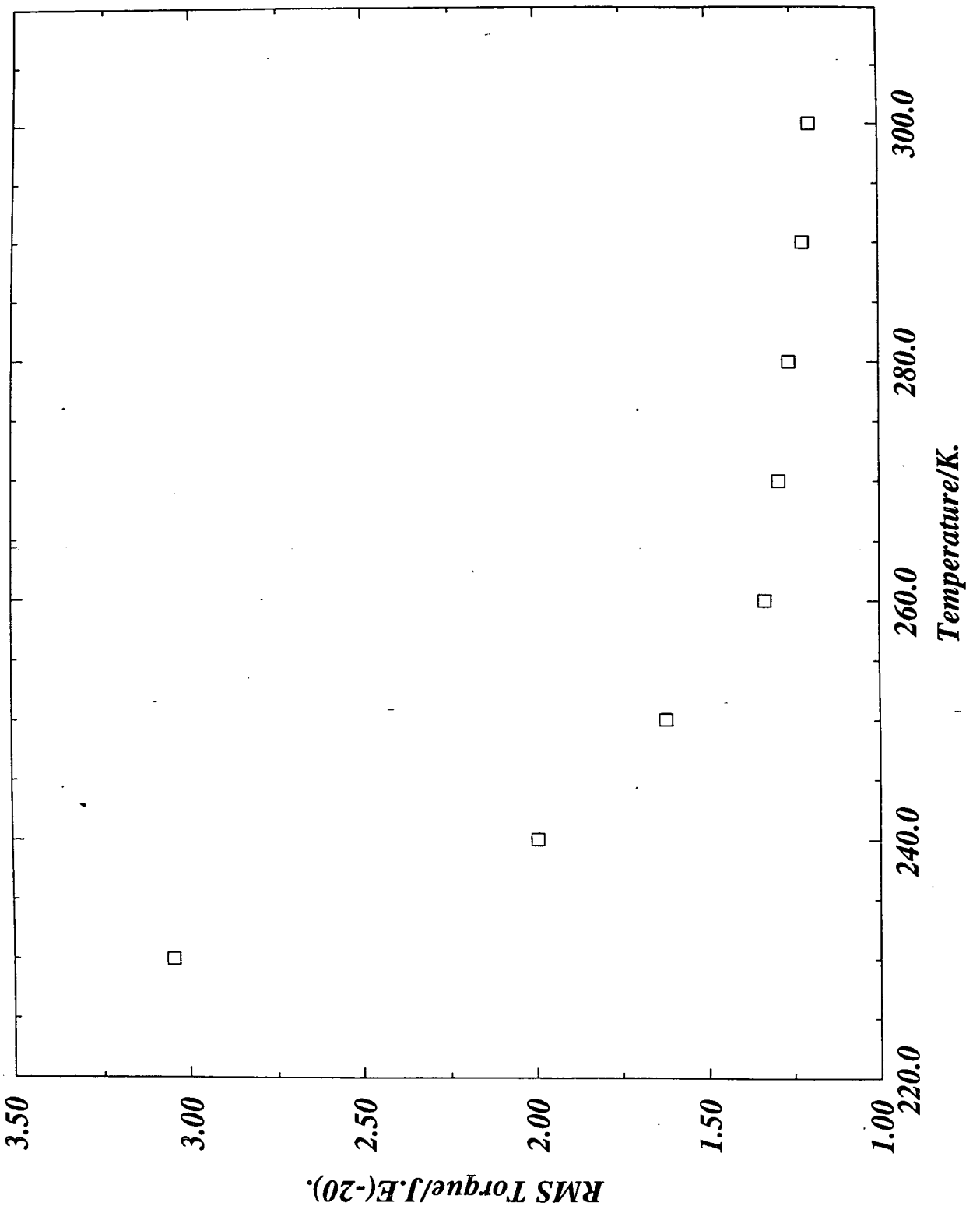

Fig. 9 Moments Analysis at 180K

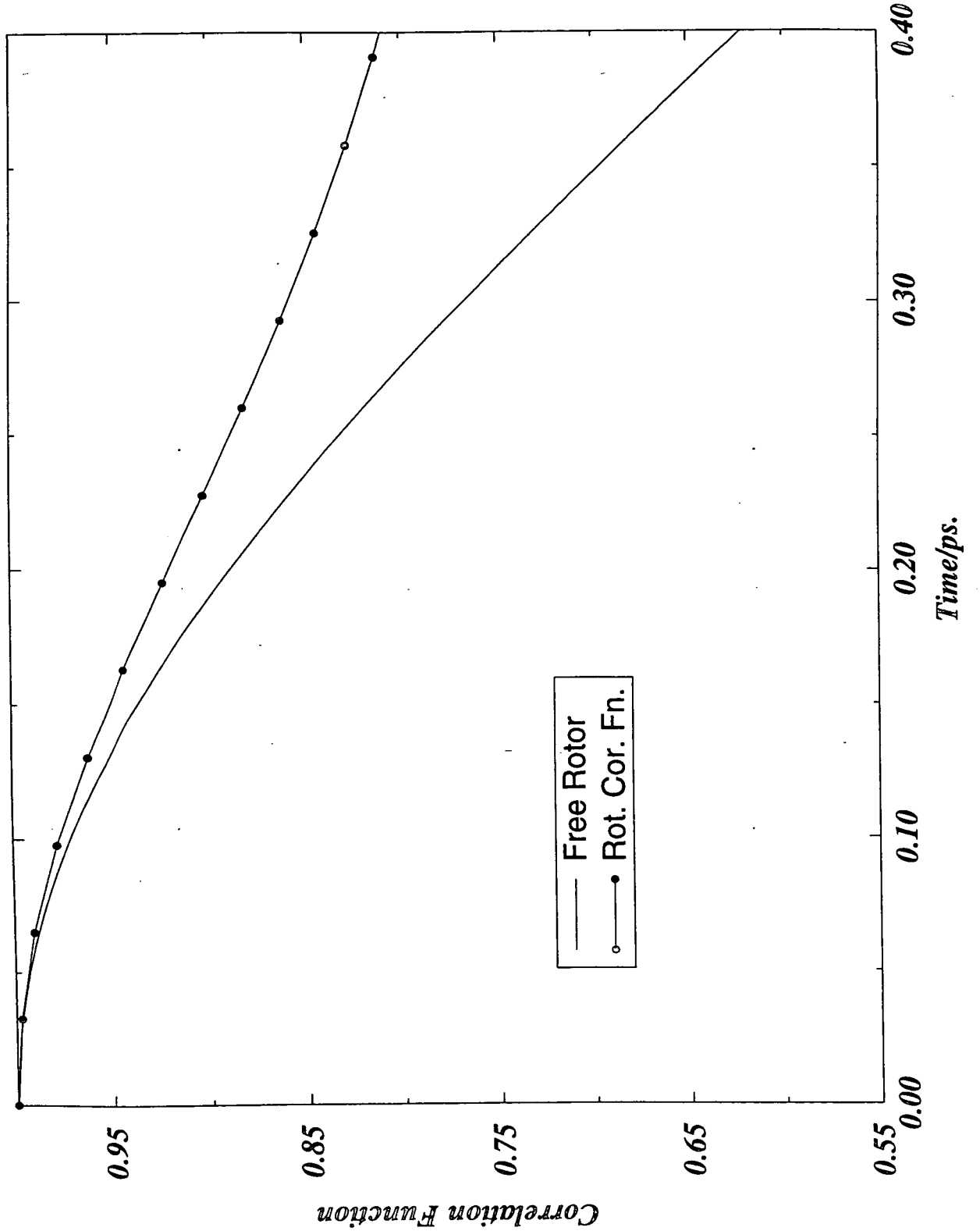

Fig. 10 CS_2 Correlation Function: Theory and Experiment

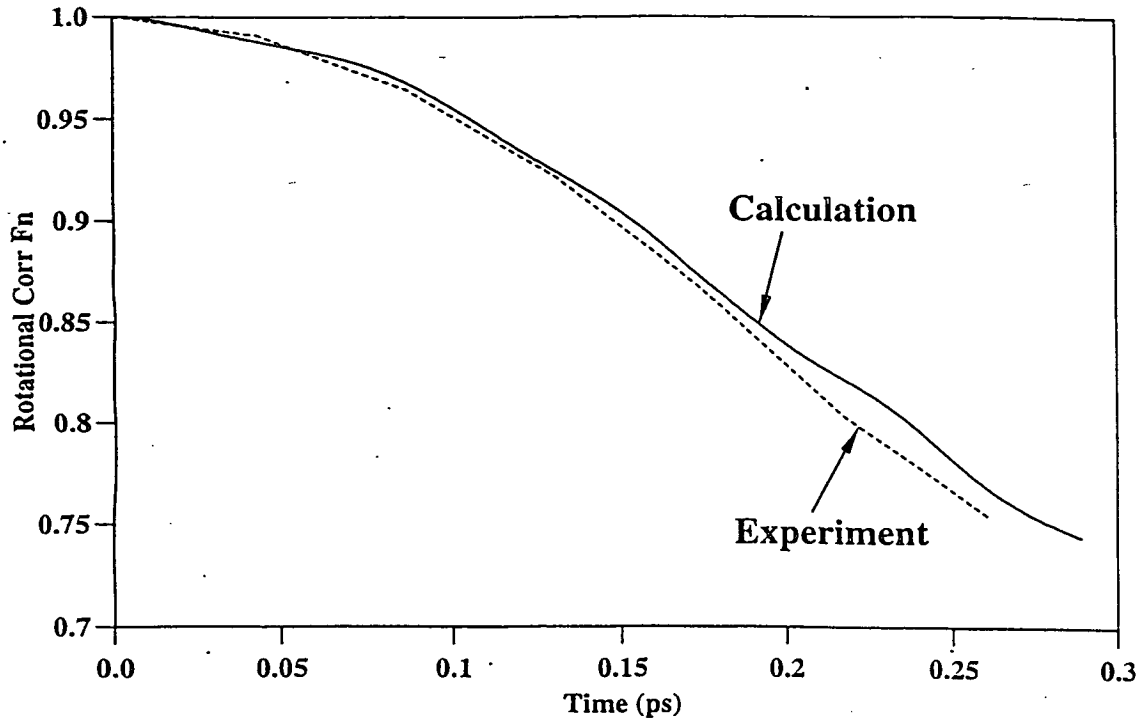

Fig. 11 CS_2 Vibrational Density of States

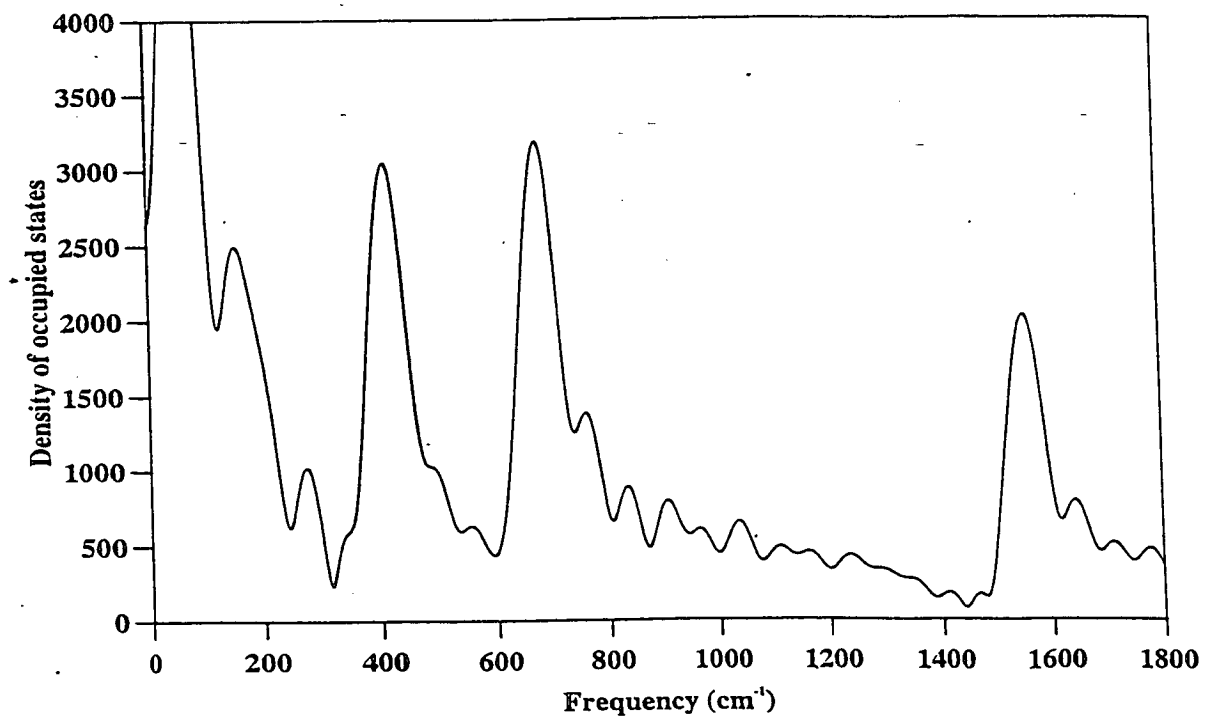

Fig. 12 CS_2 Intermolecular Torque at 300K

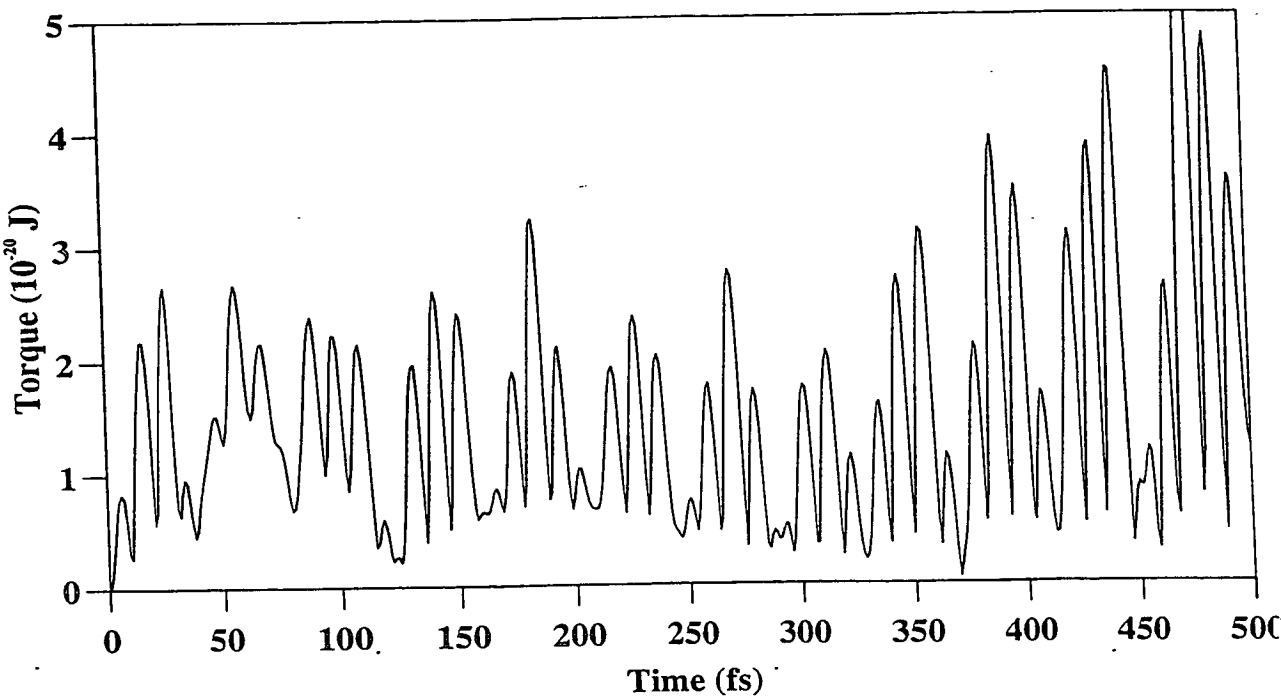

Fig. 13 CS_2 Radial Distribution Functions

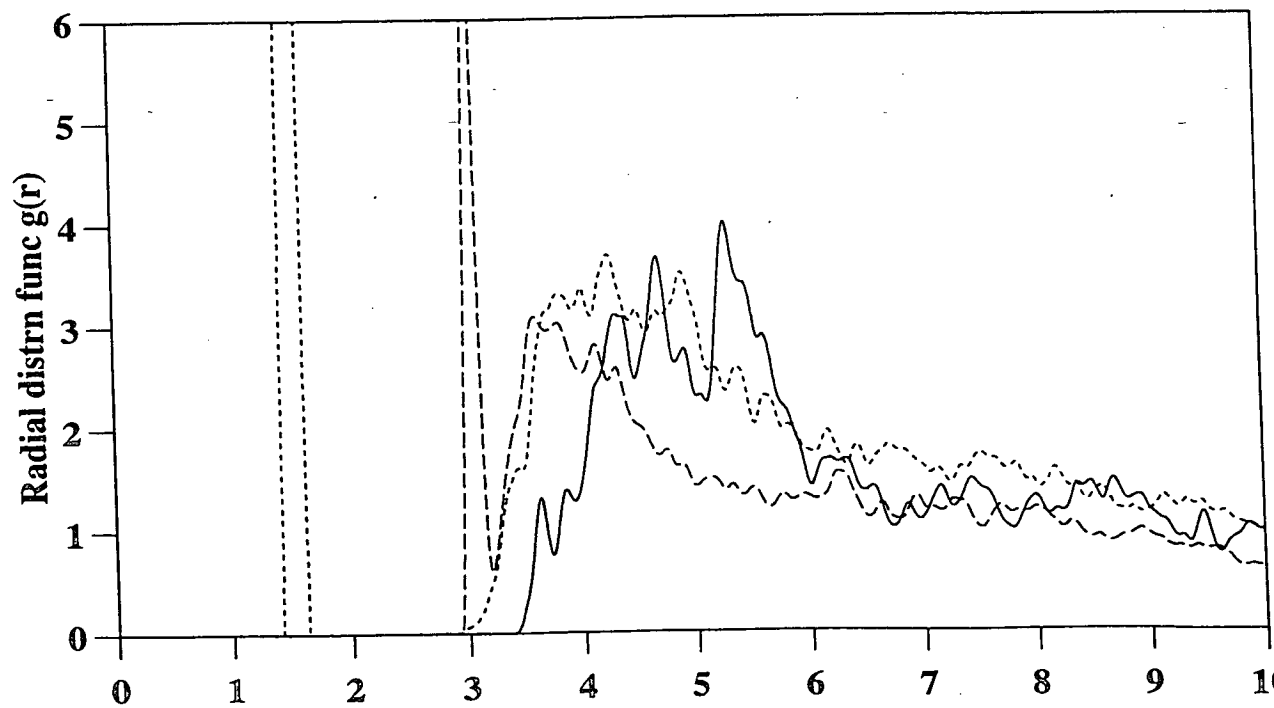

Chapter 5

Solvation Dynamics: CS_2 in Cyclohexane

5.1 Introduction

In the previous chapter, results were presented for the prototypical liquid system, CS_2. As discussed CS_2 lends itself well to Raman lineshape analysis, due to its size, rigidity and high degree of molecular symmetry. Unfortunately this is not true for all systems of interest. Larger molecular systems in general provide two intrinsic problems. Although the molecule might be a strong Raman chromophore, the suitable vibrational band is often not isolated well enough from the rest of the spectrum to perform accurate lineshape analysis techniques. Secondly, larger molecular systems are more flexible with more than one possible geometric conformation. The molecular flexibility results in a coupling of the different modes of reorientation, in particular, spinning and tumbling, which makes the calculation of quantitative parameters, such as the intermolecular torque, impossible.

One means of probing the dynamics of more complex molecular systems is to use a dopant. In this chapter results are provided for the reorientational dynamics of CS_2 molecules dissolved in cyclohexane, C_6H_{12}, which undergoes a temperature-induced liquid to plastic crystal transition. The correlation functions are compared to those of CS_2 dissolved in n-propanol (which vitrifies at low temperatures). Whilst the correlation functions for CS_2 as a dopant cannot be compared quantitatively to those in the previous chapter, due to differences in

the density of the system, it is the aim of this chapter to show how the functional form of the correlation functions provides qualitatively an insight into the interactions and dynamics of the host system.

5.1.1 The Physical Properties of Cyclohexane

The molecular properties and phase diagram of cyclohexane are well established [74,75]. The cyclohexane molecule can exist in two possible molecular conformations, the chair and boat conformations, of which the chair conformation is the most energetically stable. As such, the molecule exhibits D_{3h} point group symmetry and is nearly spherical. The pure material at atmospheric pressure forms a plastic phase upon cooling at $279.8K$ and undergoes a second-order solid-solid transition at $186.1K$. The plastic crystal phase is face-centred-cubic with $a = 8.76\mathring{A}$, which, asssuming close packing and spherical molecular units, gives an effective molecular diameter of $6.2\mathring{A}$.

Due to the fact that cyclohexane exhibits an easily accessible liquid to plastic crystalline phase transition, there have already been several studies into the reorientation dynamics of the pure system. In a very early study by Bartoli and Litovitz [4], the symmetric stretch Raman band was fitted to a Lorenzian and the FWHH for the VV and VH spectra were calculated. This technique assumes that the correlation functions at all time scales are exponentials with a single time exponent and, like previous NMR studies [76], only give the integrated relaxation time. A more recent Raman study by Bansal and Roy [77] suggested that there was a monotonic slowing of the reorientational motion across the liquid-plastic crystal transition, exhibiting no anomalous behaviour due to the onset of long-range positional order. However, it is impossible to draw unambiguous conclusions concerning the reorientational dynamics from this study because of the irregular shape and conformational freedom of the cyclohexane molecule which prevents the determination of the pure tumbling motion of the C_3 axis.

5.2 Experimental Procedure

The specific Raman experimental apparatus has already been described in the previous chapter. Pure liquid samples of C_6H_{12} (> 99%) and CS_2 (> 99.8%) were obtained from Fison and BDH respectively and used without further purification.

Solutions of 2 – 20% wt. CS_2 in cyclohexane were prepared and sealed in $1mm$ diameter capillary tubes. Polarised Raman scattering spectra were collected in the 90° scattering geometry over the temperature range of $300K$ to $185K$. The $514.5nm$ line of an Argon ion laser was used as the excitation source with an estimated power at the sample of $250mW$. Spectra were taken of the high energy side of the $655cm^{-1} A_{1g}$ CS_2 symmetric stretch band out to $40cm^{-1}$ from the centre of the band with a step frequency of $\frac{1}{8}cm^{-1}$ and a slit size set to $100\mu m$ which provides a spectral resolution better than $0.9cm^{-1}$.

5.3 Results and Analysis

Figures 14a and 14b show the CS_2 reorientational correlation functions over the studied temperature range in the 20% solution. Differential Scanning Calorimetry experiments of this system concluded that the liquid-plastic crystal transition occurs at $230K$ and the solid-solid transition occurs at $180K$. It is at this stage not clear if this latter transition corresponds to the plastic to monoclinic crystal transition, as observed in pure cyclohexane, or to some as yet unidentified phase transition. It is however clear that the temperature range studied here allows us to observe the reorientation dynamics across the liquid-plastic crystal transition. As the temperature is lowered in the liquid phase, the reorientational motion (not unexpectedly) slows down over the whole range of times probed in our experiments. At and just below the liquid to plastic crystalline transition, T_p, however, we see that the reorientational motion in the short time limit speeds up relative to the liquid at temperatures just above the phase transition. At temperatures well below the phase transition, continued cooling results in a slowing down of the short-time reorientational motion. At short time scales, the system exhibits an anomalous non-monotonic temperature dependence. At longer timescales (t)$0.5ps$) the decay of the reorientational correlation function exhibits a near monotonic slowing down with decreasing temperature through the phase transition. The same trend was observed in the 2% solution, however, due to very weak scattering from the CS_2 the effect is not as clearly observable as in the 20% solution.

In order to explain the long and short time-scale dynamics of this system it is necessary to formulate a suitable model. Widom [78] has discussed a model of the liquid state in which he argues that at that critical point the attractive forces between molecules produce correlations that can propagate beyond the range

of the forces themselves and these are more significant than the short-ranged repulsive forces. However, as a liquid approaches its triple point, the correlations due to the short-ranged forces become more significant, which can be understood when one considers that the density of a liquid at its triple point is approximately three times greater than at its critical point. Widom then further argues that as the attractive forces between molecules are relatively weak and long ranged compared to the very steep repulsive forces, it follows that in a fluid as dense as a liquid at its triple point the attractive forces exerted on any molecule by its neighbours largely cancel, while the negative potentials largely add, so that each molecule in such a liquid may be thought of as a hard sphere in a deep but uniform negative background potential. The freezing transition of hard spheres is driven entirely by entropy: the densest random packing of hard spheres in $3D$ occurs at a volume fraction of $\phi \sim 0.64$ [79], while the densest crystalline packing occurs at $\phi = \pi/3\sqrt{2} \approx 0.74$. As the density of the system increases, there must come a point when the loss of (single particle) configurational entropy upon ordering is more than compensated for by the increase in local free volume (or many-body correlational entropy). This means that the volume accessible to each particle (i.e, the free volume) is greater in the hard sphere crystal at the melting density than in the hard sphere fluid at the freezing density [80].

We are now in a position to explain the unusual speeding up of the molecular reorientational motion at short times at the phase transition. Due to the comparable size of the rotation spheres for CS_2 and C_6H_{12}, we expect the dopant CS_2 to be incorporated substitutionally into the cyclohexane plastic crystalline lattice. As has been discussed above, it can be proved rigorously that the free volume increases when hard spheres crystallise. Widom's arguments suggest that this likely to be true for the freezing of simple liquids far from criticality [78,81]; each particle is moving in an almost constant attractive potential well set up by its nearest neighbours, and experiencing nearly zero force, so that the entropic (or free volume) and dominant part of the free energy remain hard-sphere-like. For the first time, we observe experimentally direct evidence of the predicted increase in free volume as the cyclohexane freezes into the plastic crystalline phase. The dopant CS_2 molecules in their substitutional sites are permitted to rattle more rapidly due to an increase in the extra local free volume at the plastic crystal phase transition, resulting in the observed speeding up of the reorientational correlation function in the short-time limit. In the case of a perfectly spherical solute molecule, faster orientational relaxation would be observed over all time scales. However the CS_2 dopant molecules are structurally anisotropic. The presence of

an ordered lattice structure with finite rigidity and the anisotropic nature of the solute, means that the longer-time reorientation is slowed down because decorrelating end-over-end rotations are surpressed. This accounts for the observed cross-over behaviour at about $t = 0.4ps$.

In order to justify this explanation, we now compare the results to those for the system of 20% CS_2 in n-propanol, which vitrifies. In this case we do not expect a discontinuity in the free volume across the glass transition temperature [82], and this is verified by the monotonic temperature dependence of the correlation functions at all time-scales (Fig. 15).

5.4 Conclusions

The correlation functions presented here provide, for the first time, direct evidence for the increase in local free volume across a liquid to plastic crystal phase transition. The results are interpreted in terms of a model which involves both the changes in the local solvent structure at the freezing transition and the solute molecular shape, which appear to play competing roles in the molecular reorientation process. We observe a very complex behaviour in solvation dynamics correlation functions, particularly at the phase transition: the increase in free volume leads to less hindered motion of the solute resulting in faster reorientational motion at short times, whilst the solute anisotropy restricts the end-over-end motion, as signified by the slower orientational relaxation at longer times. Such behaviour has been observed in idealised rough hard sphere molecular dynamics simulations of plastic crystals [83].

Fig. 14a CS_2 in Cyclohexane

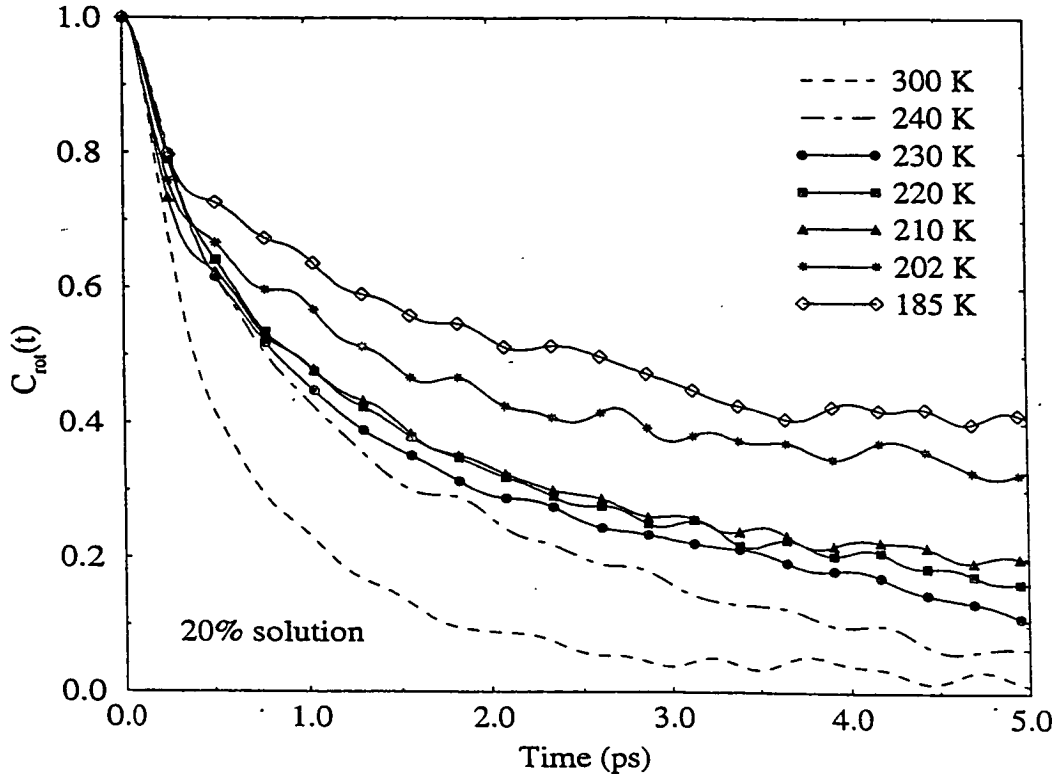

Fig. 14b CS_2 in Cyclohexane: The Short Time Limit

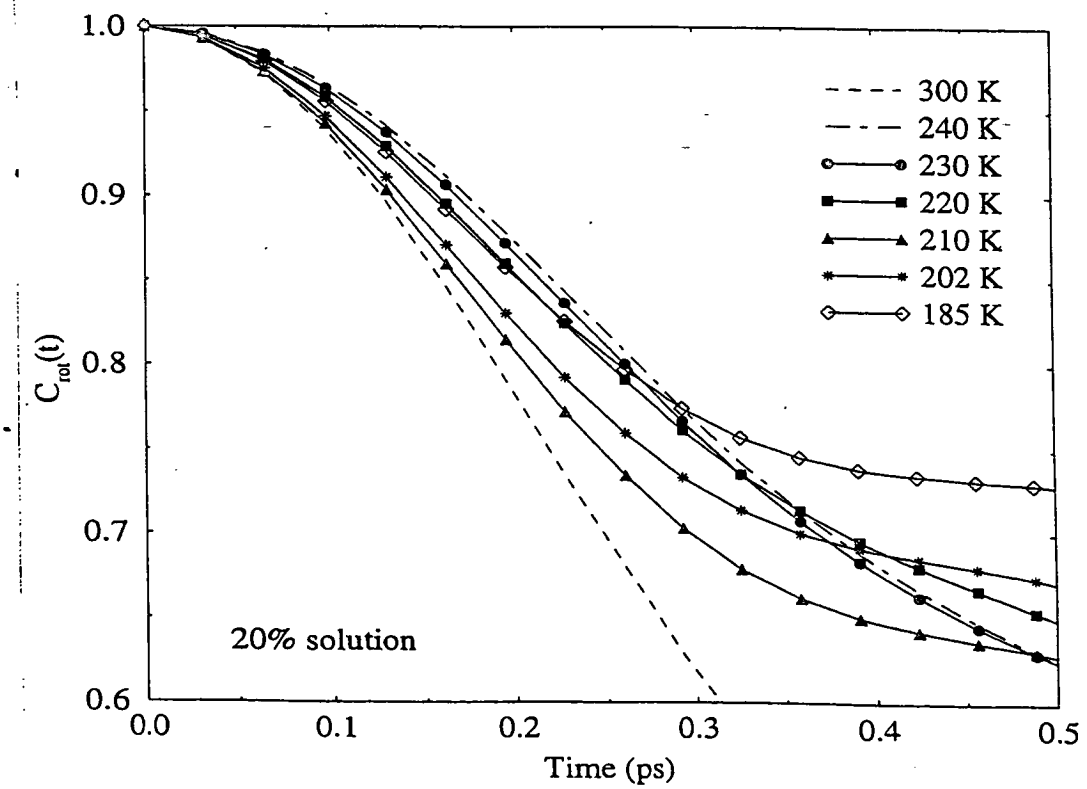

Fig. 15 CS_2 in Propanol, 100K, 150K, 175K, 200K, 225K, 250K and 300K Top to Bottom

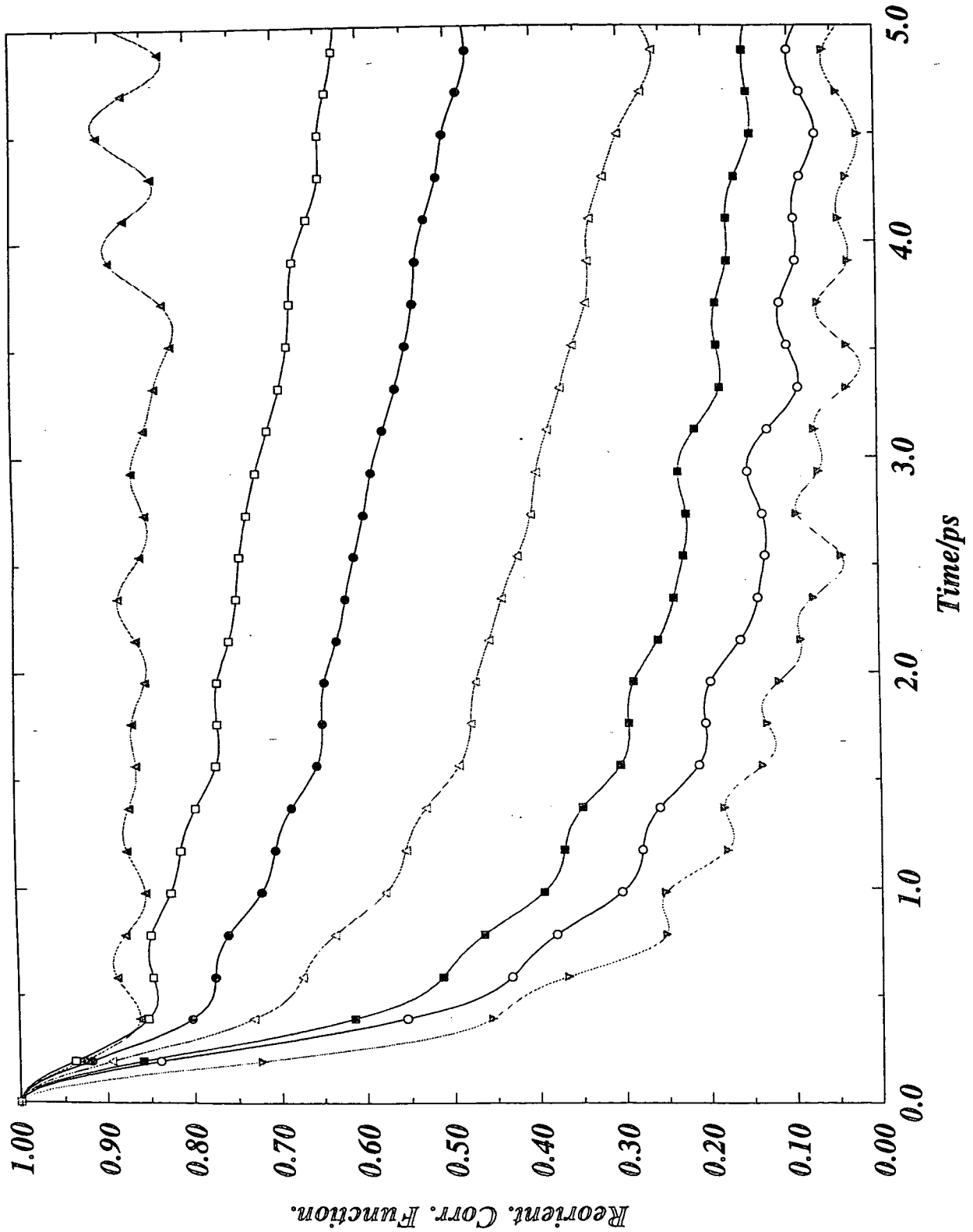

Chapter 6

Reorientation Dynamics of Single Flexible Anisotropic Molecules

6.1 Introduction

The results presented in chapter 4 showed that the bending mode vibration in CS_2 plays a major role in the intermolecular interactions and reorientation dynamics in partially disordered condensed matter phases, as the vibration destroys the linear symmetry of the molecule resulting in an intermolecular torque. In this chapter we investigate the effect of molecular flexibility in more detail by considering the single molecule reorientation dynamics of several members of the nCB (4-n-alkyl-4'-cyanobiphenyl) homologous series. The two phenyl rings and the cyano group act as a rigid rod and the variation in the flexibility of the homologues is provided by the differing lengths of the alkyl chain. Here we study the homologues 2CB, 4CB and 5CB. 5CB and all higher members exhibit liquid-crystalline phase behaviour at easily accessible temperatures. Attention to the dynamics of anisotropic systems in general, and liquid crystals in particular can be partly ascribed to the many technical applications of mesophases, in particular, liquid crystal displays (LCD's).

Computational advances have opened opportunities to expore the relationship between molecular structure and dynamics at many levels of sophistication ranging from ensembles of simple spherocylindrical particles to fully atomistic electronic structure descriptions of individual molecules [84-91]. There have as yet been very few experimental studies of reorientational dynamic processes in condensed

phases of large flexible anisotropic molecules. The reason for this is two-fold. First, the anisotropy of the system complicates the execution and analysis of the most sensitive dynamical measurements, and secondly, the reorientational motion of large molecules, such as mesogens is very slow.This was first shown by Bulkin and Brezinsky [92], who concluded that vibrational dephasing is primarily responsible for the bandwidth and shape of Raman bands of mesogenic molecules in their isotropic and liquid crystalline phases, as well as in solutions. Fontana *et al.* [93,94] developed a small step diffusion model for molecular reorientational relaxation in a mean-field nematic orienting potential in order to probe the spinning and tumbling diffusion coefficients of various mesogens. Such a model suggests that the reorientational correlation function is a single exponential. More recent studies [95] definitively show that this is not the case. In fact defining a suitable model for the reorientation dynamics of large anistropic molecules is problematic as the flexibility of the molecules means that no definable symmetry of the consituent molecules exists.

Previous studies of liquid crystals in the isotropic phase have concentrated on the collective reorientation dynamics of the system [96]. It is now well understood that at temperatures above the nematic to isotropic phase transition there exists substantial local structural anisotropy. This temperature region, which is referred to by Fayer [96] as the pretransitional region, is characterised by the presence of pseudonematic domains, whose local order exists over a distance scale ξ, the correlation length. On cooling towards the isotropic-nematic phase transition ξ increases, before diverging at a specific temperature T_c just below the phase transition temperature T_{ni}.

The dynamics of the pseudonematic domains can be separated into two distinct time scales. The fast time-scale orientational relaxation ($1ps$ to $1ns$) is attributed to intradomain dynamics which are temperature and viscosity independent, suggesting that the local pseudonematic structures are preserved during the relaxation. The anisotropy of the domains themselves decays as a single exponential on a much longer time scale ($\rangle 1ns$) with a decay rate that is highly temperature dependent. This slow dynamical behaviour is well described by the Landau-de Gennes (LdG) theory. In a recent publication, Sengupta and Fayer [96] analysed such collective reorientational dynamics of the pretransitional region in terms of fluctuation modes of the pseudonematic domains. Using the Ising model and including critical correlations of fluctuations, this theory predicts a universal temperature-independent power law to describe the fast time-scale orientational

dynamics in the isotropic phase of liquid crystals. Transient grating optical Kerr effect (TG-OKE) experiments performed at various temperatures on the liquid crystals 5CB and MBBA in their isotropic phases supporteded the theories discussed above. In 5CB the pretransitional region extends approximately 30° above the nematic-isotropic transition temperature, T_{ni}. Above $T_{ni} + 30°$, the slow dynamics start deviating from LdG theory as thermal fluctuations change the local structures and the overall domain relaxation. Simultaneously the collective intradomain reorientation dynamics becomes temperature dependent.

In this chapter we present for the first time a systematic study of single molecule reorientation dynamics in the nCB homologous series over a range of temperatures including the pretransitional region. The main objectives are to understand how the reorienational dynamics varies with molecular structure and flexibility, to explore how the onset of orientational order influences the dynamics and to provide unambiguous data for comparison to computer simulations.

6.2 Experimental Procedure

The general procedure for obtaining good correlation functions has been discusssed previously in Chapter 3. Raman spectra (VV and VH) were taken of the 2225 cm $^{-1}$ CN A_{1g} stretch of 2CB, 4CB and 5CB in the isotropic phase close to the respective phase transition [2CB and 4CB exhibit a solid-isotropic transition, whilst 5CB exhibits a solid-nematic transition]. The samples were acquired from Merck, and loaded into $1mm$ diameter capillary tubes. The samples were initially heated to 60° above their respective melting points, and cooled to the phase transition. Temperature readings were accurate to within an error of 0.1°. The incident beam at $514.5nm$ with a power of $240mW$ was obtained from an Argon ion laser. A Coderg T800 triple grating spectrometer was used in a 90° configuration. The slit size was set to $50\mu m$ allowing a spectral resolution better than $\frac{1}{4}$ cm $^{-1}$ FWHH and the data was collected in steps of $\frac{1}{8}$ cm $^{-1}$ out to 85 cm $^{-1}$ from the centre of the band. The typically observed FWHH was 7-10 cm $^{-1}$. Count times varied from $4sec$ per step to as much as $80sec$ per step according to the relative intensities of the VV and VH bands. In the case of such large anisotropic molecules, the reorientational contribution to line broadening is very small, and therefore differences in the S/N for VV and VH spectra can cause anomalies in the obtained correlation functions. It was observed whilst taking the spectra that the relative intensities (and hence the relative S/N) of the VV

and VH spectra changed as a function of temperature. Particularly for $4CB$ and $5CB$, the VH band intensity was seen to increase with decreasing temperature, whilst the VV band intensity was seen to decrease with decreasing temperature. This phenomenon is the result of an increase in the orientational anisotropy of the system. Each spectrum was taken three times, and the obtained correlation functions were averaged.

At high temperatures all the nCB homologues studied here undergo a slow thermally-activated irreversible reaction. The author assumes this to be thermal oxidation. Whilst the product of this reaction is unknown it manifests itself in Raman spectra by raising the background signal as much as one-thousand-fold. This makes accurate baseline correction techniques and thereby the acquisition of realistic correlation functions at higher temperatures impossible.

6.3 Results and Discussion

6.3.1 Ramifications of the TG-OKE Experiments

The nonlinear time-resolved spectroscopic results discussed in section 6.1 have very interesting ramifications. In this section we will discuss the results of the TG-OKE experiments performed by Fayer and Sengupter [96]. The TG-OKE response function is directly related to frequency domain dynamical light scattering data via Fourier inversion. The OKE response function is therefore a direct measurement of the collective orientational relaxation of the system [97]. The susceptibility fluctuation due to the reorientational motion of the molecules in liquids generally has an exponentially decaying correlation function at sufficiently long times, as described by the rotational diffusion equation. This results in an exponential decay of the OKE response in the long time scale:

$$G_{OR}(t) \propto \Theta(t) \exp(-t/\tau_{col})[1 - \exp(-t/\tau_{\nu})] \tag{6.1}$$

where $\Theta(t)$ is the normalised step function and τ_{col} is the collective orientational relaxation time. The ultra-fast nature of the response function is complicated by the finite decay rate of the molecular angular momentum, given by the relaxation time of the angular momentum, τ_{ν}, librational motion and interaction-induced (I-I) phenomena. The relation of τ_{col} to the single-particle orientational relaxation

time is given by [98]:

$$\tau_{col} = (g_2/j_2)\tau_r \tag{6.2}$$

where g_2 and j_2 are the static and dynamic orientational correlation coefficients of the liquid, respectively. In the temperature range of the pretransitional region for 5CB, the very slow hydrodynamic modes do decay as single exponentials. However, the faster, intradomain dynamics are not coupled to these hydrodynamic modes and the response function exhibits a power law decay:

$$G_{OR}(t) \propto \Theta(t)t^{-0.63} \tag{6.3}$$

suggesting that the dynamics are strongly influenced by the pseudonematic domain structure. The time scales for single molecule reorientation for a molecule the size of 5CB are of the same order as the time scales of these collective intradomain dynamics.

6.3.2 Results for 5CB

Reorientational correlation functions for 5CB at different temperatures are presented in fig.16. It is evident from the data that there are two distinct dynamical regions: in the first $0.25ps$ the correlation functions decay rapidly and non-exponentially. This rapid decay is temperature independent, within experimental error, close to the transition temperature, $T - T_{ni} < 30K$, and much faster than would be expected considering the moment of inertia for 5CB. At higher temperatures, $T - T_{ni} > 35K$, the initial decay of the correlation functions becomes temperature dependent, the rate of decay increasing with temperature. At time scales greater than $0.25ps$ the correlation functions decay as very slow single exponentials. The time exponent, τ:

$$C(t)_{rot,t>0.25ps} = A\exp(t/\tau) \tag{6.4}$$

has a complicated temperature dependence. As shown in Fig. 17, close to the transition temperature, the correlation time decreases slowly with increasing temperature. At $T - T_{ni} > 35K$ the correlation time is extremely temperature dependent and decreases rapidly. This occurs with the onset of temperature dependence in the short time regime, ($t < 0.25ps$). At time-scales greater than $1ps$, the total and vibrational correlation functions fall below 0.25. As the reorientational correlation function is given by the ratio of these two correlation functions, the

calculated data error increases rapidly at time scales greater than $1ps$ and the reorientational correlation functions become unreliable.

On the basis of these results we conclude that the fast initial decay of the correlation functions represents intra-molecular librational motion of a fragment of the flexible molecule in a cage formed by neighbouring molecules. The molecule is subject to strongly fluctuating intermolecular forces across the cage, which cause the conformational structure of the molecule to relax rapidly on a similar time-scale. The molecular flexibility couples the rotations about different molecular axes, causing spinning and twisting motions to contribute to the tumbling motion. In the pretransitional region exhibited by 5CB, this response is temperature independent as the local pseudonematic structures are preserved, and the rate of decay is dependent on the force coefficient of the well potential representing the cage. When $T - T_{ni} > 35K$ the pseudonematic domains start to break down and the fast relaxation becomes temperature dependent as the flexible molecule possess a greater degree of freedom. The slow single exponential decay observed at time-scales greater than $0.3ps$ is indicative of reorientation diffusion. Using the small-step reorientation diffusion model (SSRDM), reorientation diffusion coefficients, $D_\perp$ for the tumbling motion of the molecule can be obtained simply as:

$$D_\perp = 1/6\tau \ . \tag{6.5}$$

For 5CB just above the transition temperature $D_\perp = 3.47 \times 10^9 sec^{-1}$. This value is much lower than one would expect by comparison to the results obtained for 2CB taking into account the differences in the molecular mass and actual temperature (the solid-isotropic transition temperature, T_{si} for 2CB is $340K$ whereas the nematic-isotropic transition temperature, T_{ni} for 5CB is $308K$), and is also lower than other reorientation diffusion coefficients obtained from liquids comprising of non-liquid-crystalline molecules of comparable size. This is indicative of the presence of substantial local structural anisotropy. At high temperatures 5CB behaves as an isotropic liquid, the single molecule reorientation diffusion coefficient increases rapidly with temperature. Lowering the temperature to $340K$, 5CB enters the pretransitional region. At this point the single molecule reorientation is severely hindered by the formation of a localised structure, or pseudonematic domain, and the reorientation diffusion coefficient slowly decreases on cooling to the nematic-isotropic phase transition. This complicated temperature dependence may be entropically driven, suggesting that the dynamics of single molecules in the system are affected by long-range interactions over distances comparable to

ξ. Alternatively, single-molecule dynamics in the pretransitional region could be determined by short-range interactions which maintain an optimised local order in the system. There exists considerable evidence that the mesogen 5CB aligns in an anti-parallel configuration [99,100]. Intermolecular forces created, for example, by dipole-induced dipoles (DID's) which relax on very fast time-scales (usually $100 - 800fs$) maintain the local structure and play a significant part in the dynamics of single molecules on much longer time-scales. Such intermolecular interaction manifests itself directly in Rayleigh light scattering and is referred to as an interaction-induced (I-I) phenomenon. Recent computer simulations show that considerable I-I phenomena exist in systems comprised of large molecules such as mesogens [101].

6.3.3 Results for 2CB

In comparison to the data for 5CB discussed above, the reorientational correlation functions for 2CB show markedly different behaviour, (Fig. 18). There still exist two dynamical regions, yet, especially at higher temperatures, they are not so distinct. The initial fast decay is temperature-dependent across the entire temperature region studied. This fast decay is slower than that observed for 5CB. The 2CB molecules act as rigid rotors, which are subjected to a temperature-dependent inter-molecular torque in the short time limit. The slower response is highly temperature dependent, and the respective correlation times decrease rapidly with increasing temperature.

Due to the small degree of flexiblility, assuming that 2CB is linear, such correlation functions can be interpreted in terms of extended diffusion models, such as the J-diffusion model using a large collision frequency parameter. This collision frequency parameter like the inter-molecular torque for the inflexible 2CB molecule are temperature dependent.

6.3.4 Results for 4CB

The dynamics of 5CB and 4CB are remarkably similar. The short-time behaviour of the correlation functions is temperature independent over a temperature range of $25K$ above the melting point, and this rapid decay is much faster than would be expected for a rigid rotor. The similarity between the data for 4CB and 5CB in this short-time region suggests that the two molecules possess a similar degree

of flexibility.

On the grounds of the above discussion, the results for 4CB shown in Fig. 19 suggest that, whilst not actually existing in a liquid-crystalline phase, this system exists over a temperature range of $25K$ above its melting point in a pseudonematic state.

6.4 Summary

The reorientation dynamics of mesogenic molecules in the isotropic phase is extremely complex. In the pretransitional region collective orientational relaxation of the pseudonematic domains occurs on time-scales greater than $1ns$ and is temperature/viscosity dependent, whilst the intradomain dynamics ($1ps$ to $1ns$) are temperature/viscosity independent. The single-molecule reorientational relaxation shows two distinct time-scales. The fast initial non-exponential decay is temperature independent. This non-diffusional behaviour in the short time-limit is a manifestation of the interaction between the intermolecular potential and molecular flexibility. Its temperature independence suggests the existance of significant local structural anisotropy in the pretransitional region. The slowly decaying single exponential component represents single-molecule reorientation diffusion. This component is weakly temperature dependent in the pretransitional region. At temperatures greater than $343K$ the pseudonematic domains in 5CB break down. The fast initial decay of the autocorrelation function becomes temperature dependent and reorientational diffusion increases rapidly. Decidedly different behaviour has been observed for 2CB.

On the basis of these results, we conclude that local structural anisotropy is related to the complex dynamics in the short-time limit determined by rapidly decaying electronic interactions between molecules, such as DID's. This means that there exists a preferential local structure which optimises interaction between the molecules, thereby lowering the free energy of the system. Molecular flexibility enables the system to maintain local anisotropy despite thermal fluctuations by the rapid variation of the interaction potential between a single molecule and the cage around it. At a certain temperature, the kinetic energy of the molecules overcomes the potential energy well of the cage, local structural anisotropy breaks down and the reorientational autocorrelation function becomes

temperature dependent in the short-time limit, whilst at longer times the temperature dependence of molecular motion is comparable to that of extended diffusion models.

On cooling the system into and through the nematic phase, ξ grows, the order parameter increases rapidly and the long-range orientational correlation of the pseudonematic domains is maintained indefinitely. This occurs as the potential energy well of the cage becomes narrower and deeper. The interaction between the flexible molecule and the cage around it increases. Whilst the macroscopic structure of the system is now entropically driven, the dynamics of the system are determined by the fast relaxation of the molecule as it interacts with its neighbours. It is a tantalising prospect that this complex relaxation occurring over several hundred femtoseconds could determine the reorientational dynamics of the system at much longer time-scales. In the following chapters we concentrate on the dynamics of liquid-crystalline molecules in different mesophases.

Fig. 16 Reorientational Correlation Functions for 5CB

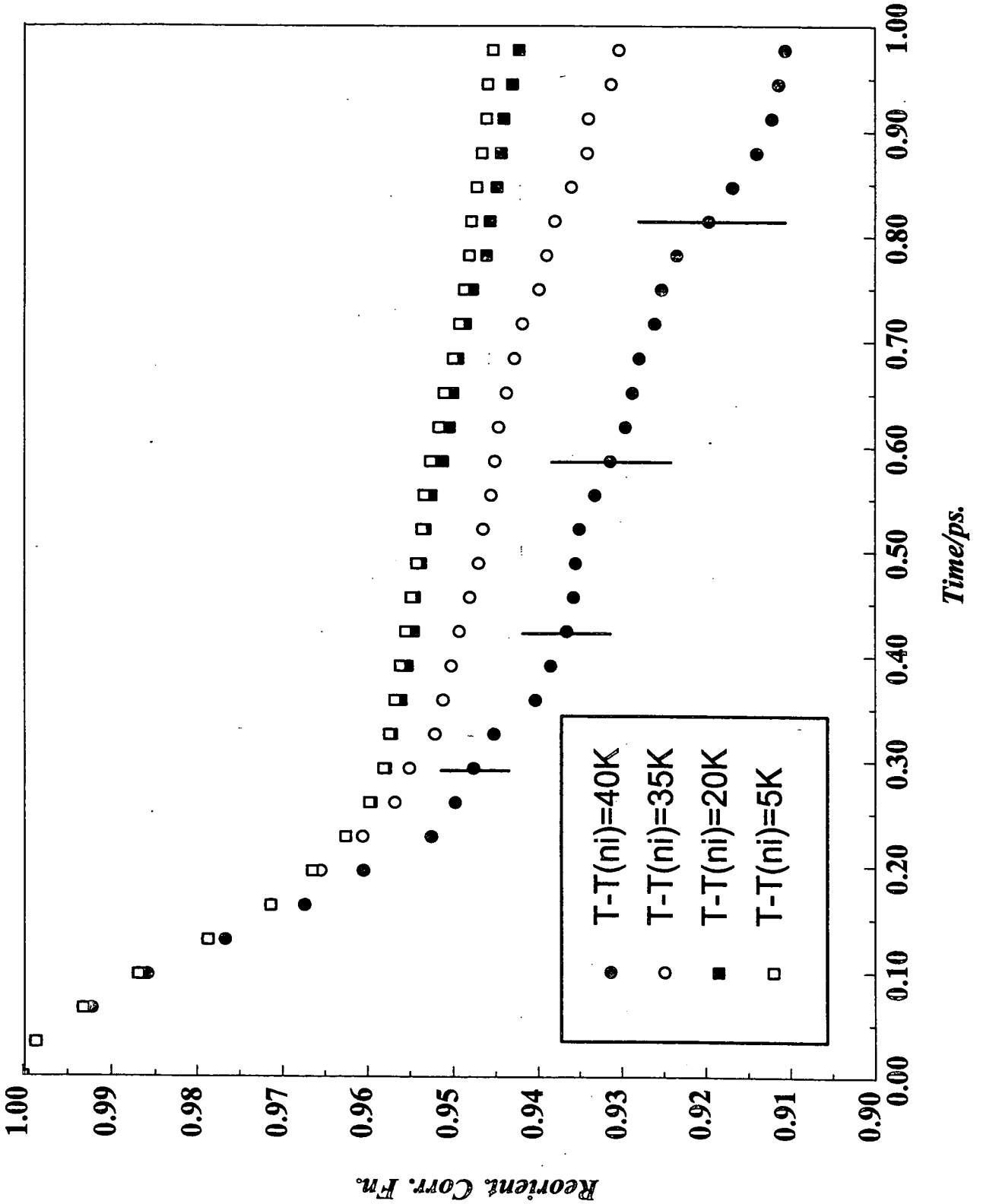

Fig. 17 Reorientational Correlation Times
Long Time-scale Rotational Relaxation t>0.3 ps.

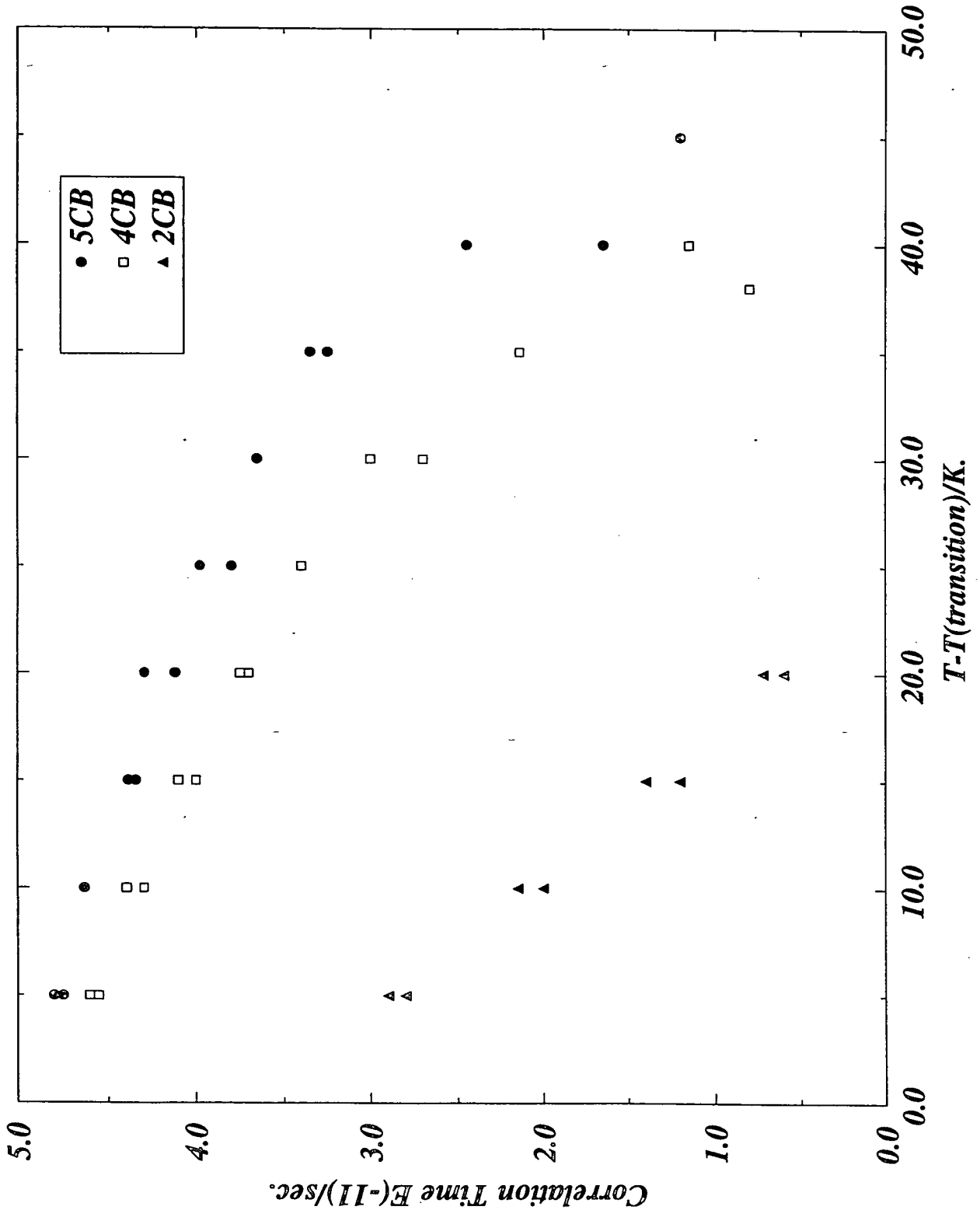

Fig. 18 Reorientational Correlation Functions for 2CB

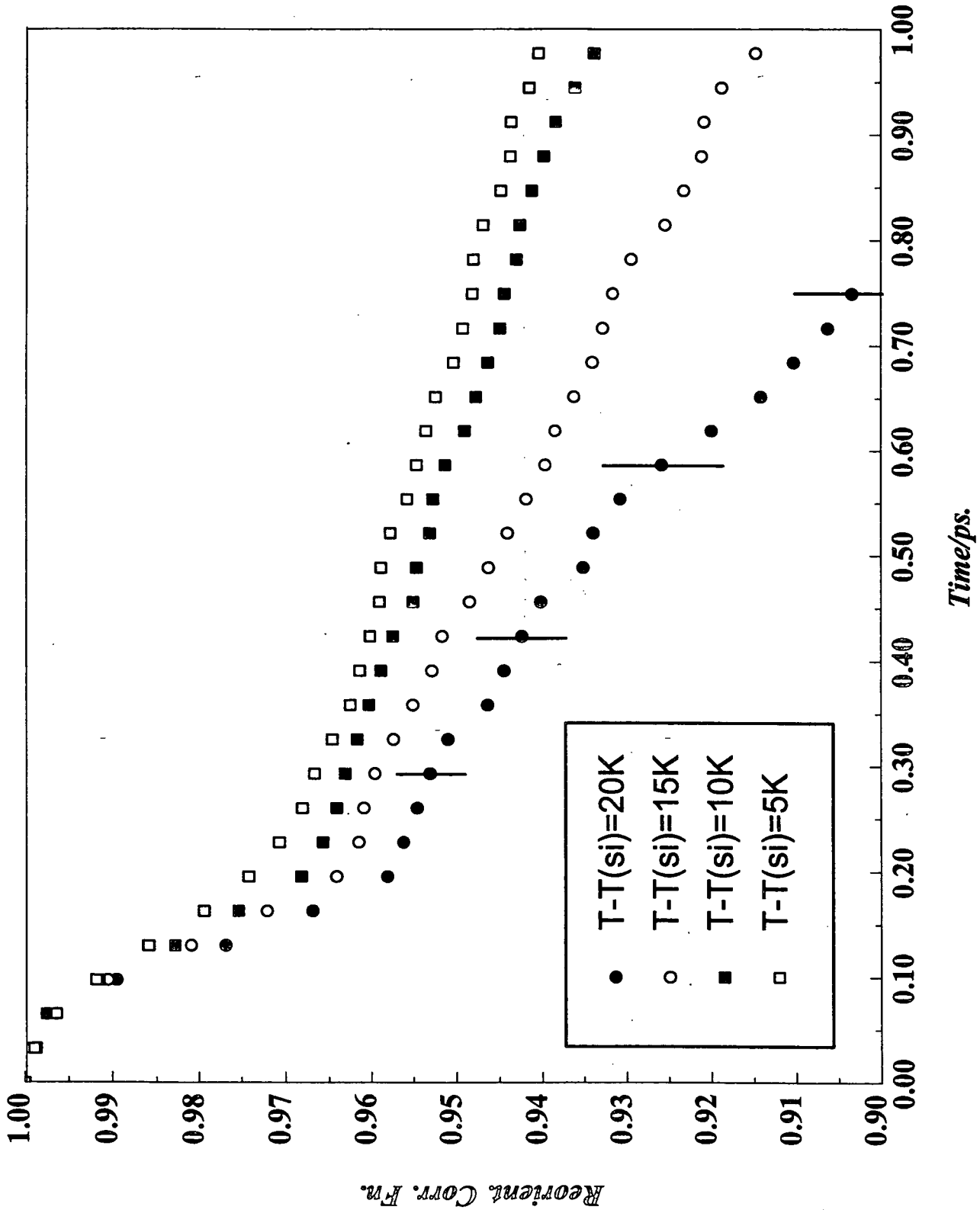

Fig. 19 Reorientational Correlation Functions for 4CB

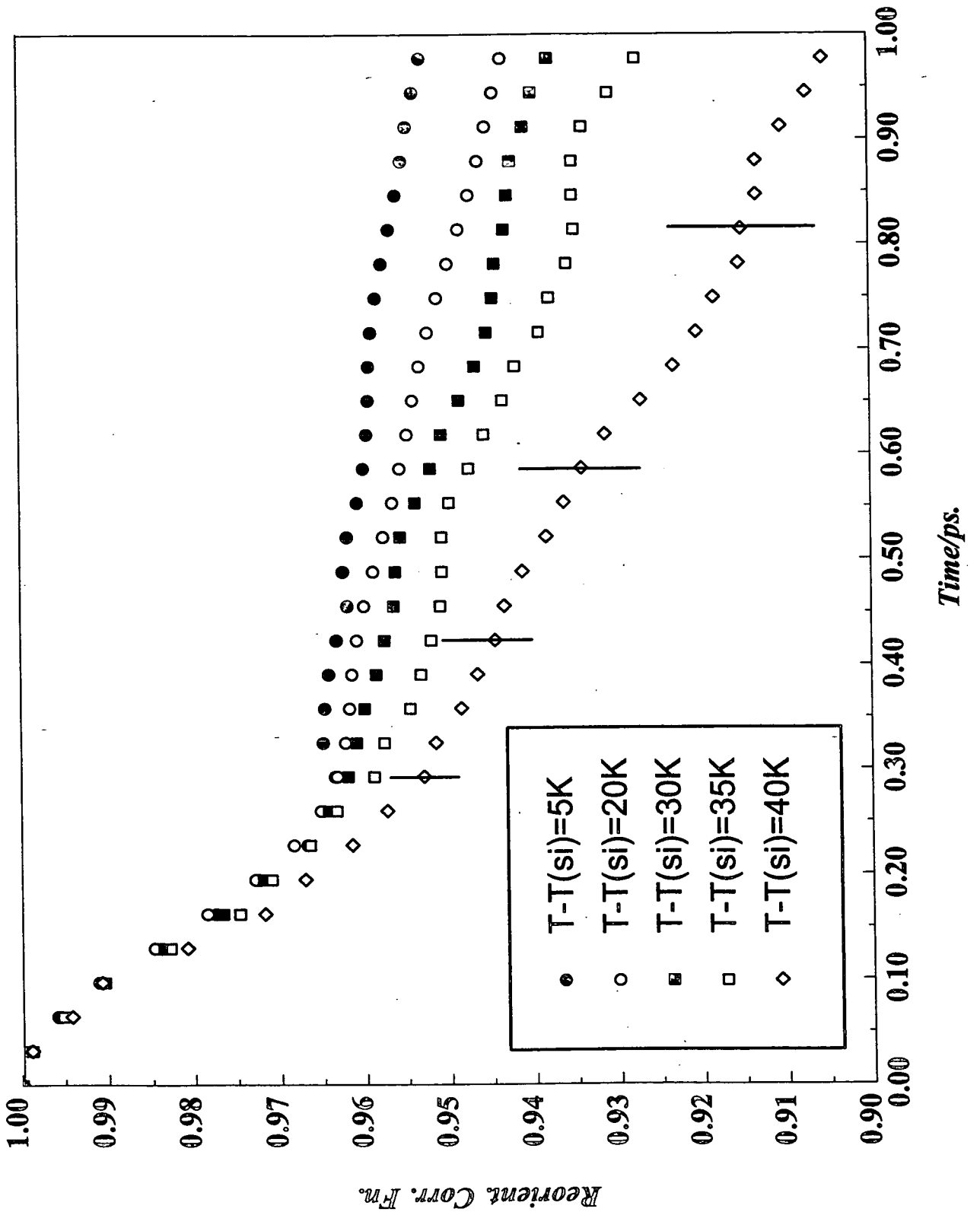

Chapter 7

The Theory of Dielectric Relaxation

7.1 Introduction

The results from chapter 6 showed that, whilst Raman lineshape analysis is a good technique for isolating and analysing the reorientational correlation function in condensed matter systems, it is best suited to systems comprised of small rigid molecules, where the line broadening is dominated by reorientational rather than vibrational relaxation. In the case of large flexible anisotropic molecules, such as those higher members of the nCB homologous series, the reorientational line broadening is so small that obtaining reorientational correlation functions becomes increasingly more difficult. It is therefore unsuitable to use Raman lineshape analysis to study the dynamics of the higher members of the nCB homologous series in the nematic and smectic liquid-crystalline phases, where the contribution to reorientational line broadening is even smaller than in the isotropic phase. To this end we must use an alternative experimental technique. The most suitable technique for studying reorientational relaxation in polar mesogenic systems is that of dielectric relaxation, where we measure the frequency-dependent dielectric constant expressed as a complex permittivity, $\varepsilon^* = \varepsilon' - i\varepsilon''$. In the following section the theory of the static dielectric constant and dielectric relaxation is discussed and applied to the particular case of polar mesogenic systems.

7.2 The Static Dielectric Constant

The well-known Onsager theory [102,103,104] describes the static dielectric constant, ε_s, of isotropic, non-associative, polar liquids. The theory does not take into account intermolecular interaction potentials and assumes the constituent molecules to be of spherical symmetry. Maier and Meier [105] extended the Onsager theory to describe the dielectric properties of uniaxial nematic liquid-crystalline phases. In order to account for the orientational order observed in nematic mesogenic systems, they invoked a parameter called the nematic potential, q. It is considered that the potential energy of the molecule is lowest when its molecular long-axis lies either parallel or anti-parallel to the director, $\mathbf{n}$. Whilst the order parameter, S provides a measure of the degree of molecular alignment, it is the nematic potential that defines the amount of energy the molecules need to overcome the reorientational potential energy barrier. The static dielectric constant is expressed as a tensor. Assuming that the laboratory z-axis coincides with the director, $\mathbf{n}$, the dielectric tensor has the form of a sphero-cylinder with the principle elements, $\varepsilon_{s\parallel} = \varepsilon_{zz}$ and $\varepsilon_{s\perp} = \varepsilon_{xx} = \varepsilon_{yy}$. Applying the incident electric field parallel or perpendicular to the director then yields $\varepsilon_{s\parallel}$ or $\varepsilon_{s\perp}$ respectively. The anisotropy of the dielectric constant is defined as:

$$\Delta\varepsilon_s = \varepsilon_{s\parallel} - \varepsilon_{s\perp} \; . \tag{7.1}$$

The magnitude and sign of the dielectric anisotropy are determined by the molecular structure of the nematic phase. $\Delta\varepsilon_s$ depends on the extent of orientational alignment of neighbouring molecules, and therefore on the order parameter S. As in the isotropic case, it is necessary to consider the induced and orientational polarisation. The induced polarisation is ostensibly due to the displacement of electrons in an external electric field. The orientation polarisation is concerned with the alignment of the permanent dipole moment of the constituent molecules in the direction of the incident electric field. Following the theory of Maier and Meier [106] we assume that the permanent dipole moment lies at an angle β to the molecular long-axis. The polarisability anisotropy, $\Delta\alpha$, is comprised of a longitudinal part α_l and a transverse part α_t. In the microscopic molecular-fixed coordinate system, the components of the dipole moment are expressed as:

$$\mu_l = \mu \cos\beta \tag{7.2}$$

and

$$\mu_t = \mu \sin\beta \ . \tag{7.3}$$

The aim is now to find expressions for the components $\alpha_{||}, \alpha_{\perp}, \mu_{||}$ and $\mu_{\perp}$, which refer to the laboratory fixed frame. These components are therefore dependent on the orientation of the molecular long-axis with respect to the z-axis of the laboratory-fixed frame and are naturally coupled to the order parameter S:

$$\langle\alpha_{||}\rangle = \frac{1}{3}(\alpha_l(2S+1) + \alpha_t(2-2S)) \tag{7.4}$$

$$\langle\alpha_{\perp}\rangle = \frac{1}{3}(\alpha_l(1-S) + \alpha_t(2+S)) \tag{7.5}$$

$$\langle\mu_{||}^2\rangle = \frac{1}{3}(\mu_l^2(2S+1) + \mu_t^2(1-S)) = \frac{1}{3}\mu^2(1-[1-3cos^2\beta]S) \tag{7.6}$$

$$\langle\mu_{\perp}^2\rangle = \frac{1}{3}(\mu_l^2(1-S) + \mu_t^2(2+S)) = \frac{1}{3}\mu^2(1+\frac{1}{2}[1-3cos^2\beta]S) \ . \tag{7.7}$$

Maier and Meier use the same assumptions as Onsager to simplify the problem. The molecules are considered to sit in spherical cavities with radius r, given by the molecular volume ($M/\rho = \frac{4}{3}\pi N_A r^3$). The so-called cavity-field factor is expressed as $h = 3\bar{\varepsilon_s}/(2\bar{\varepsilon_s}+1)$ with $\bar{\varepsilon_s} = \frac{1}{3}(\varepsilon_{s||} + 2\varepsilon_{s\perp})$. The so-called reaction-field is expressed as $f = (\bar{\varepsilon_s}-1)(2\pi\varepsilon_0 r^3[2\bar{\varepsilon_s}+1])$. The resulting equations express the relationship between $\varepsilon_{s||}$ and $\varepsilon_{s\perp}$ and their dependence on the orientation polarisation and induced polarisation [106,107,108].

$$\begin{aligned}\varepsilon_{s||} - 1 &= (NhF/\varepsilon_0)(\langle\alpha_{||}\rangle + F\langle\mu_{||}^2\rangle/(kT)) \\ &= (NhF/\varepsilon_0)(\bar{\alpha} + \tfrac{2}{3}\Delta\alpha S + (F\langle\mu^2\rangle/(1-(1-3cos^2\beta)S))/(3kT))\end{aligned} \tag{7.8}$$

$$\begin{aligned}\varepsilon_{s\perp} - 1 &= (NhF/\varepsilon_0)(\langle\alpha_{\perp}\rangle + F\langle\mu_{\perp}^2\rangle/(kT)) \\ &= (NhF/\varepsilon_0)(\bar{\alpha} + \tfrac{1}{3}\Delta\alpha S + (F\langle\mu^2\rangle(1+\tfrac{1}{2}(1-3cos^2\beta)S))/(3kT))\end{aligned} \tag{7.9}$$

$$\Delta\varepsilon = \varepsilon_{s||} - \varepsilon_{s\perp} = (NhF/\varepsilon_0)(\Delta\alpha - (F\langle\mu^2\rangle(1-3cos^2\beta)S)/(2kT)) \ . \tag{7.10}$$

In the above equations $F = 1/(1-f\alpha)$, $\Delta\alpha = \alpha_l - \alpha_t$, $\bar{\alpha} = \frac{1}{3}(\alpha_l + 2\alpha_t)$ and ε_0 is the permittivity of free space. The last equation shows that the induced polarisation is proportional to the order parameter, whilst the orientation polarisation shows S/T dependence. In nematic liquid crystals composed of rod-like

molecules $\Delta\alpha$ is always greater than zero. The contribution of the induced polarisation to $\Delta\varepsilon$ is always positive. The contribution of the orientation polarisation depends on the size of the permanent dipole moment and the angle, β, between the dipole moment vector μ and the molecular long-axis. Only in the special case, where $3cos^2\beta = 1, (\beta = 54.74°)$ is the contribution of μ to $\varepsilon_{||}$ and $\varepsilon_{\perp}$ the same. For an angle $\beta < 54.74°$, the contribution of the orientation polarisation to $\Delta\varepsilon$ is positive. Similarly the contribution of the orientation polarisation is negative for all angles $\beta > 54.74°$. It follows that the sign (+ or -) of the total dielectric anisotropy is determined by the relative magnitudes of the induced and orientation polarisation. In the case of molecules possessing a large dipole moment in the direction of the molecular long-axis, such as the case for para-cyano substituted mesogens, $\Delta\varepsilon$ is positive. In some cases, particularly for substances with lateral dipolar moments, the negative part of the orientation polarisation dominates, which leads to a negative dielectric anisotropy.

If averaged values are used for ε_s and ε_∞: $\bar{\varepsilon_s} = \frac{1}{3}(\varepsilon_{s||} + 2\varepsilon_{s\perp}); \varepsilon_\infty \approx n^2$ (ε_∞ is the high frequency dielectric constant, n is the refractive index), Onsager's equation for the isotropic phase is recovered and can be used to estimate the permanent dipole moment of the constituent molecules in the system:

$$\mu^2 = \frac{9kT\varepsilon_0 M(\bar{\varepsilon_s} - \bar{\varepsilon_\infty})(2\bar{\varepsilon_s} + \bar{\varepsilon_\infty})}{N_A \rho \bar{\varepsilon_s}(\bar{\varepsilon_\infty} + 2)^2} \ . \tag{7.11}$$

In many cases (such as with the alkyl-cyanobiphenyls) the calculated dipole moment is much smaller than expected, considering the polar nature of the constituent molecules. This is accounted for using a correlation factor g_k such that:

$$\mu_{eff}^2 = g_k \mu^2 \ . \tag{7.12}$$

This correlation factor gives an indication of the parallel or anti-parallel alignment of the constituent molecules [109]. In the case of the nCB homologous series,the anti-parallel correlations give a value of g_k less than 1. For further discussions of the static dielectric constant, the reader is referred to the references provided [110,111].

7.3 Dielectric Relaxation

In a static electric field, the total polarisation is a combination of the induced and orientation polarisation. When the external field is removed, the relaxation of the induced polarisation occurs on a timescale faster than $10^{-11}s$ due to the high velocity of the electrons. In contrast to this, the reorientation of the dipole moments requires a finite time t. The macroscopic relaxation time τ is defined as the time in which the orientation polarisation falls to $1/e$ of its initial value after removing the external electric field. The resulting dielectric correlation function of the orientation polarisation is then assumed to be an exponential.

Dielectric relaxation measurements are usually performed in the frequency domain using an alternating electric field. There then exists a Fourier-transform relationship between the time-dependent correlation function and the dielectric data collected in the frequency domain. At sufficiently high frequencies, the orientation polarisation lags behind the external electric field, resulting in a decrease in the permittivity. The reduction of the static dielectric constant ε_s to the high-frequency dielectric constant ε_∞ is described as dielectric relaxation. The dielectric relaxation is associated with a characteristic adsorbtion of energy. This energy adsorbtion is known as the dielectric loss and forms the imaginary part of the complex dielectric constant:

$$\varepsilon^*(\omega) = \varepsilon'(\omega) - i\varepsilon''(\omega) \; . \tag{7.13}$$

Obviously the functional forms of the real and imaginary parts of the complex frequency-dependent dielectric constant (dielectric relaxation and dielectric loss respectively) are dependent on the reorientation dynamics of the system. The models developed in chapter 2 are equally applicable to dielectric relaxation experiments as to Raman experimental data. However, we should note that as dielectric relaxation is an absorbtion process, we are now working in the first spherical harmonics index ($l = 1$). For the simplest case, of the small-step rotation diffusion model with a single relaxation time τ, the real and imaginary parts of the complex dielectric constant are given by the well-known Debye equations [112]:

$$\varepsilon'(\omega) - \varepsilon_\infty = \frac{\varepsilon_s - \varepsilon_\infty}{1 + \omega^2\tau^2} \tag{7.14}$$

$$\varepsilon''(\omega) = \frac{\varepsilon_s - \varepsilon_\infty}{1 + \omega^2\tau^2}\omega\tau \; . \tag{7.15}$$

Figure 20 shows the typical functional form of the dielectric relaxation and dielectric loss curves. The dielectric loss curve is completely symmetric with a maximum at $\omega_{max} = 2\pi/\tau$. Usually, however, one finds that the loss curve is not completely symmetric. Such deviation is best shown by plotting ε'' against ε', a 'Cole-Cole plot'. From the Debye equations it is apparent that the Cole-Cole plot should be a semi-circle:

$$[\varepsilon' - \frac{\varepsilon_s + \varepsilon_\infty}{2}]^2 + \varepsilon''^2 = [\frac{\varepsilon_s - \varepsilon_\infty}{2}]^2 \,. \tag{7.16}$$

Deviation from the Debye relation results in a characteristic distortion of the semi-circle. Several equations [113] have been developed with variational parameters in order to describe these deviations. The Cole-Cole, Cole-Davidson and Havriliak-Negami equations describe both the real and imaginary part of the complex dielectric constant. The Havriliak-Negami equation is:

$$\varepsilon^*(\omega) - \varepsilon_\infty = \frac{\varepsilon_s + \varepsilon_\infty}{(1 + [i\omega\tau]^{1-\alpha})^\beta} \,. \tag{7.17}$$

For the case that $\alpha = 0, \beta = 1$ the above equation reduces to the Debye equation. The Cole-Cole equation is obtained for $\alpha \neq 0, \beta = 1$ and the Cole-Davidson equation is given for $\alpha = 0, \beta \neq 1$. The Jonscher equation only describes the imaginary part of the dielectric constant expressed as:

$$\varepsilon''(\omega) = \frac{A}{(\omega/\omega_p)^{-m} + (\omega/\omega_p)^{1-n}} \,. \tag{7.18}$$

In the particular case that $m = 1, n = 0$ and $\omega_p = 2\pi/\tau$ the Jonscher equation is identical to the imaginary part of the Debye equation. The fit-parameters α, β, A, m and n are sufficient to describe the observed dielectric loss curves, though their physical meaning is not well defined. In general, deviations from the Debye equation occur when there exists a distribution of relaxation times τ, or when more than one relaxation process is occurring simultaneously.

7.4 Thermodynamics

The temperature and pressure dependence of the dielectric relaxation time τ can be used to express reorientational activation parameters [114,115]. The activation

enthalpy is given by:

$$\Delta^{\dagger}H = R[\frac{\partial ln\tau}{\partial(1/T)}]_p = T\Delta^{\dagger}V[\frac{\partial p}{\partial T}]_\tau \ . \tag{7.19}$$

The activation energy is expressed as:

$$\Delta^{\dagger}U = R[\frac{\partial ln\tau}{\partial(1/T)}]_V = \Delta^{\dagger}H - T[\frac{\partial p}{\partial T}]_V\Delta^{\dagger}V \ . \tag{7.20}$$

Similarly the activation volume is given by:

$$\Delta^{\dagger}V = RT[\frac{\partial ln\tau}{\partial p}]_T \ . \tag{7.21}$$

The activation volume can be understood as the *excess* volume a molecule requires in order to rotate. Therefore this value is not dependent on the molecular volume, but rather on the molecular shape and rigidity, and the structuring of the local molecular environment. In a similar manner, the activation enthalpy and energy are measurements of the *excess* enthalpy and energy required for a molecule to rotate. The activation energy can only be calculated with the use of PVT data. By comparing the relative magnitudes of the activation enthalpy and energy it is possible to determine the extent steric hindrance plays in intermolecular interaction. All the activation parameters are based on Arrhenius-type relationships, assuming that the partial derivatives remain constant.

7.5 The Retardation Factor

According to Maier-Saupe theory [116], when a nematic liquid crystalline molecule is aligned parallel to the director, it lies at an energy minimum on the potential energy surface. In order to rotate, the molecule must therefore overcome a potential energy barrier, given by the nematic potential, q. It is not surprising that the tumbling motion of the molecule slows dramatically when crossing the transition point from the isotropic phase to the nematic phase. It is logical to assume that there exists a simple relationship between the degree to which the relaxation rate is lowered and the nematic potential q that hinders tumbling motion in the nematic phase. Maier and Saupe found that the retardation factor $g_{\|} = \tau_{\|}/\tau_0$, ($\tau_0$ being the relaxation time at $q = 0$) is related to the nematic potential energy

barrier as:

$$g_{\|} = \frac{e^{\sigma} - 1}{\sigma} \tag{7.22}$$

where $\sigma = q/RT$. τ_0 is estimated by extrapolation of the isotropic isotherm (see Fig. 21). Assuming Debye-type motion, it has been found that the presence of the nematic potential reduces the relaxation rate of the tumbling motion, whilst increasing the relaxation rate of the spinning motion such that $g_{\|} > 1, g_{\perp} < 1$. More recently an exact analytic solution for the retardation factors as a function of the nematic potential has been derived by Coffey *et al.* [117,118,119]. To a close approximation, the exact solution for $g_{\|}$ can be written as:

$$g_{\|} = \frac{e^{\sigma} - 1}{\sigma}\left(\frac{2}{1 + 1/\sigma}(\sigma/\pi)^{1/2} + 2^{-\sigma}\right)^{-1} . \tag{7.23}$$

The retardation factors are related to the order parameter S as follows:

$$g_{\|} = \frac{2S + 1}{1 - S} \tag{7.24}$$

$$g_{\perp} = \frac{2 - 2S}{2 + S} . \tag{7.25}$$

7.6 Summary

Dielectric relaxation experiments provide not only information about the reorientational relaxation times in liquid-crystalline systems, but also generate a wealth of information about the type and extent of intermolecular interaction and the thermodynamics and energetics of reorientational motion. Most importantly, the experiment also provides a means of calculating the order parameter S, which is the single most important parameter used to define liquid-crystalline systems as it is a measure of the degree of anisotropy. In the following chapters we use the theories discussed here to analyse the relationship between single molecule motion and orientational order in such systems.

Fig. 20 Generalised Result for Dielectric Relaxation

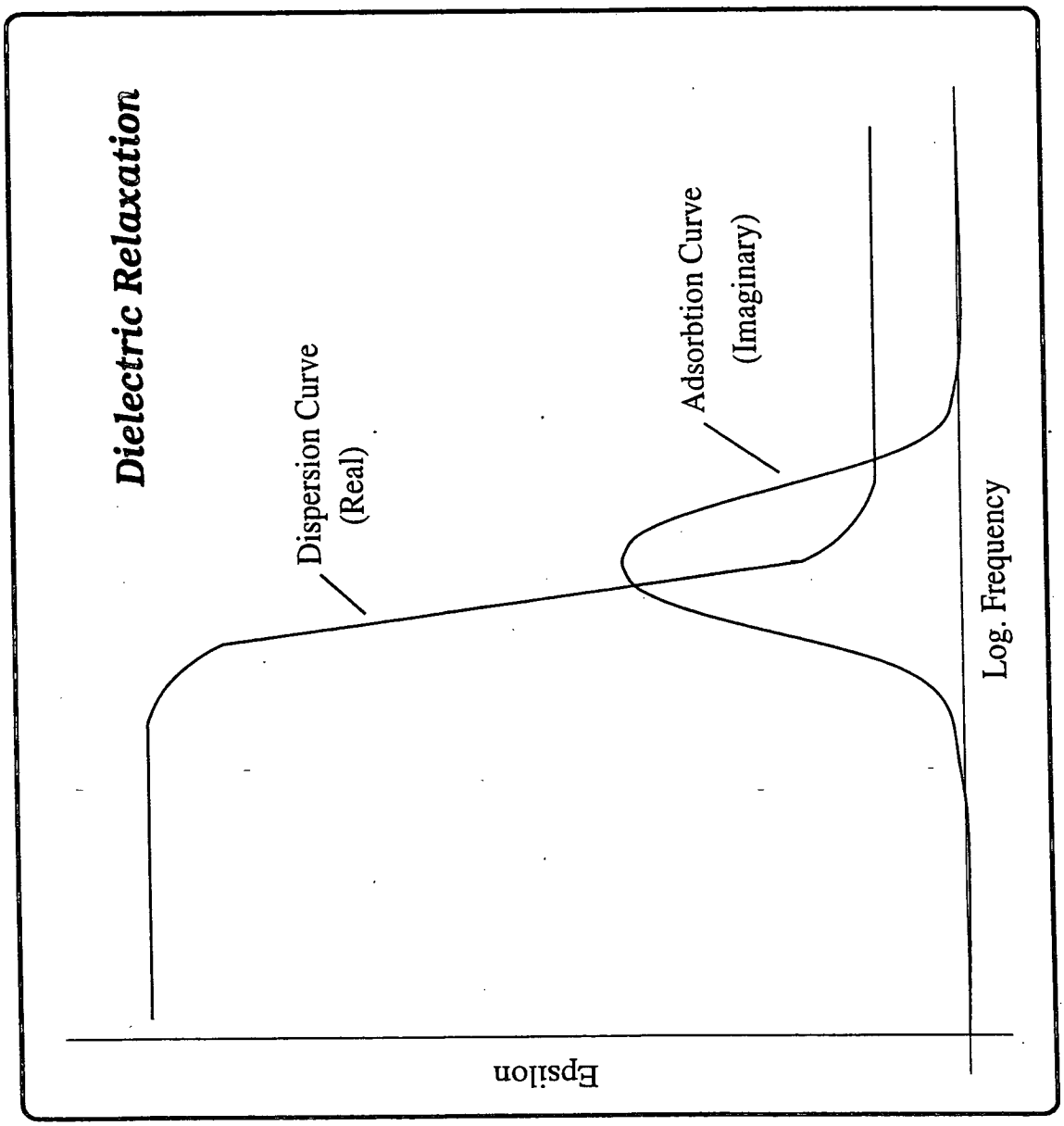

Fig. 21 Calculation of the Retardation Factor

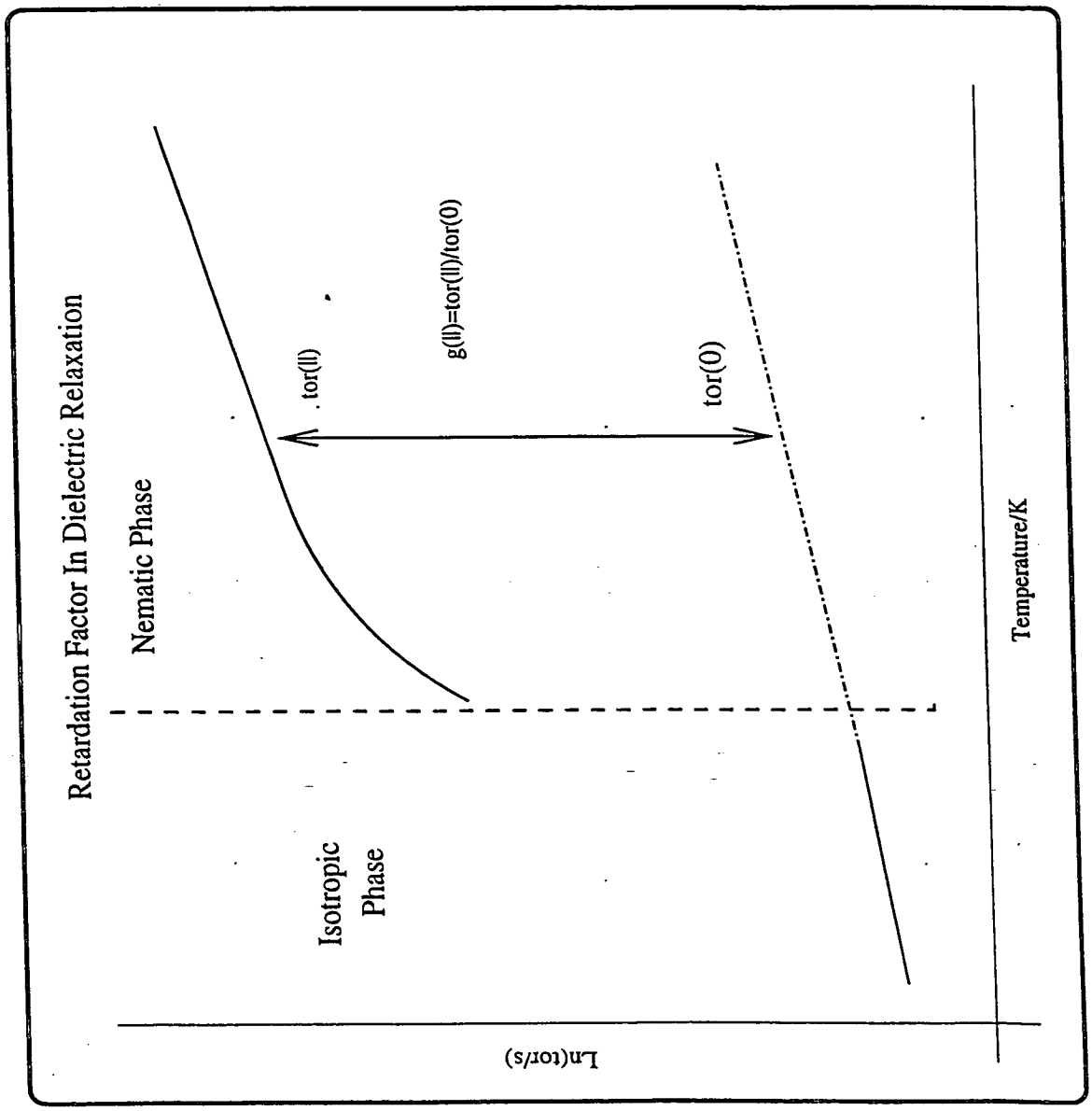

Chapter 8

Dielectric Studies on Liquid Crystals under High Pressure: Low Frequency Relaxation Processes in the Nematic Phase of 6PCH

8.1 Introduction

In this and the following chapter the results of dielectric studies on two liquid crystalline materials under high pressure are presented. It is the study of liquid crystals at both variable temperature and pressure, which allows the extraction of thermodynamic data.The two chosen prototypical liquid crystals are 6PCH (4-trans-4'-n-Hexyl-Cyclohexyl-Benzonitrile) and 8CB (4-n-Octyl-4'-Cyanobiphenyl). Due to the substitution of a cyclohexyl ring for a phenyl ring in the 6PCH, the two molecules are comparable in length. However the 6PCH is much more flexible than the 8CB. In the present chapter the experimental procedure is discussed followed by the presentation, discussion and analysis of results obtained for 6PCH, which exhibits a nematic liquid-crystalline phase. The theories discussed in chapter 7 are used to calculate activation parameters and the order parameter. In the following chapter, results are presented for 8CB, which exhibits both a nematic and a smectic A phase. Comparisons are then made between 6PCH and 8CB in order to analyse the effect of rigidity on the structural anisotropy and reorientation dynamics in liquid crystalline phases. The work presented here was carried out at the Ruhr Universitaet Bochum, in Germany in collaboration with Prof. Wuerflinger.

8.2 Experimental Procedure

An overview of the experimental apparatus is presented in Fig. 22. The autoclave is pressured with compressed oil *via* a spindle press up to a maximum pressure of $300MPa$. A heating and cooling jacket around the autoclave serves to adjust the temperature, which is calibrated using ice-water as a reference. The impedance is measured automatically with a Hewlett-Packard analyser HP 4192, controlled by a personal computer. The high-pressure vessel is made of copper beryllium alloy and closed by a Bridgeman piston with two bores for the electrical leads to the capacitor. Special care is taken to avoid short-circuits between the leads and the vessel. A detailed cross-section view of the measuring cell, which is housed in the autoclave is presented in Fig. 23. The measuring cell is cylindrical and made of stainless steel. It is approximately $5cm$ long with a diameter of $3cm$. The outer electrode is separated from the stainless steel housing by a cylindrical Teflon spacer. There is a $2mm$ gap between the outer and inner electrodes, where the test substance is to be found. At the base of the measuring cell is a reservoir to hold the test substance. The filled measuring cell holds approximately $2cm^3$ of the sample. A special moving piston consisting of two parts separated by an indium seal transmits the pressure on the test substance in the reservoir, which can penetrate to the space between the two electrodes.

The dielectric relaxation was measured in the frequency range between $1kHz$ and $13MHz$. The low conductivity of the test samples allowed the use of a DC bias field $E \simeq 300V/cm$ which was used to orient the sample in the nematic phase parallel to the measuring field. After filling the capacitor with the sample (at a temperature corresponding to the isotropic phase) the dielectric spectra under pressure were obtained by gradually decreasing the pressure at constant temperature, starting from state points close to the melting curve. The temperature stabilisation was better than $\pm 0.2K$, and the accuracy for the pressure measurements was $\pm 0.2MPa$. All results were repeated to check reproducibility.

8.3 Results for 6PCH

The phase diagram for 6PCH is presented in Fig.24 [120]. As can be seen, 6PCH exhibits three distinct thermodynamic phases: isotropic liquid, nematic liquid crystal and the solid crystalline state. At higher temperatures the nematic phase

exists over a broader pressure range. An example of the static permittivity as a function of pressure for a given isotherm is presented in Fig.25. In the nematic phase, the static permittivity is relatively large, indicating a large degree of molecular alignment. On reducing the pressure, the static permittivity slowly decreases. This can be attributed to fact that, as the density decreases at constant temperature, the average intermolecular distance increases, thereby causing a reduction in the extent of intermolecular interaction, which leads to a relaxation in the molecular alignment. At $33MPa$, the system reaches the nematic-isotropic phase transition and the static permittivity drops suddenly to a value of 9.5. Such a result is a distinct sign that a dramatic change in the structural anisotropy of the system has occurred. In the isotropic phase there is no orientational order (by definition, the order parameter is $S = 0$ in the isotropic phase). Due to the fact that the molecules in the nematic phase were aligned parallel to the electric field, it is the parallel component of the static permittivity that is being measured. Assuming the molecule to be a sphero-cylinder, the permittivity tensor can be assumed to be diagonal, with principle elements $\epsilon_{\|}$, $\epsilon_{\perp}$, and $\epsilon_{\perp}$. The static permittivity in the isotropic phase can then be assumed to be the average of these three priciple elements. Decreasing the pressure further results in a negligible change in the static permittivity. This result was obtained for all experimentally investigated isotherms. In each case, the static permittivity well into the nematic phase has a value of 15, which gradually reduces until the phase transition occurs, causing the static permittivity to drop to 9.5, where it remains constant. This result is similar to other experimental results which probe anisotropic properties, in particular optical birefringence.

In Fig.26 some examples of the frequency dependence of the real and imaginary parts of the complex permittivity measured at different pressures in the nematic and isotropic phases of 6PCH are presented. The maxima of the loss curves are shifted to higher frequencies with decreasing pressure. The loss curves were fitted to the Jonscher equation in order to calculate the dielectric relaxation time $\tau_{\|}$ from the frequency of maximum loss. It should be pointed out that it is only the low frequency relaxation that is being measured in the nematic phase (that is the end-over-end tumbling motion). The high frequency relaxation, representative of the spinning motion about the molecular long axis cannot be accessed due to the frequency limit of the impedance bridge at $13MHz$. In the isotropic phase, the low and high frequency processes merge to give one broad relaxation spectrum, which can only be measured in part. The Cole-Davidson equation was employed with a fixed value for ϵ_{∞} to fit the incomplete loss curves.

For each of the dispersion and dielectric loss curves at $337K$ presented in Fig.26, the equivalent Cole-Cole plots are presented in Fig.27. Well in the nematic phase, at $75MPa$, the dielectric spectrum appears to obey a single Debye-type relaxation process very well, resulting in a near perfect semi-circular Cole-Cole plot. On decreasing the pressure, the functional form of the Cole-Cole plots deviates from this semi-circular form. In the isotropic phase the Cole-Cole plot is not semi-circular.

The relaxation times calculated for all isotherms studied are presented in semi-logarithmic form in Fig.28. The most distinctive feature in all isotherms is the dramatic reduction in correlation time at the nematic-isotropic transition. Particularly in the nematic phase, it is clear that the relaxation times are not a strictly exponential function of the pressure, and the $\ln\tau_{\|}$ *vs.* p curves deviate from a straight line, especially for the high-temperature isotherms. Fig.29 shows the activation volumes calculated for the nematic and isotropic phases of 6PCH as a function of temperature, using equation 7.21. For each semi-logarithmic isotherm shown in Fig.28, the gradient over the available pressure range has been calculated. For example, at $334K$ relaxation times were measured at $10MPa$, $15MPa$, $20MPa$ and $25MPa$. Having taken the logarithm of these relaxation times and plotted them against the pressure (see Fig.28), we see that the four points lie, to a good approximation, in a straight line with a gradient of $0.22/15MPa$. Taking this gradient and mutiplying by the gas constant, R, and the temperature, $334K$ (see equation 7.21) gives a value for the activation volume of $40.7cm^3mol^{-1}$, as shown in Fig.29. Due to experimental limitations, it was not possible to accurately measure the relaxation time at $334K$ at pressures less than $10MPa$, and between $25MPa$ and $30MPa$ the 6PCH undergoes a phase transition to the nematic phase. Similarly, activation volumes have been calculated for the other isotherms in the isotropic phase, but over different pressure ranges. The upper most pressure is determined for each isotherm by the phase transition to the nematic phase, whilst the lowest pressure for which a relaxation time could be experimentally measured is determined by the limitations of the experimental equipment. The highest frequency of the external alternating electric field that could be achieved was $13MHz$. As the relaxation time increases, the maximum in the absorption curve shifts to higher frequencies. When the maximum in the absorption curve is greater than $13MHz$ no accurate determination of the relaxation time can be made.

In the case of the nematic phase, calculation of the activation energies is complicated by the fact that the semi-logarithmic isotherms shown in Fig.28 are curved. In this case, the two slowest and fastest relaxation times were ignored, and the gradient was averaged over the remaining data. As an example, the activation volume for the $334K$ isotherm in the nematic phase was calculated over the pressure range $40MPa - 55MPa$ in $5MPa$ steps and then an average overthe calculated values was taken. From the variation in the activation volume as calculted for each $5MPa$ step, it was possible to determine the experimental error. In the same way, using the gradient of the semi-logarithmic isochores and equation 7.19, the activation enthalpy was calculated for the nematic phase as a function of pressure as shown in Fig.30. Due to inaccuracies in the estimation of the very fast relaxation times in the isotropic phase at low pressures, no accurate values of the isotropic activation enthalpy could be calculated.

Using the theory discused in the previous chapter (see equations 7.22 and 7.24), the order parameter in the nematic phase of 6PCH was calculated from the retardation factor as a function of pressure (Fig.31). The author points out, that as the order parameter is dependent on both the temperature and the pressure, in order to be able to compare the results for different isotherms, a physically meaningful reference is required. For this reason the order parameter is plotted for each isotherm as a function $p - p(NI)$, the pressure difference between the absolute pressure at which the order has been calculated and the nematic-isotropic phase transition pressure, which is obviously dependent on the temperature. This will be discussed in more detail in the next section. For all isotherms, the order parameter takes on values between 0.42 and 0.44 deep in the nematic phase. The order parameter decreases very slowly with pressure until the system is $25 - 30MPa$ above the nematic-isotropic phase transition, at which point the order parameter decreases rapidly as the transition pressure is approached.

8.4 Analysis Of Results: Discussion of the Reorientation Dynamics and Molecular Interactions in 6PCH

The analysis of the reorientation dynamics and molecular interactions in 6PCH is complicated by the fact that, unlike in the case of Raman lineshape analysis, the dielectric relaxation experiments only give the correlation times, rather than the

correlation functions. If we are to formulate a model to describe the reorientation dynamics in the nematic phase, it must predict all our available data. In particular the model must explain the large difference in correlation times between the isotropic and nematic phases. It must also account for the non-exponential relationship between τ and p, and the deviation from the Debye type motion as the system approaches the nematic-isotropic transition, indicated by the non-semi-circular form of the Cole-Cole plots. Further, the model must account for the observed decrease in activation volume on increasing temperature, and the observed decrease in activation enthalpy with increasing pressure.

Fig.31 shows the order parameter of 6PCH as a function of the pressure using the nematic-isotropic phase transition pressure as a reference. It is apparent that the order parameter for all isotherms increases with increasing pressure. However, taking a closer look, the order parameter is seen to be larger at higher temperatures for the same $p-p(NI)$. As a specific example, the order parameter for the $340K$ isotherm at $p - p(NI) = 50MPa$ is 0.415 ± 0.1, whilst the order parameter for the $352K$ isotherm at $p - p(NI) = 50MPa$ is 0.435 ± 0.1. From the phase diagram of 6PCH, (Fig.24), the nematic-isotropic phase transition at $340K$ occurs at $30MPa$, whilst at $352K$ the phase transition occurs at $65MPa$. In terms of absolute values, this means that the order parameter of 6PCH is 0.435 ± 0.1 at $352K$, $115MPa$ and 0.415 ± 0.1 at $340K$, $80MPa$. A change in temperature and pressure affect the molecular system in different ways. The effect of a change in pressure is to reduce the space available for the molecules to reorientate. A small change in the pressure applied to a system results in a large change in the density of the system. This steric interaction stabilises the system. It is observed that over the temperature and pressure ranges studied here, the change in pressure has a greater influence on the order parameter which suggests that collisions between molecules cause reorientational relaxation.

The increase in the order parameter, and therefore the molecular alignment in the nematic phase on increasing the pressure is also observed when examining the effect of variation of pressure on the static dielectric constant (Fig.25). In the nematic phase the static dielectric constant increases with increasing pressure. This can be understood as an example of Le Chatelier's principle. In the case of an anisotropic system, such as a nematic liquid crystal, the easiest way to remove the constraint of applied pressure is to increase the molecular alignment. In the isotropic phase, an increase in presssure only results in a decrease of the average intermolecular distance, and so the static dielecric constant in independent of

pressure.

It is unlikely that there is just a single mechanism which accounts for all the intermolecular interactions and reorientation dynamics. It is well understood that in mesogenic molecules possessing a cyano-group, there exists substantial dipole-dipole moment interaction. The nematic phase has a high degree of long-range orientational order, but no long-range translational order. The strong dipole-dipole moment interactions result in an anti-parallel alignment of the mesogenic molecules. Such strong molecular associations could lead to a monomer-dimer equilibrium, which will be temperature and pressure dependent.

A second important factor is the flexibility of the 6PCH molecule. The 6PCH molecule is more flexible than the 5CB molecule, which, as we have already seen, exhibits very fast intra-molecular reorientational relaxation in the short-time limit. The flexibility of the molecule couples the perpendicular and parallel reorientation diffusion coefficients, and thereby could facilitate the end-over-end tumbling motion of molecules in the nematic phase. The onset of molecular alignment and the increased density of the system in the nematic phase might however hinder the flexibility of the molecule.

The dramatic decrease in the relaxation time on passing from the nematic to the isotropic phase can only be rationalised by considering a large change in density at this phase transition. This is visually observed: in the nematic phase, 6PCH is a viscous, opaque substance, whilst in the isotropic phase it is a transparent mobile fluid. It can therefore be argued that in the dense nematic phase, the intermolecular associations due to dipole-dipole moment interactions are very strong. Initially this would appear to be the case, as the activation volume decreases with increasing temperature: as the temperature increases, the molecules acquire more thermal motion, the intermolecular distance increases and the extent of molecular associations decreases. The molecules find that they have more volume in which to reorientate, and so the excess volume (the activation volume) decreases. Unfortunately this model must be relinquished as the activation enthalpy also decreases in the nematic phase as the pressure increases. Following a similar argument to before, an increase in pressure would cause the average intermolecular distance to decrease, and the extent of intermolecular associations would therefore also increase. In order to reorientate, the molecules must find the excess enthalpy to overcome the intermolecular interaction, and so the activation enthalpy would be seen to increase with pressure. This process might well occur, but it certainly isn't the predominent mechanism, as the activation enthalpy is

seen to decrease with increasing pressure.

The flexibility of the molecule also fails to provide a suitable solution: as the pressure increases, the flexibility of the molecule in the nematic phase decreases, and hence the molecule is less capable of bending round the neighbouring molecules in order to achieve reorientation. The less flexible the molecule, the more it must push the surrounding molecules out of its path in order to rotate, which would once again result in an increase in activation enthalpy with increasing pressure.

Having dismissed the molecular flexibility and the diple-dipole molecular association theories as the primary reorientation mechanism, only the argument based on collisions between molecules remains. It does not initially appear too promising, that as the pressure increases, the collision frequency decreases, resulting in the decrease of the activation enthalpy. However, it can be argued that an increase in the orientational alignment of the molecules facilitates reorientational motion: in a system where the constituent molecules are aligned, any molecule attempting to reorientate will be channelled between neighbouring aligned molecules. The effect of an increase in pressure, as previously discussed, is to increase the orientational alignment, and hence the order parameter. As the order parameter increases, the reorientational motion of the constituent molecules is aided by the channelling effect and the activation enthalpy is seen to decrease with increasing pressure.

In order to support the proposed model, it is necessary to justify the other observed experimental results. The are two arguments to explain how the activation volume might decrease with an increase in temperature in the nematic phase. On the one hand we can argue that the increased thermal motion of the molecules reduces the extent of molecular alignment. Paradoxically, however, at the same time the average intermolecular distance increases, causing the molecular flexibility to increase. The molecules can now bend around their neighbours thereby lowering the activation volume. However, the author prefers a more subtle argument as follows: at each subsequent value of the activation volume with increasing temperature, the absolute value of the pressure has also increased. As the order parameter is more susceptible to increases in absolute pressure, rather than absolute temperature, the net effect is a very slight increase in the order parameter from one isochore to the next. Due to the increase in order parameter, the reorientational motion of the molecule, as previously discussed, is aided by a channelling effect, resulting in a decrease of activation volume with an increase in temperature.

It remains to discuss the non-exponential behaviour of the τ *vs.* p graph and the deviations in the Cole-Cole plots. At very high pressures in the nematic phase, close to the respective freezing curve, the order parameter is (comparatively) very large. The molecules are well aligned and the system is dense. The individual molecules do not possess a high degree of flexibility and, due to molecular alignment, one molecule's immediate environment is fairly similar to any others. The molecular orientation is aided by the alignment of the molecules. The time-scale on which the each molecule rotates is similar, as any deviations are simply due to the orientational distribution of the surrounding molecules (as S is not at unity). There is therefore a single relaxation process with a single associated relaxation time, dependent on the extent of molecular alignment. The Cole-Cole plot shows Debye-type motion. As the pressure decreases, there is initially only a very small change in the order parameter. However, the average intermolecular distance increases and so does the molecular flexibility, whilst the the extent of dipole-dipole interactions decreases. The combined effects of a decrease in density, a decrease in the extent of dipole-dipole interactions and an increase in the average intermolecular distance and the residual orientational order combine to give an increase in the reorientational relaxation time. As the distribution of molecular orientations has increased, the relaxation is now affected by several competing mechanisms. The Cole-Cole plot becomes increasingly skewed, as the relaxation time deviates from an exponential function of pressure. When the system reaches the nematic-isotropic phase transition, the density reduces dramatically, molecular orientation is lost and the relaxation time falls steeply. The molecules in the isotropic state are extremely flexible and the average intermolecular distance very large, rendering the activation volume temperature independent.

In the following chapter the proposed model will be applied to 8CB, a less flexible mesogenic molecule, and will be extended to include the reorientation dynamics in the smectic A phase. A summary of the discussion provided in this chapter will be presented in chapter 9, after comparing the results for 6PCH and 8CB.

Fig. 22 Dielectric Relaxation Apparatus

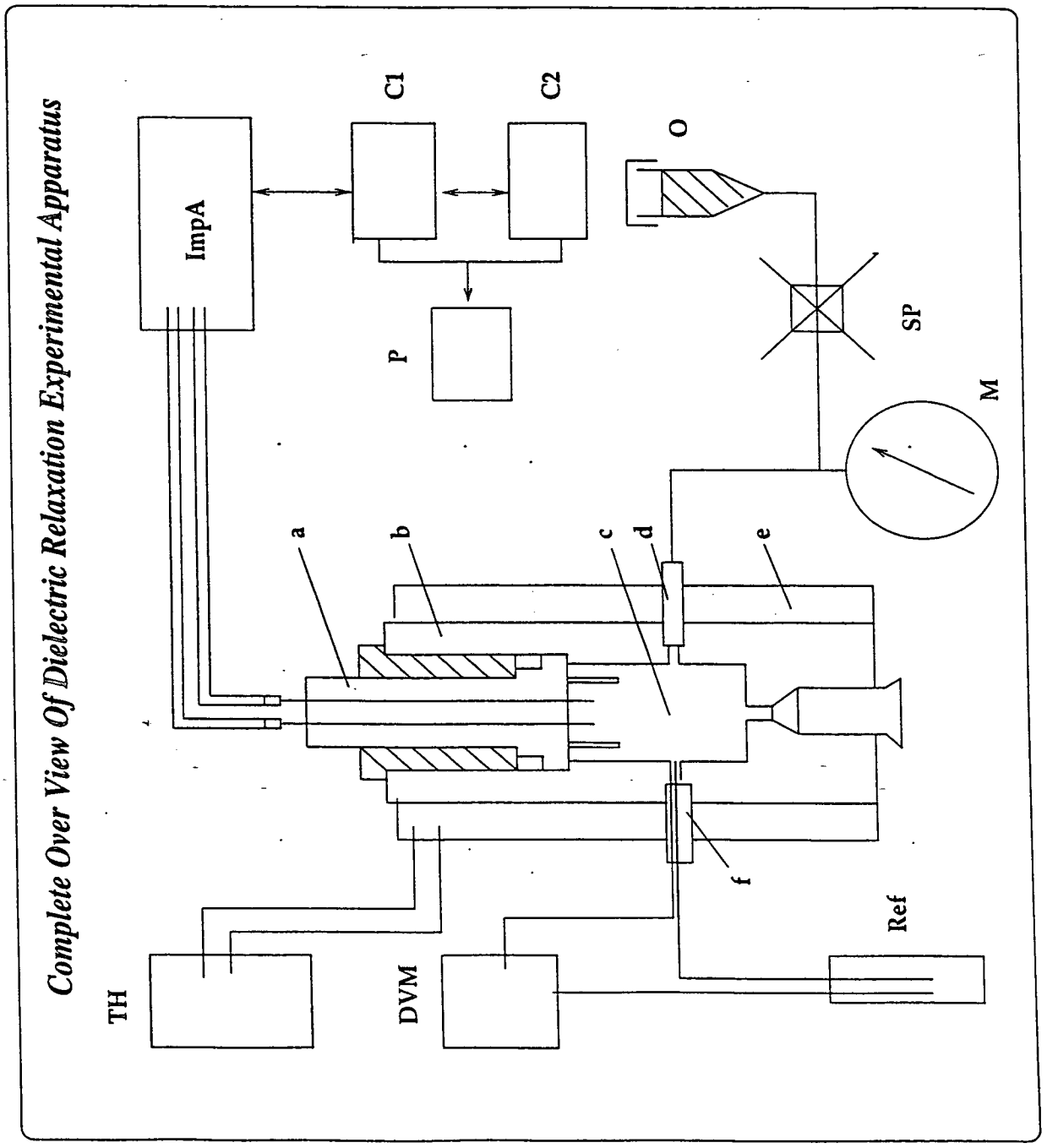

TH: Thermostat, DVM: Digital Volt Multimeter, Ref: Ice-Water Reference, M: Manometer, SP: Spindle Press, O: Oil Reservoir, C1: Computer 1, C2: Result Analysis Computer, P: Printer, ImpA: Impedence Analyser.
a: Bridgeman Piston, b: Autoclave, c: Cavity for Measuring Cell, d: High Pressure Capillary, e: Heating/Cooling Jacket, f: Chrome-Aluminium Thermoelement.

Fig. 23 The Dielectric Mesuring Cell

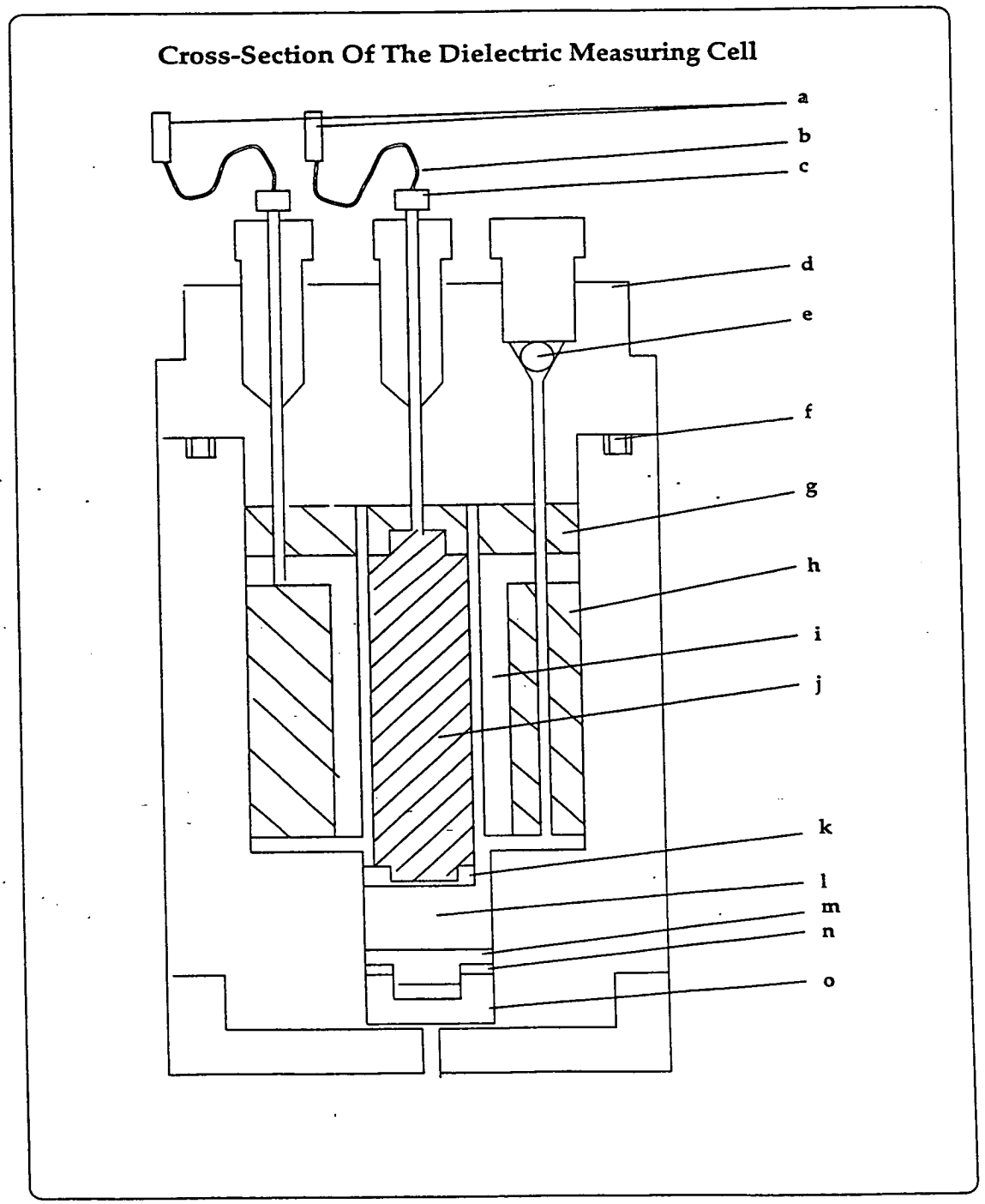

a: Electrical Contacts, b: Flexible Insulated Connection Wires, c: Insulating Cap, d: Stainless Steel Casing of Cell, e: Stopper, f: Rubber Washer, g: Upper Teflon Insulating Cap, h: Teflon Insulator to separate Outer Electrode from Cell Casing, i: Outer Electrode, j: Inner Electrode, k: Lower Teflon Insulating Cap, l: Cavity to hold Sample, m: Upper Part of Moving Piston, n: Indium Sealing, o: Lower Part of Moving Piston.

Fig. 24 6PCH Phase Diagram

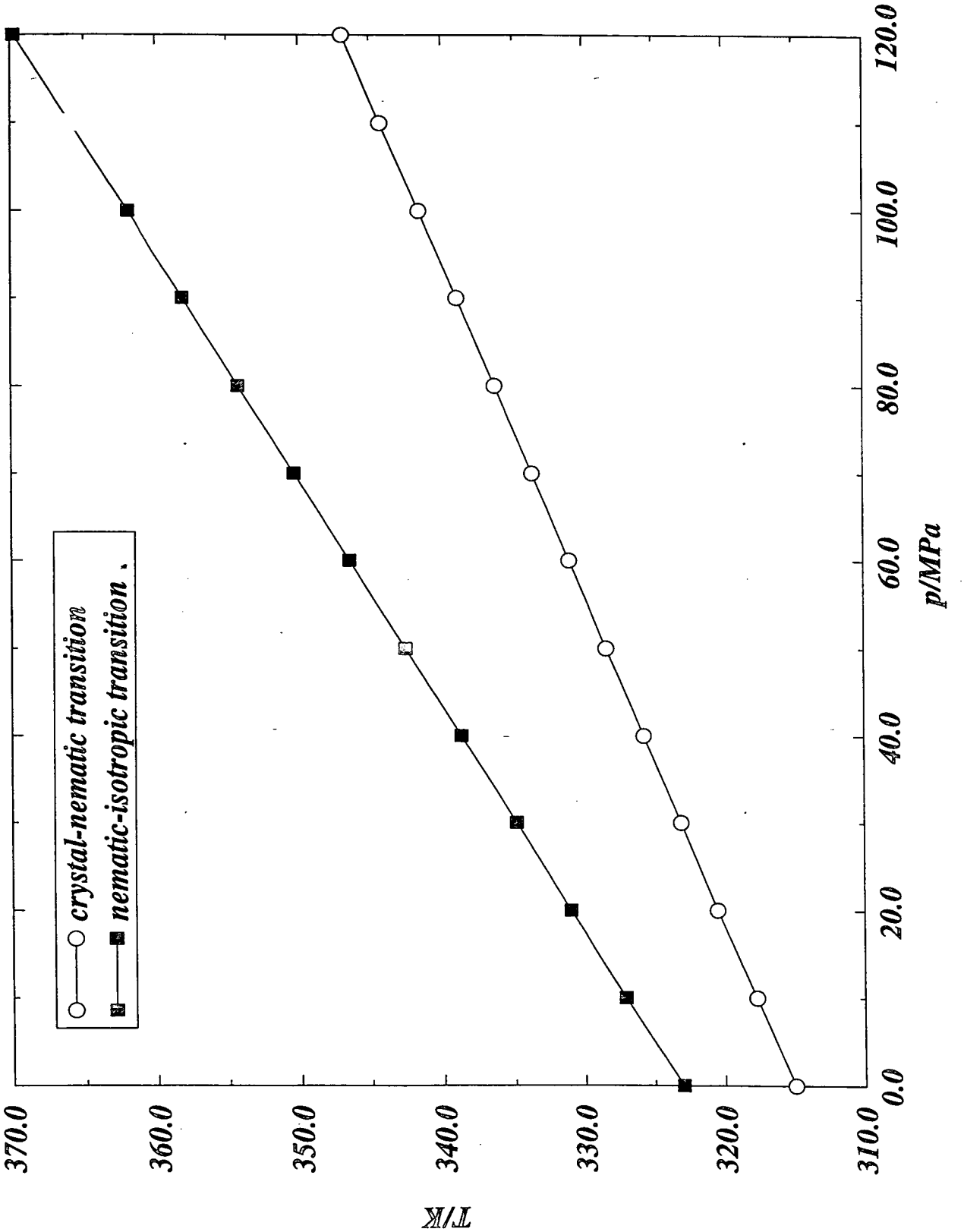

Fig. 25 Pressure Dependence of the Static Permittivity 6PCH at 337K
[Dashed Line Represents ni Phase Transition]

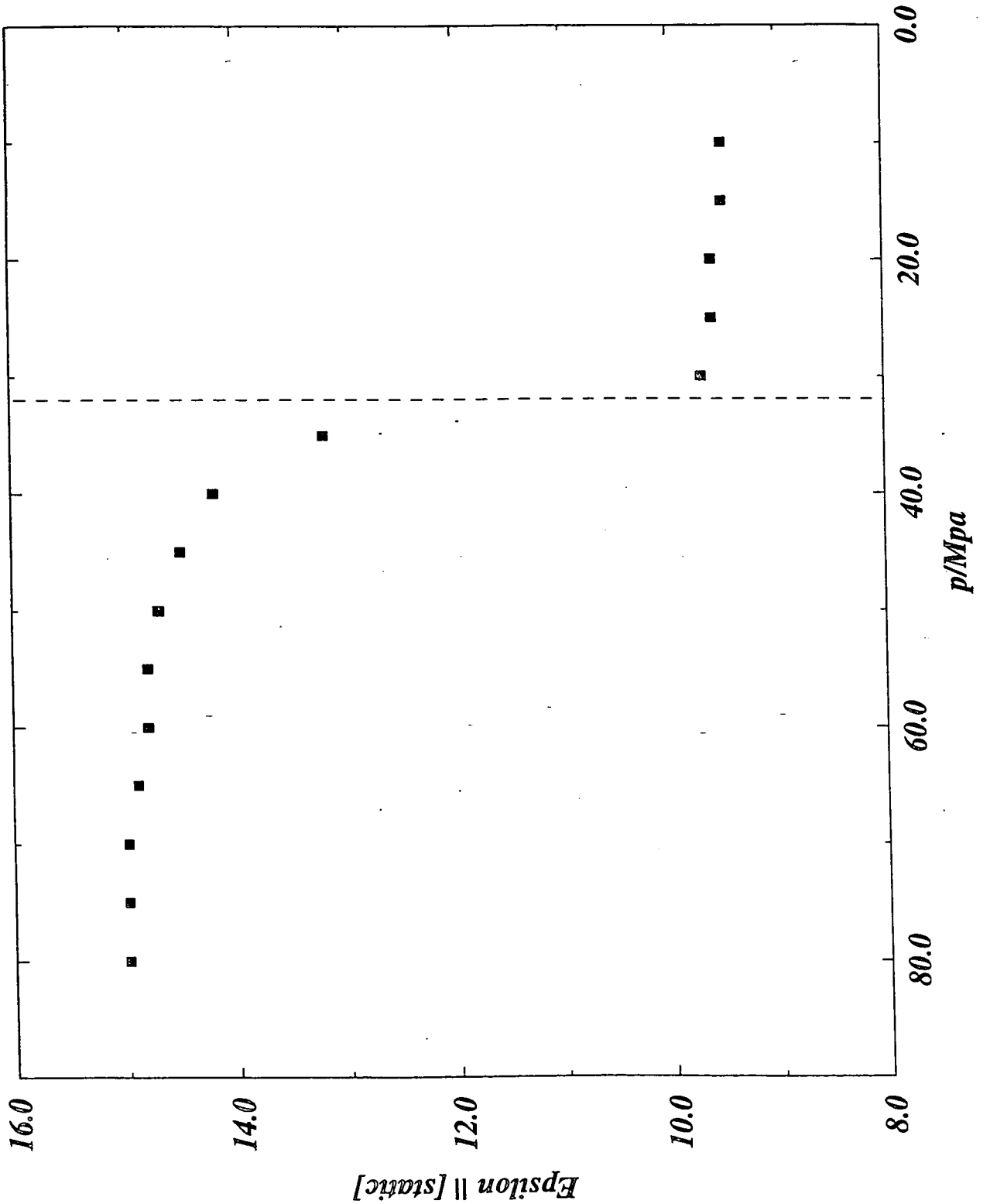

Fig. 26 Dispersion and Dielectric Loss Curves
6PCH 337K Isotherm

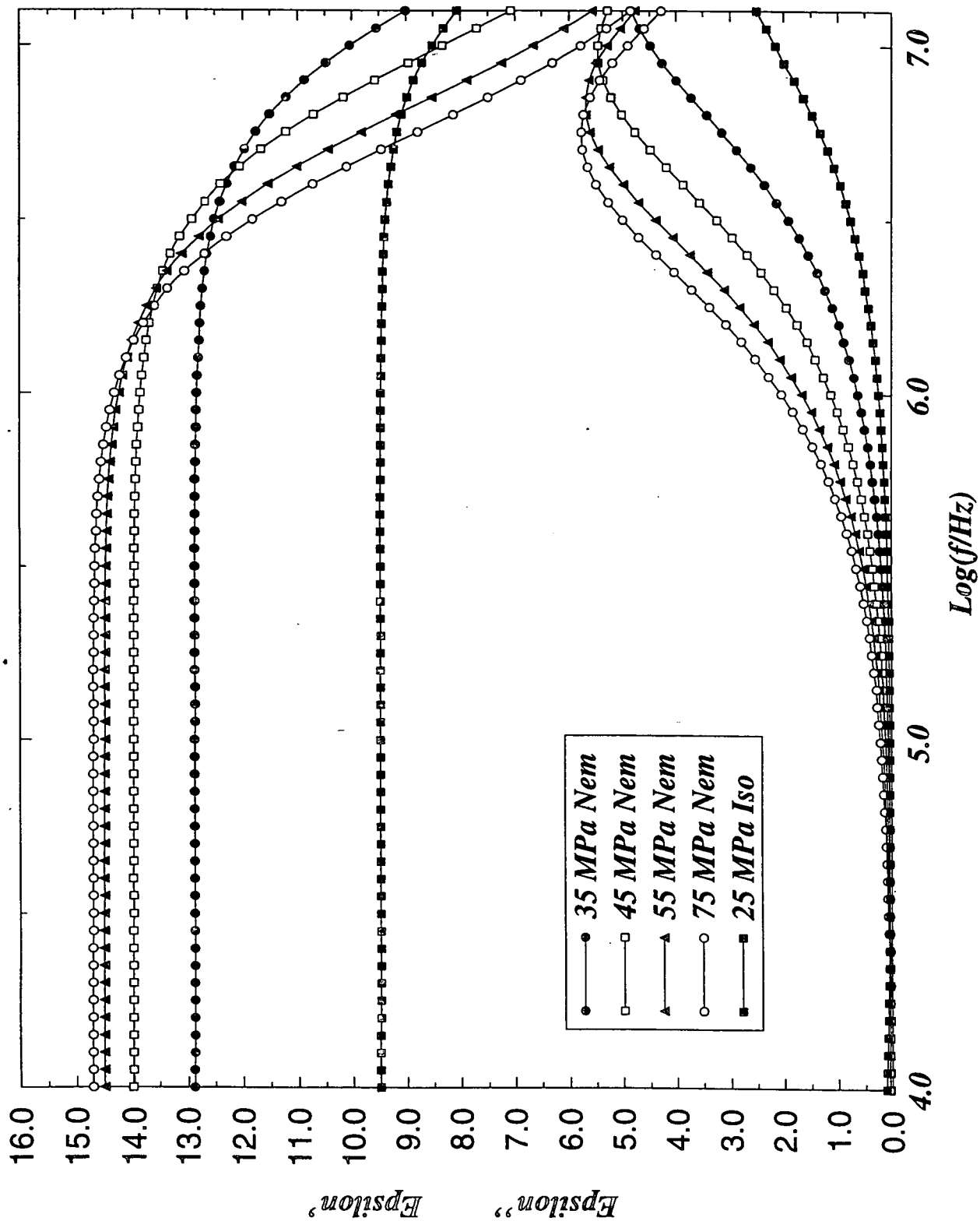

Fig. 27 Cole-Cole Plot 6PCH 337K Isotherm

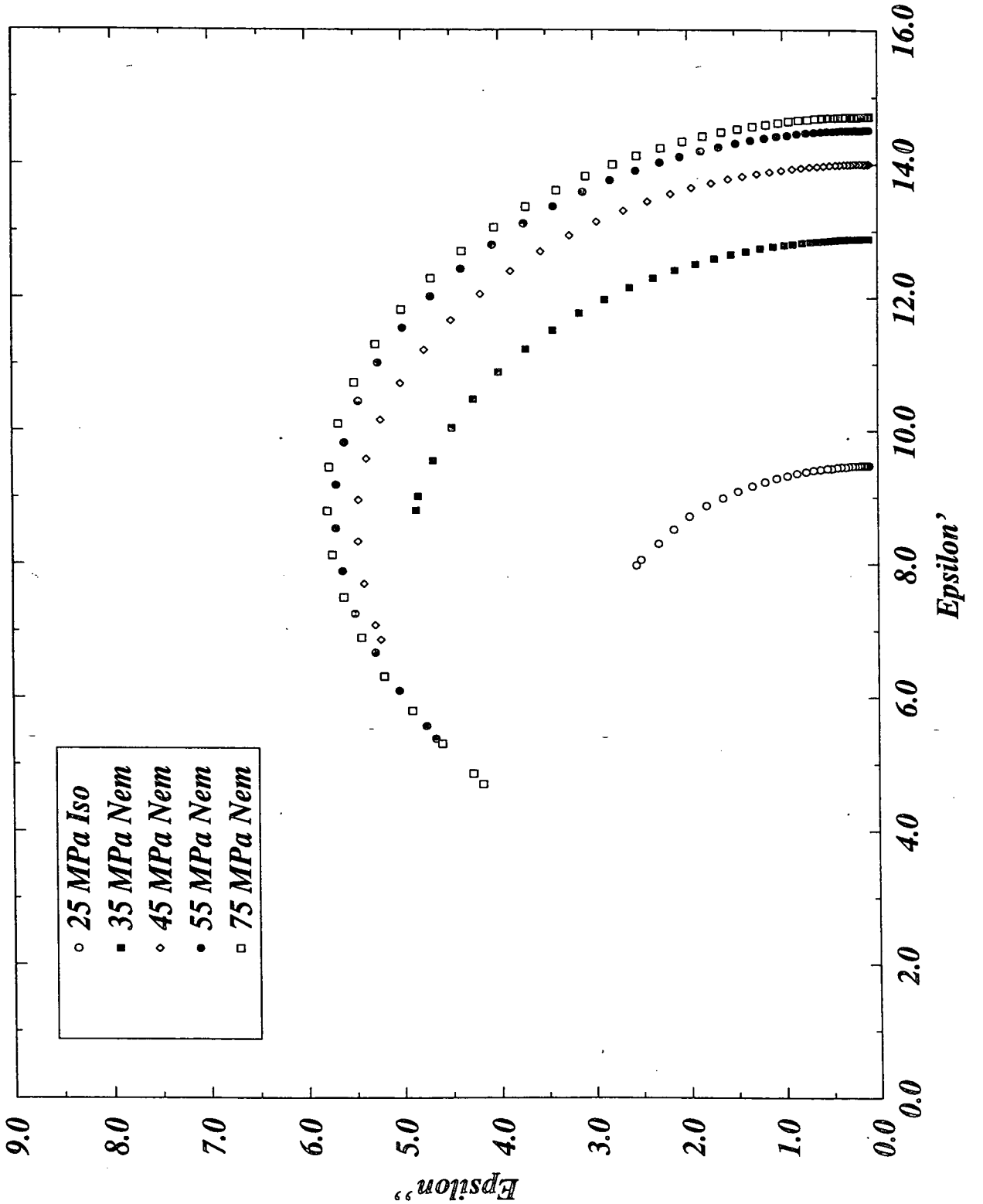

Fig. 28 Logarithm of the Dielectric Relaxation Time as a Function of Pressure 6PCH in Nematic and Isotropic Phases

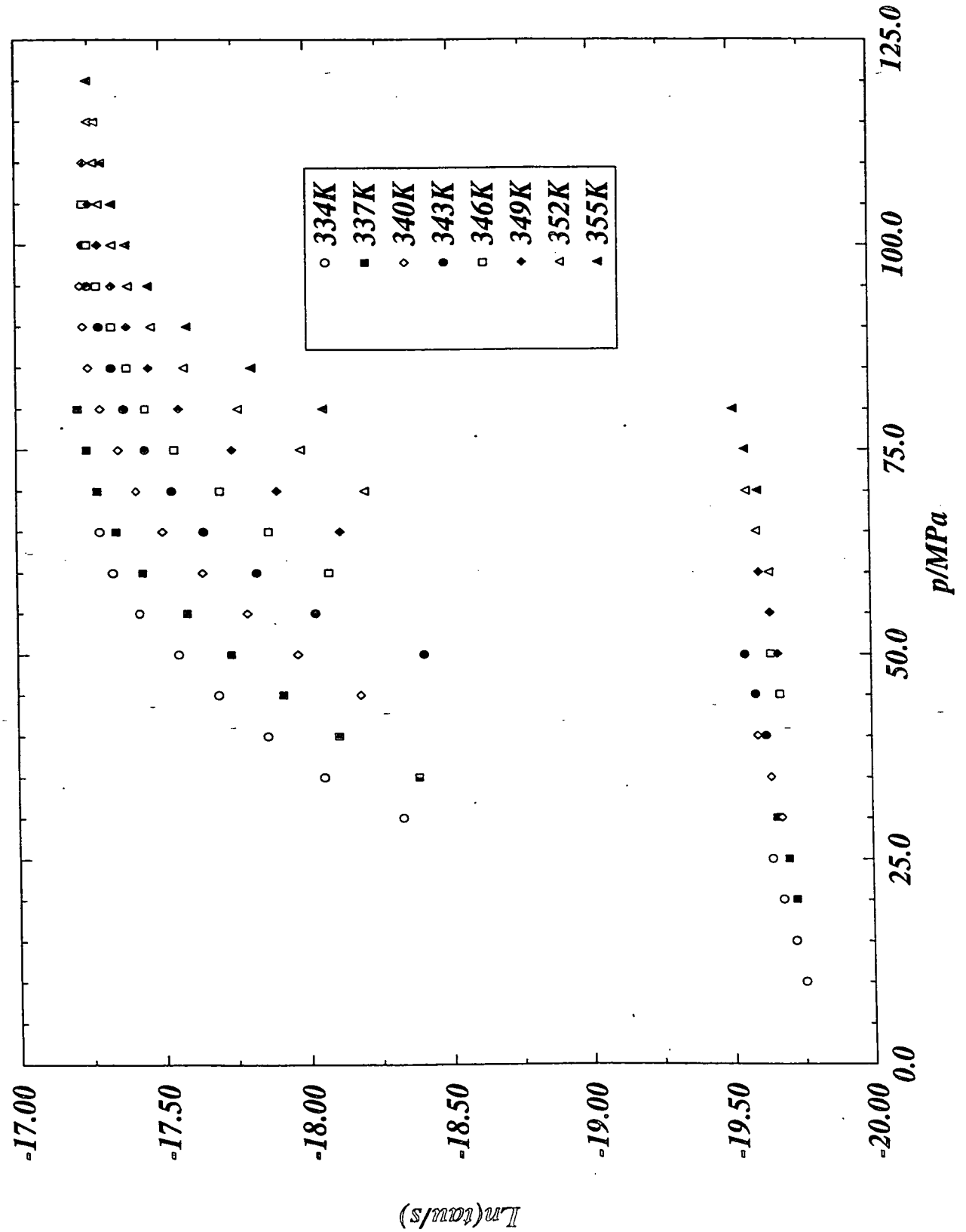

Fig. 29 Activation Volumes for 6PCH as a Function of Temperature

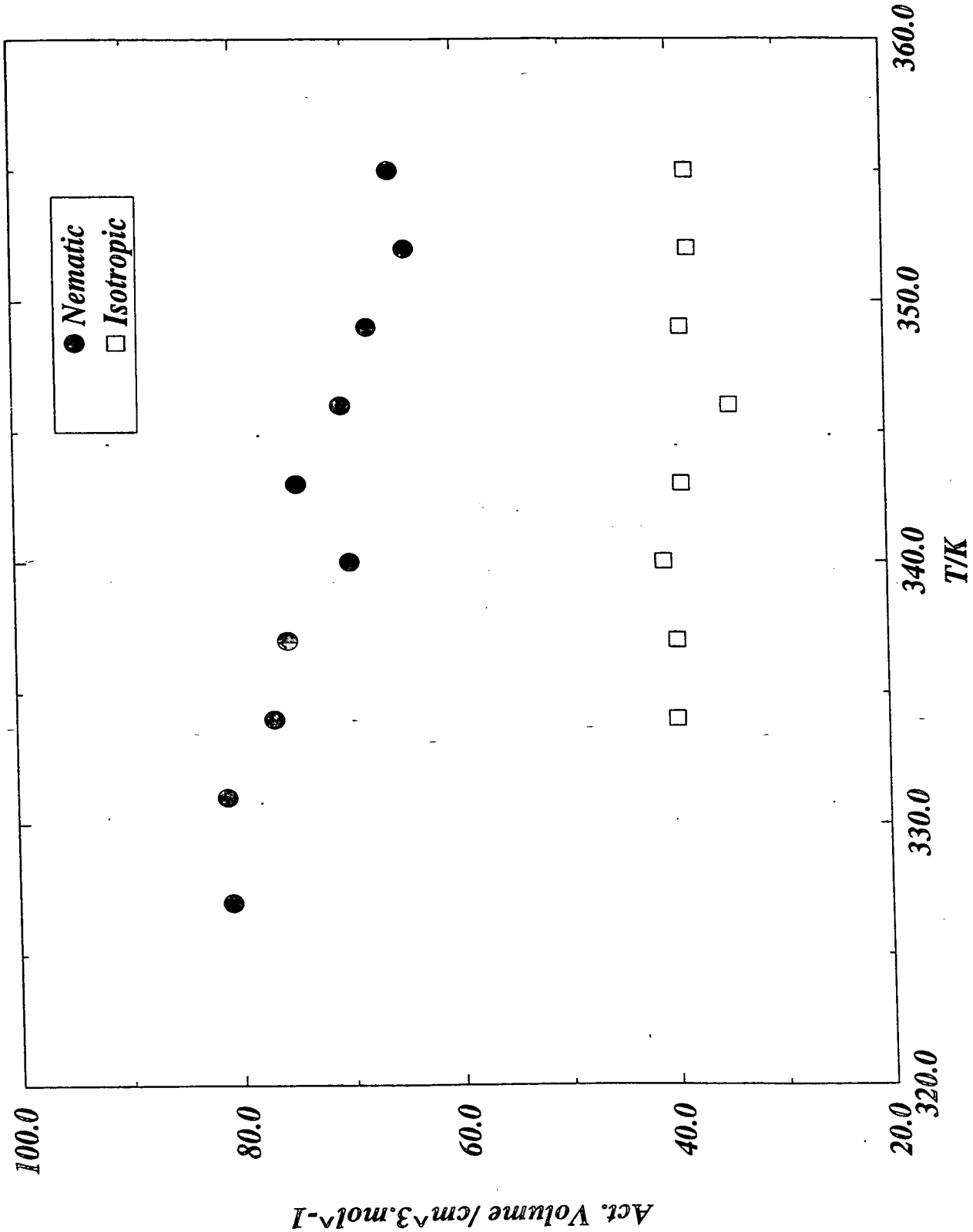

Fig. 30 Activation Enthalpies for 6PCH in the Nematic Phase

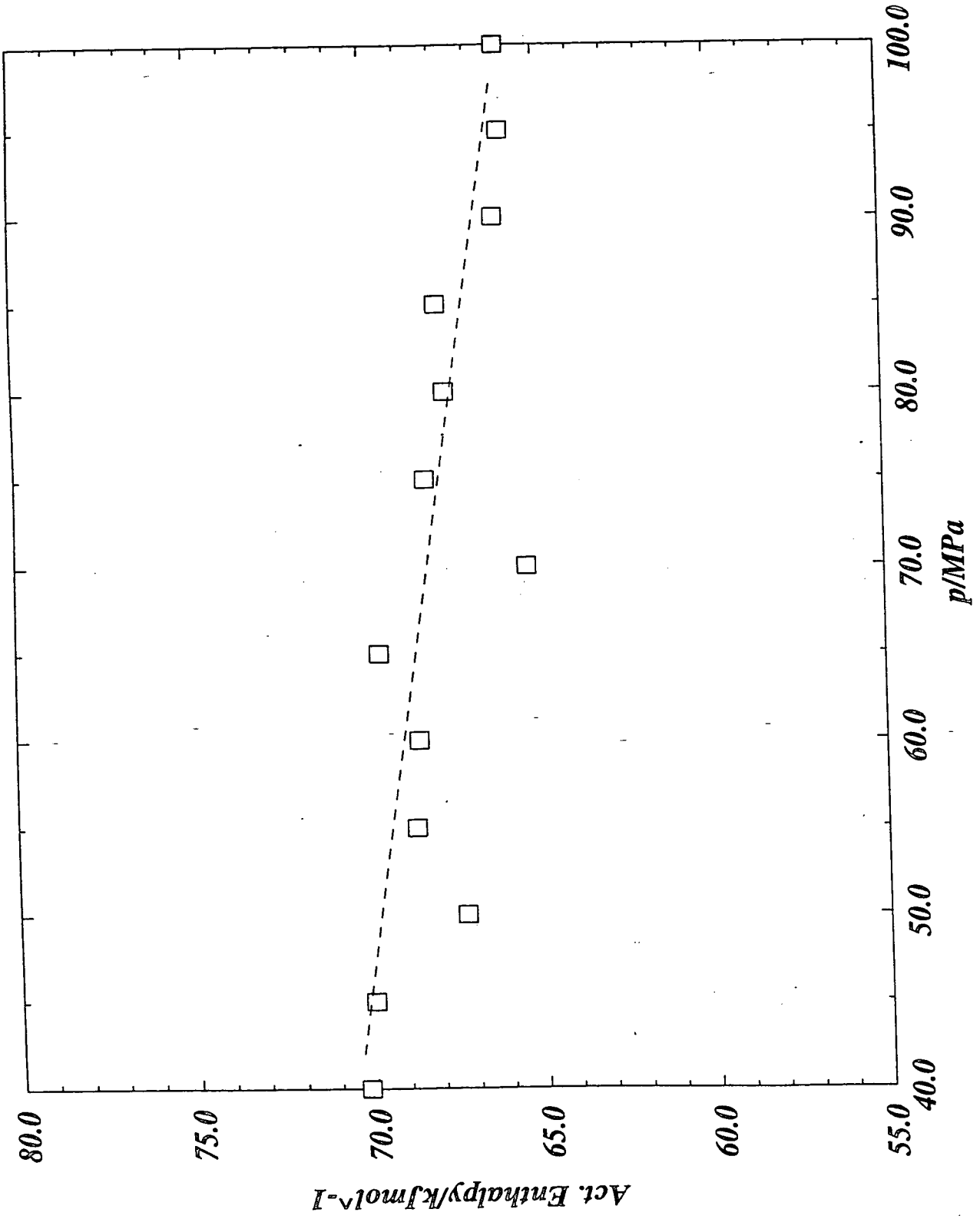

Fig. 31 6PCH Order Parameter as a Function of Pressure

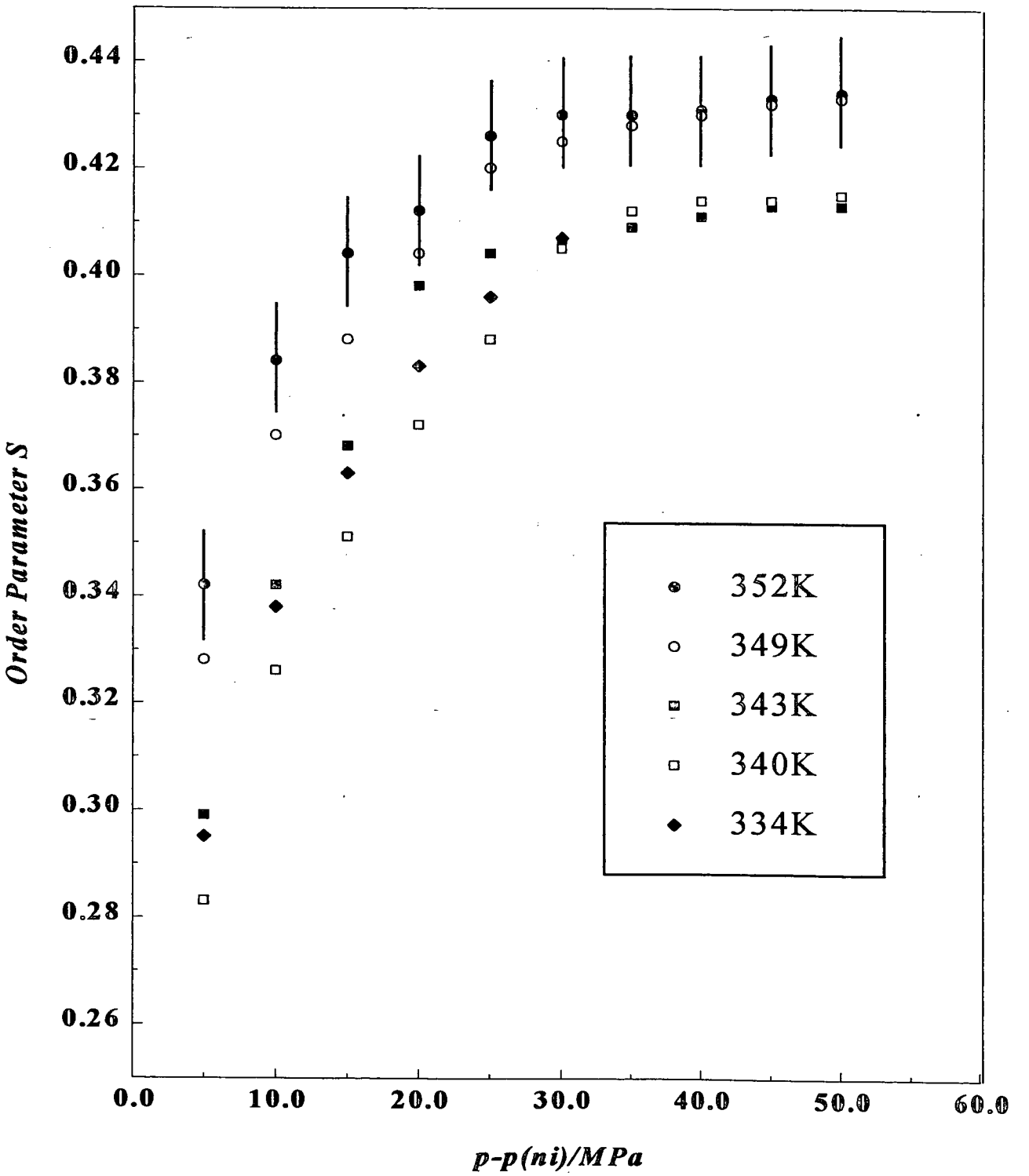

Chapter 9

Dielectric Relaxation Study of 8CB

9.1 Introduction

In this chapter results are presented for dielectric relaxation studies on 8CB at variable temperature and pressure. The experimental apparatus and procedure have already been discussed in the previous chapter. The temperature range studied was from $305K$ to $361K$, and the pressure range varied from $1MPa$ to $225MPa$. Over such a temperature and pressure range measurements were obtained for the isotropic, nematic and smectic A phases as shown in Fig.32 [121]. 8CB is the lowest homologue of the nCB homologous series to exhibit a smectic A phase. Despite the fact that it's molecular mass is different from that of 6PCH, the two molecules are comparable in terms of molecular length, but do not possess the same degree of flexibility. A direct comparison of the results obtained for 8CB and 6PCH allows an investigation into the effect of flexibility on the dynamics and structural anisotropy of molecular systems. Many of the phenomena observed in the results for 8CB in the nematic and isotropic phase are similar to those observed in 6PCH. The author therefore concentrates on the results obtained in the smectic A phase. At the end of the chapter, differences between the two mesogens are discussed.

9.2 Results of Dielectric Studies on 8CB

The static permittivity as a function of pressure for the $336K$ isotherm of 8CB is presented in Fig.33. As discussed for 6PCH the static permittivity in the isotropic phase is relatively low at a value of 9.5, and appears to be independent of pressure. There is a dramatic increase in the magnitude of the static permittivity observed in the nematic phase, qualitatively indicative of the presence of substantial structural anisotropy. At this point the author points out that the absolute value of the static permittivity in the nematic phase of 8CB cannot be compared directly to that in 6PCH in order to determine the relative degree of molecular ordering. The reason for this is that due to the anti-parallel packing arrangement seen in both nematogens, the effective dipole moment per molecule in the macroscopic system (which can be calculated from the experimentally obtained parallel component of the static permittivity) is much lower than the actual dipole moment. The Kirkwood correlation factor g_k for 8CB has been found to be 0.4 [122].

The magnitude of the static permittivity in the smectic A phase is lower than that in the nematic. Indeed there is a distinct kink in the static permittivity at the nematic-smectic A phase transition. This result is initially surprising as it suggests that the relative degree of molecular alignment in the smectic A phase is lower than that in the nematic phase. However, this unusual result can be explained by considering that the DC bias electric field used to align the molecules in the nematic phase parallel to the probing AC electric field is not strong enough to align the smectic A layers. Therefore, whilst the molecular alignment in the smectic A layers is greater than in the nematic phase, the layers themselves exist as undulating slabs, which sit at different angles relative to the probing AC electric field. The net result is that the (macroscopic) static permittivity is seen to decrease.

In Fig. 34 the dispersion and dielectric loss curves for the $336K$ isotherm are presented in the isotropic, nematic and smectic A phases. The lower static permittivity in the smectic A phase relative to the nematic phase is apparent from the dispersion curves even at higher field frequencies. Once again, the maxima of the loss curves are shifted to higher frequencies with decreasing pressure. The Jonscher equation was preferred for calculating the dielectric relaxation time $\tau_{\|}$ from the frequency of maximum loss. Semi-logarithmic plots of the relaxation time versus pressure are shown for a large number of isotherms in Fig.35. It is immediately apparent that the increase in the dielectric relaxation time at the

smectic A-nematic phase transition is nowhere near as dramatic as the increase in relaxation time at the nematic-isotropic transition. Indeed, particularly for the higher temperature isotherms, the only precise way of experimentally observing the smectic A-nematic transition from dielectric measurements is to look for the kink in the static permittivity. PVT meaurements on 8CB have shown that the volume change associated with the smectic A-nematic transition is also very small compared to that observed at the nematic-isotropic transition [123]. This suggests that whilst the nematic-isotropic transition is most definitely first-order, the smectic A-nematic transition is either very weakly first-order or second-order, as is well known. The second point to make is that the increase in relaxation rate through the nematic phase on decreasing pressure is not as fast as that observed for 6PCH, and the $\tau_{||}$ *vs.* p relationship can be much better fitted to that of an exponential.

The respective Cole-Cole plots are presented in Fig.36. The Cole-Cole plot for the nematic shows an almost perfect semi-circular form, whilst the Cole-Cole plot for the isotropic phase is skewed. The smectic A phase Cole-Cole plot is not semi-circular, but slightly skewed. Activation volumes for all three phases are shown in Fig.37. The calculation of the activation volume from the semi-logarithmic isotherms has been discussed in detail in the previous chapter. All three phases show decreasing activation volumes with an increase in temperature. The largest activation volumes are observed in the nematic phase, the smallest in the smectic A phase. Activation enthalpies for all three phases are shown in Fig.38. The largest activation enthalpies are observed in the nematic, the smallest in the isotropic phase. With increasing pressure the nematic and smectic A activation volumes are observed to decrease, whilst the isotropic activation enthalpy increases rapidly. Due to the availability of pVT data for 8CB it is possible to calculate the activation energy (Fig. 39). (At the time of writing, no 6PCH pVT data is available.) The nematic phase shows the largest activation energy, the isotropic phase the smallest. The activation energy is seen to remain constant in all phases across the entire range of activation volumes. The temperature and pressure dependences of the activation parameters correspond well to previous results on other similar liquid crystals [124,125,126,127]. Such data will prove very important in the next section when extending our model mechanism to describe the reorientation dynamics in this system. Finally, the order parameter has been calculated for the nematic phase of 8CB for various isotherms (Fig. 40). Once again, the higher temperature isotherms exhibit greater order parameters, suggesting that the order parameter in this system is also more susceptible to

changes in the absolute pressure than the absolute temperature (a steric *vs.* kT argument.) This phenomenon has been rigorously argued in the previous chapter. It can also be seen that the magnitude of the order parameter in the nematic phase for all isotherms is greater than that observed in the case of 6PCH.

9.3 Discussion of Results and Comparison of 6PCH and 8CB

In the previous chapter a model was proposed to describe the relaxation mechanism in the nematic phase of 6PCH. The author tentatively suggests that the predominent reorientation mechanism is that of steric interaction and that an increase in the molecular alignment facilitates reorientational relaxation *via* a chanelling effect. However, it did appear that other relaxation mechanisms, including the effect of molecular flexibility were playing some role in the reorientation dynamics. In 8CB the degree of molecular flexibility is much less than in 6PCH. In this chapter the author attempts to extend the model and describe the reorientational relaxation process in the smectic A phase. Comparison of experimental data from the two mesogens (8CB and 6PCH) allows us to try to interpret the effect of flexibility on the dynamics and structuring in these systems. Before beginning the discussion, the author points out that due to differences in density of the two systems, a direct comparison of the magnitude of the activation parameters is invalid. However, differences in the variations of the activation parameters as a function of temperature/pressure need to be explained.

The activation volume in the nematic and isotropic phases of 8CB is seen to decrease with increasing temperature. For the case of the nematic phase, the author has already suggested that, despite the fact that the temperature is increasing, the order parameter is more susceptible to the increase in absolute pressure, so there is a net increase in molecular alignment, which facilitates reorientational motion, resulting in the observed decrease in activation volume. In the isotropic phase for 6PCH however, the activation volume appeared to be independent of temperature. The author suggests that the flexibility of the 6PCH molecule means that it can bend around the neighbouring molecules even at relatively small intermolecular distances. The more rigid 8CB molecule cannot do this and so the activation volume is very much more dependent on the average intermolecular distance. This is a possible explanation for the marked temperature dependence

of the activation volume of 8CB in the isotropic phase. The activation volume of the smectic A phase over the entire temperature domain studied is seen to be lower than the respective activation volume in the nematic phase. The author suggests that as the molecular alignment in the smectic A phase is greater than that in the nematic phase, the reorientational motion is facilitated even further, resulting in lower values for the activation volume.

Due to the extensive pressure range study of the 8CB it was possible to calculate activation enthalpies for the isotropic phase. In comparison to the nematic and smectic A phases, in the isotropic phase the activation enthalpy increases dramatically with pressure. We can assume that as the pressure increases, the average intermolecular distance decreases dramatically. However, unlike in the nematic and smectic A phases, the increase in pressure does not result in an increase in the extent of molecular alignment (i.e.$S = 0$). As 8CB is not particularly flexible, the steric interaction between the rod-like molecules as they rotate increases with pressure, resulting in an increase in the activation enthalpy. In the nematic and smectic A phases, an increase in pressure results in an increase in molecular alignment facilitating molecular reorientation and decreasing the extent of steric hindrance resulting in a decrease in the activation enthalpy in these phases. However, the author notes that a difference of $20kJmol^{-1}$ between the nematic and smectic A activation enthalpies over the entire pressure range studied is too large to be explained purely in terms of the extent of molecular alignment. It appears that the layered structure in the smectic A phase increases the channelling effect, resulting in such a large difference in the activation volumes for the smectic A and nematic phases.

For all activation volumes, the activation enthalpy in the smectic A phase is lower than that in the nematic phase. In general, the ratio of the activation energy to the activation enthalpy gives a quantitative measurement of the extent that steric hindrance plays in the reorientational motion. Due to the decrease in activation enthalpy with increasing pressure, steric hindrance in the smectic A phase is seen to account for 80% of the total activation enthalpy at higher pressures (compare Fig.38 and Fig.39).

In comparison to 6PCH, 8CB is less flexible. This might be the reason why the τ *vs.* p relationship in the nematic and smectic A phases of 8CB shows a much better fit to an exponential. However, it is surprising that the Cole-Cole plot for the smectic A phase of 8CB is more skewed than the nematic. A possible explanation could be that the anti-parallel packing configuration of the

bilayer in the smectic A phase causes an increase in the repulsive CN dipole-dipole interaction, resulting in a secondary, less prominent reorientational relaxation mechanism.

9.4 Summary

From the dielectric relaxation results of 6PCH and 8CB, the author has proposed a model for reorientational relaxation in liquid crystalline phases. It is suggested that the predominant relaxation mechanism is controlled by steric effects, whereby molecular alignment is seen to facilitate reorientational motion *via* a channelling effect. In both mesogens over the temperature and pressure ranges studied, the order parameter appears to depend more on changes in pressure than changes in temperature. However, molecular flexibility and dipole-dipole interactions also promote alternative relaxation mechanisms. The extent that these alternative relaxation mechanisms play in the reorientation dynamics varies through the smectic A, nematic and isotropic phases. In the smectic A phase, the layered structure and the anti-parallel packing configuration promote the CN dipole-dipole interaction. The molecular flexibility seems to play a greater role on the relaxation dynamics in the nematic and isotropic phases. As a general observation, at any given phase point relative to the nematic-isotropic phase transition, the order parameter in 8CB is always greater than that in 6PCH. This suggests that the rigidity of the molecule not only determines the magnitude of the order parameter, but also the stability of the nematic phase.

The calculated activation parameters support the proposed model. By comparing values of activation energy to activation enthalpy, it appears that in all phases steric hindrance accounts for at least 50% of the total activation enthalpy. In the denser phases, such as the smectic A phase, the effect of steric hindrance increases to as much as 80% of the total activation enthalpy (compare Fig.38 and Fig.39). The observation that the activation volume in the smectic A and nematic phases decreases with increasing temperature is considered to support the argument that molecular alignment facilitates reorientational motion.

Fig. 32 8CB Phase Diagram

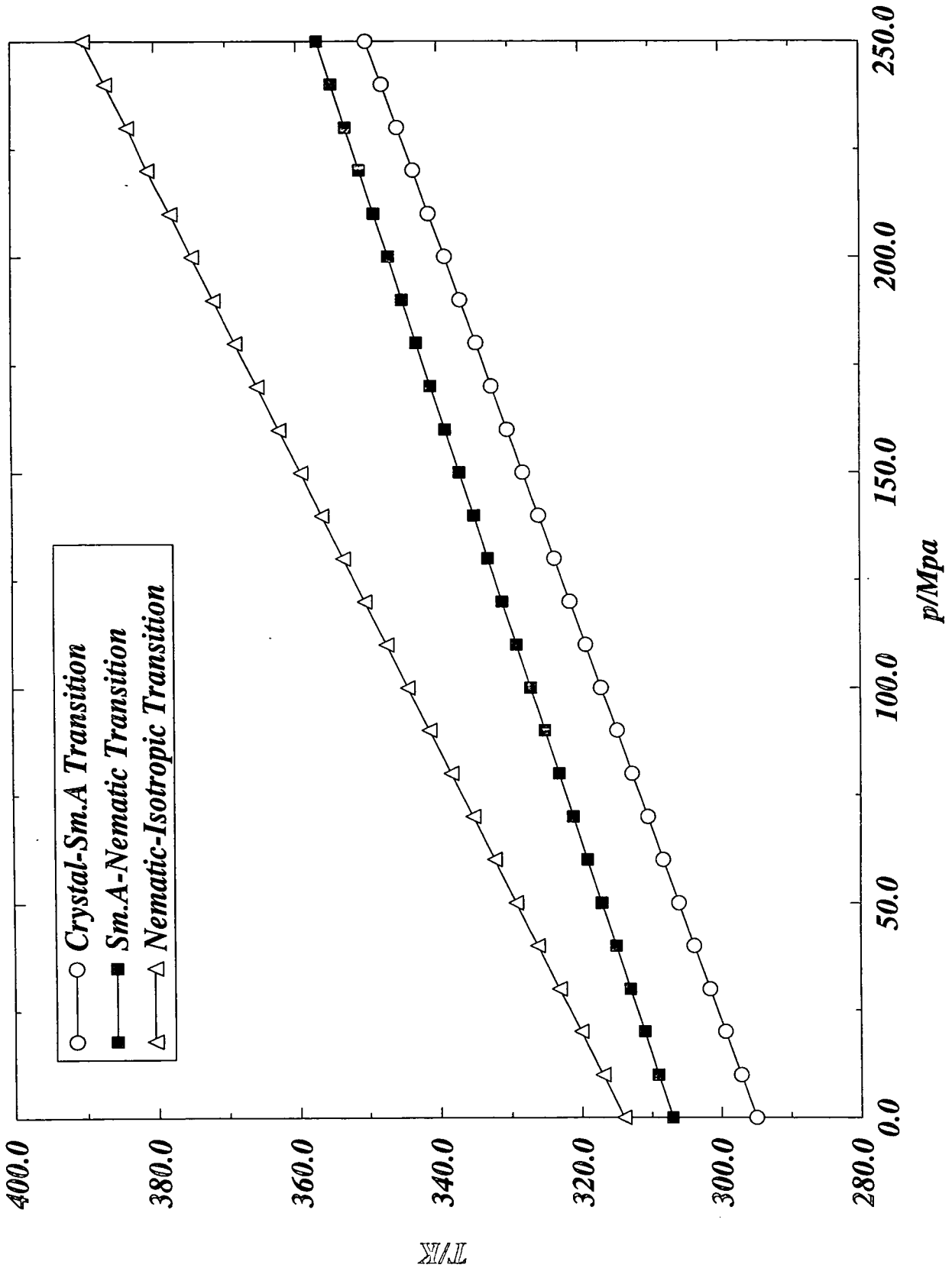

Fig. 33 Pressure Dependence of the Static Permittivity 8CB at 336K in Smectic A, Nematic and Isotropic Phases

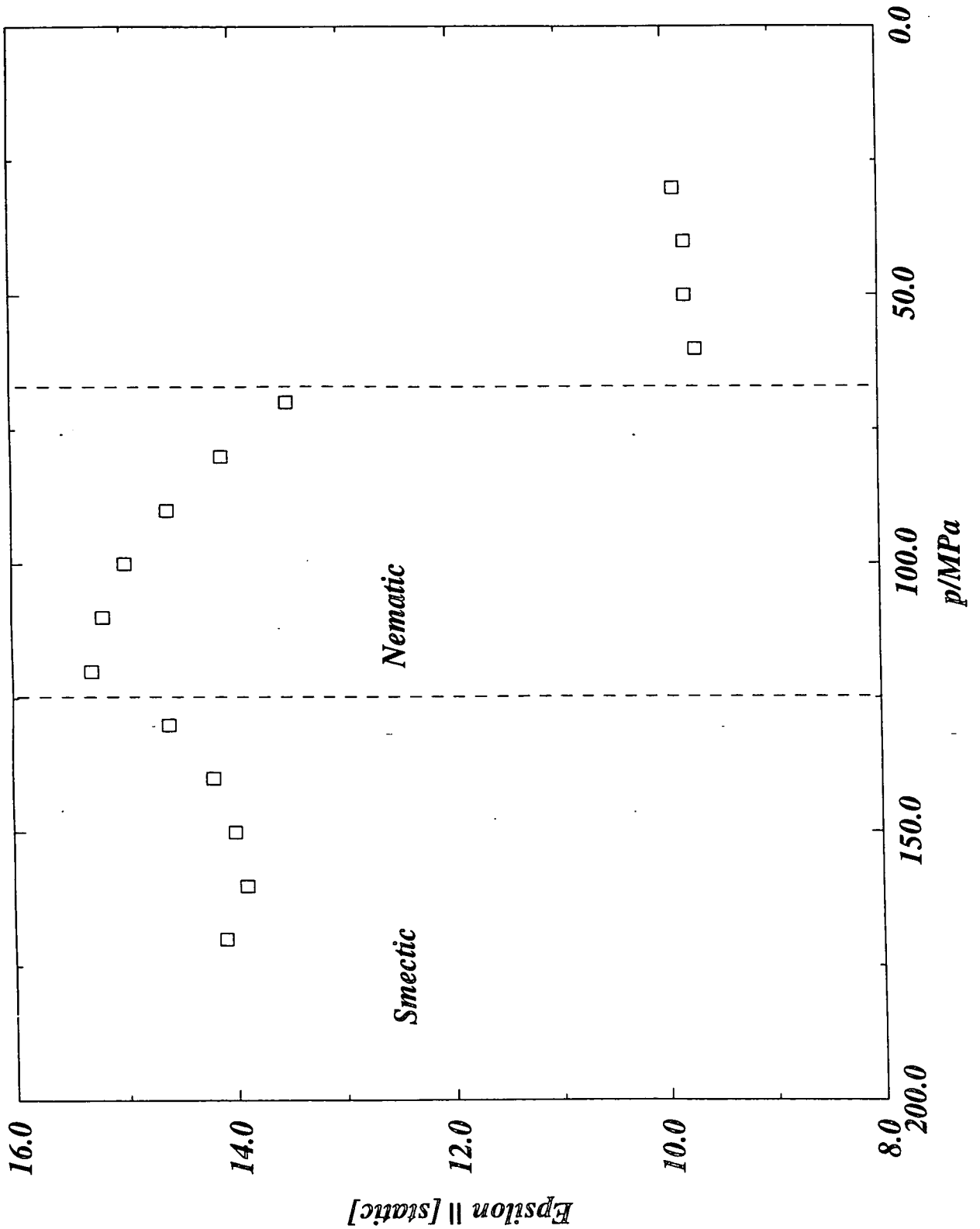

Fig. 34 Dispersion and Dielectric Loss Curves
8CB 336K Isotherm

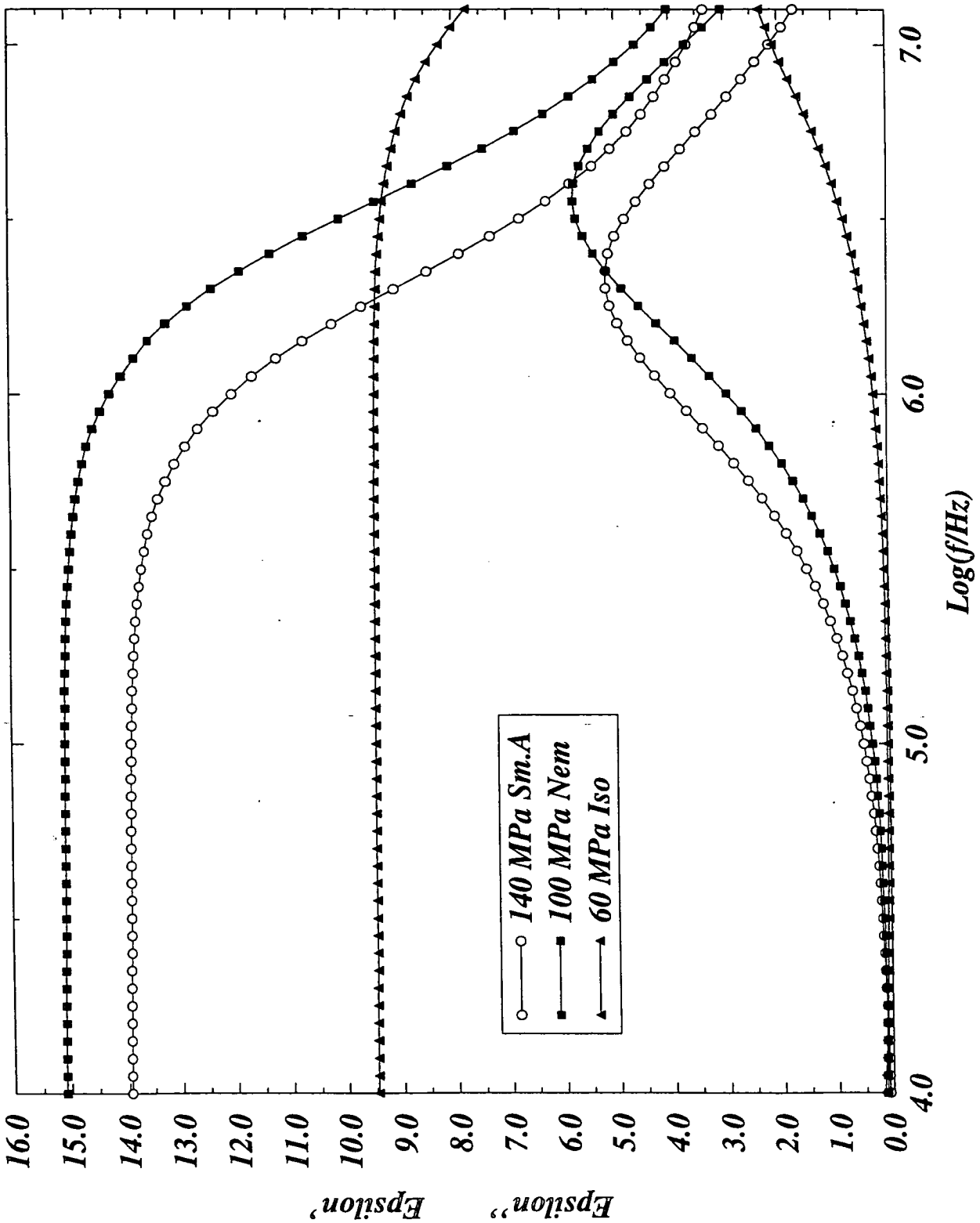

Fig. 35 Logarithm of the Dielectric Relaxation Time as a Function of Pressure 8CB in Smectic A, Nematic and Isotropic Phases

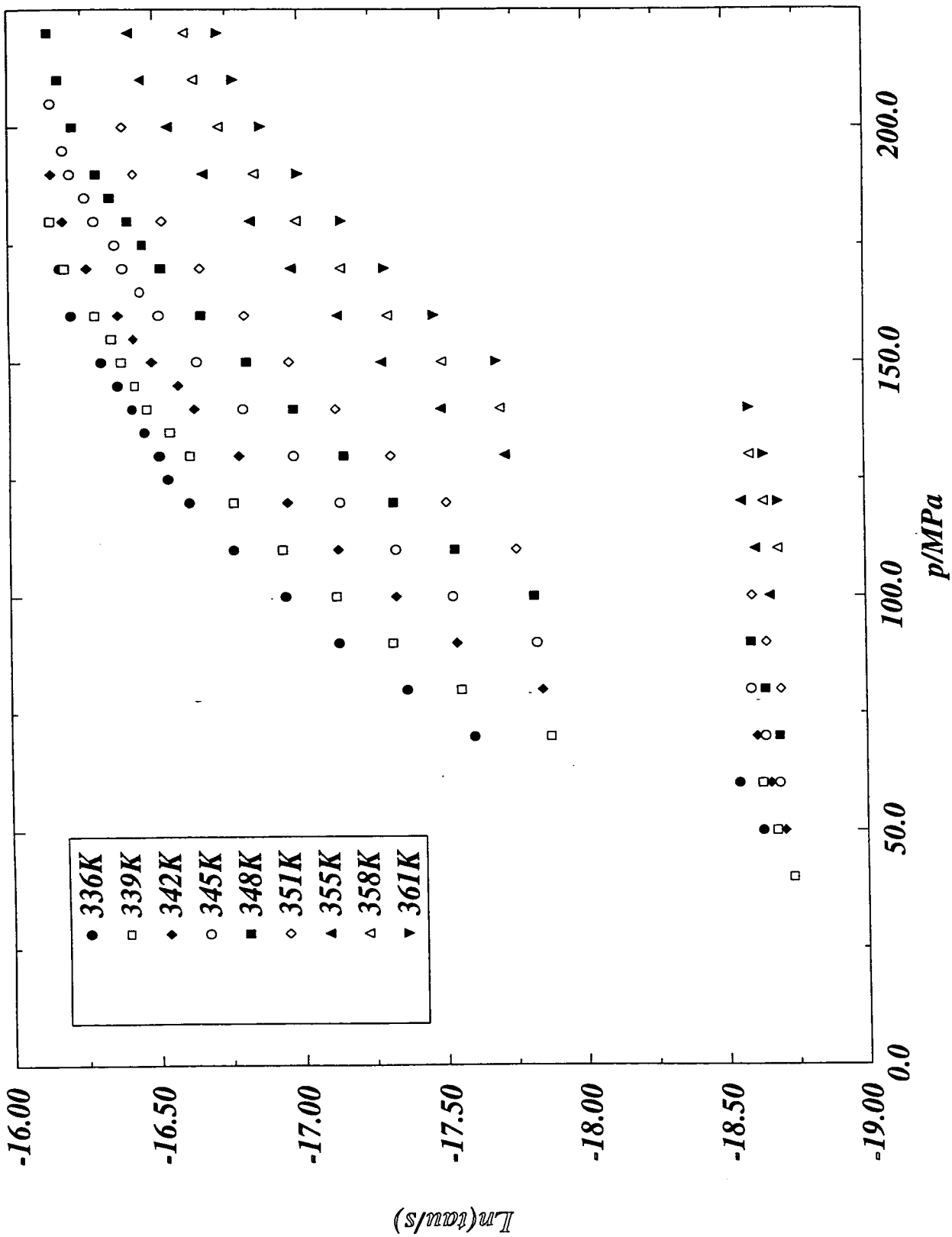

Fig. 36 Cole-Cole Plot
8CB 336K Isotherm

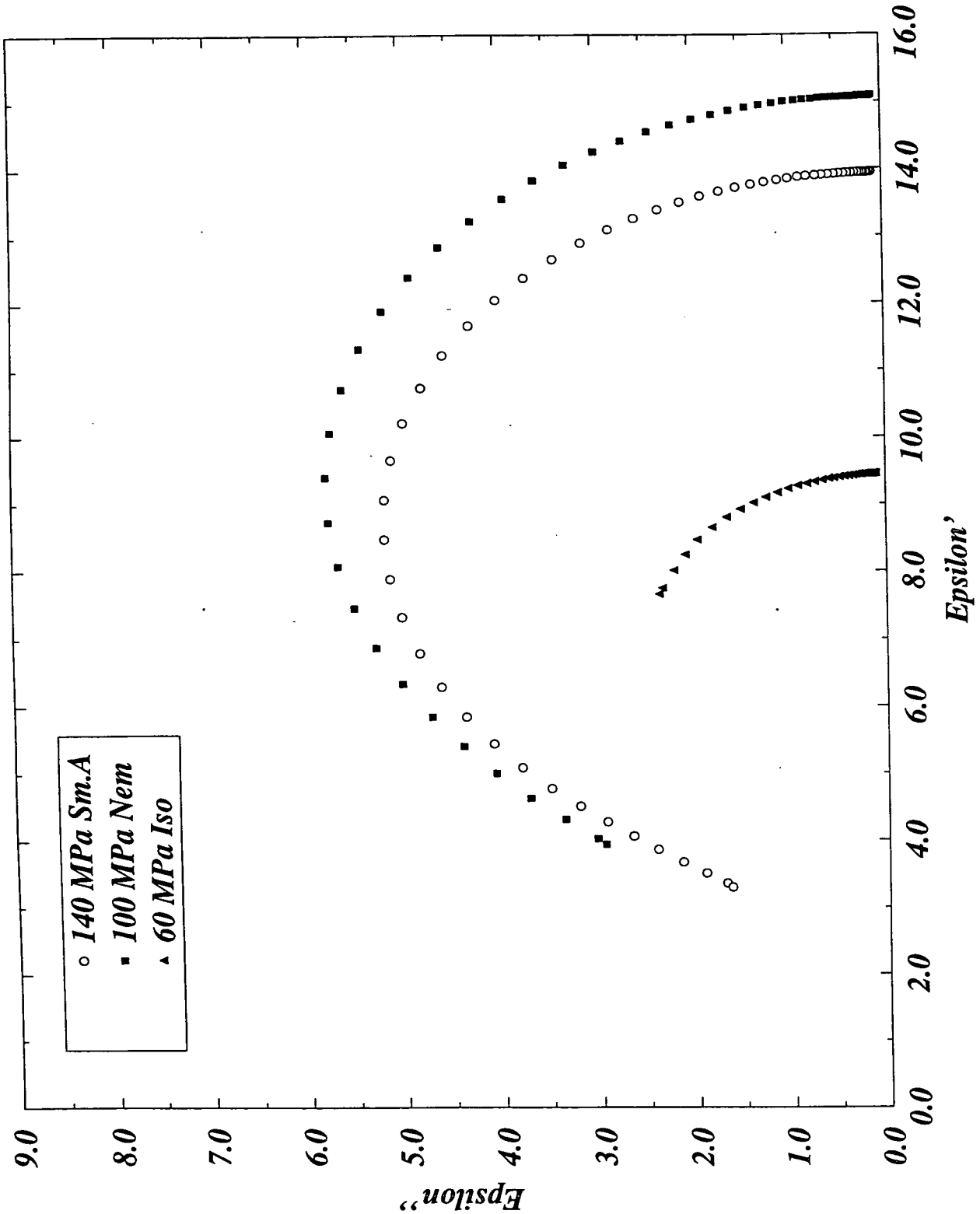

Fig. 37 Activation Volumes as a Function of Temperature 8CB in Smectic A, Nematic and Isotropic Phases

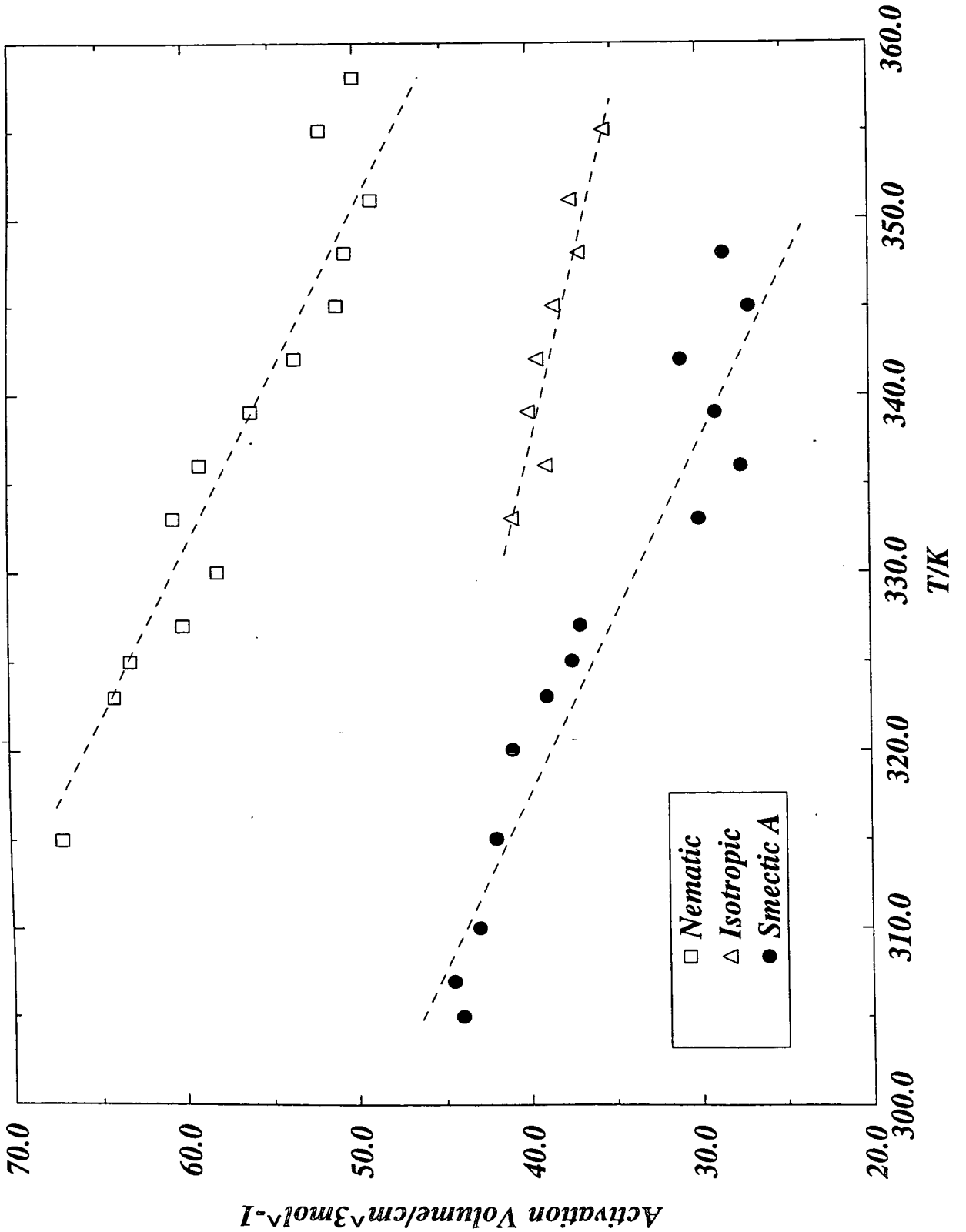

Fig. 38 Activation Enthalpies as a Function of Pressure 8CB in Smectic A, Nematic and Isotropic Phases

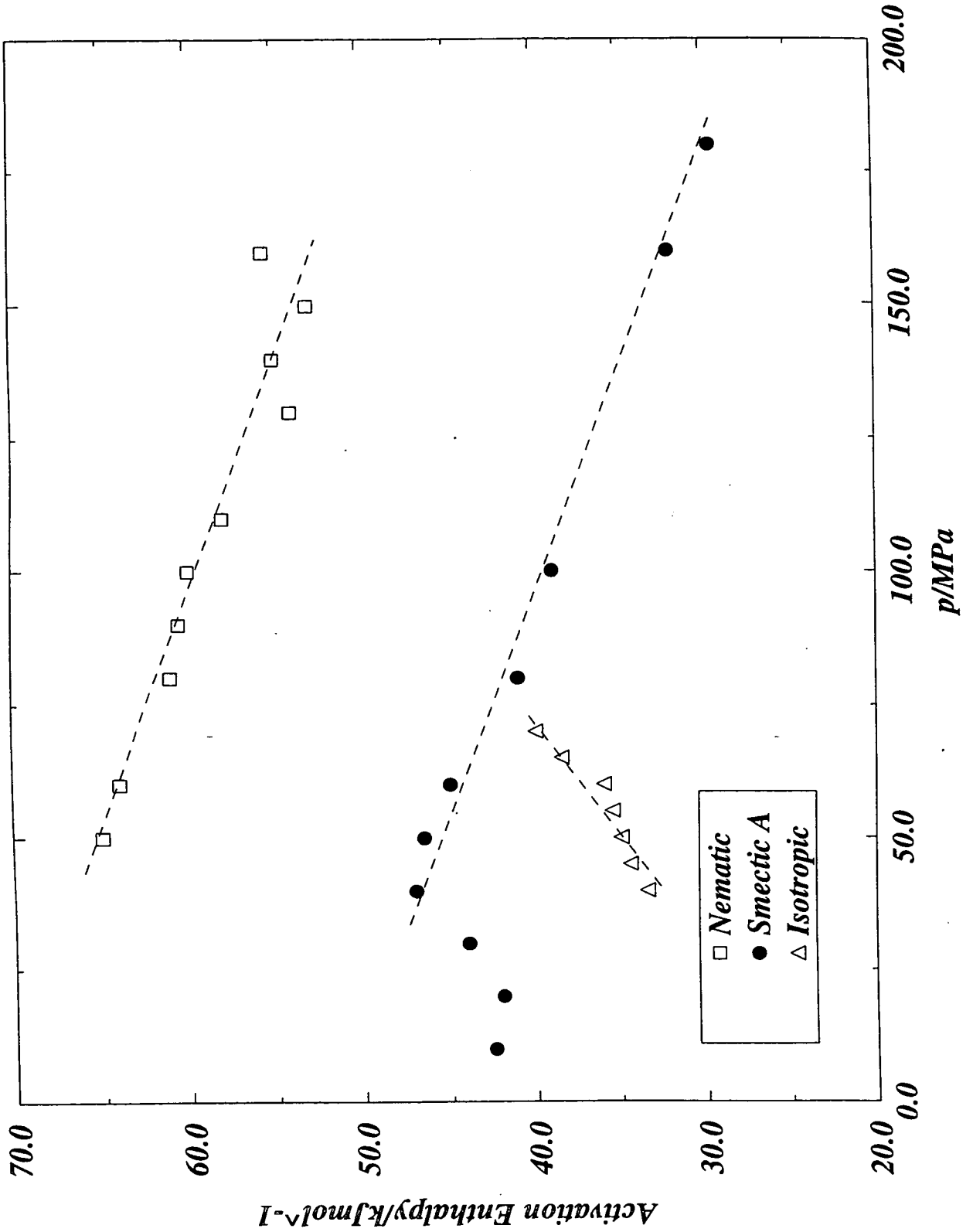

Fig. 39 Activation Energy as a Function of Activation Volume
8CB in Smectic A, Nematic and Isotropic Phases

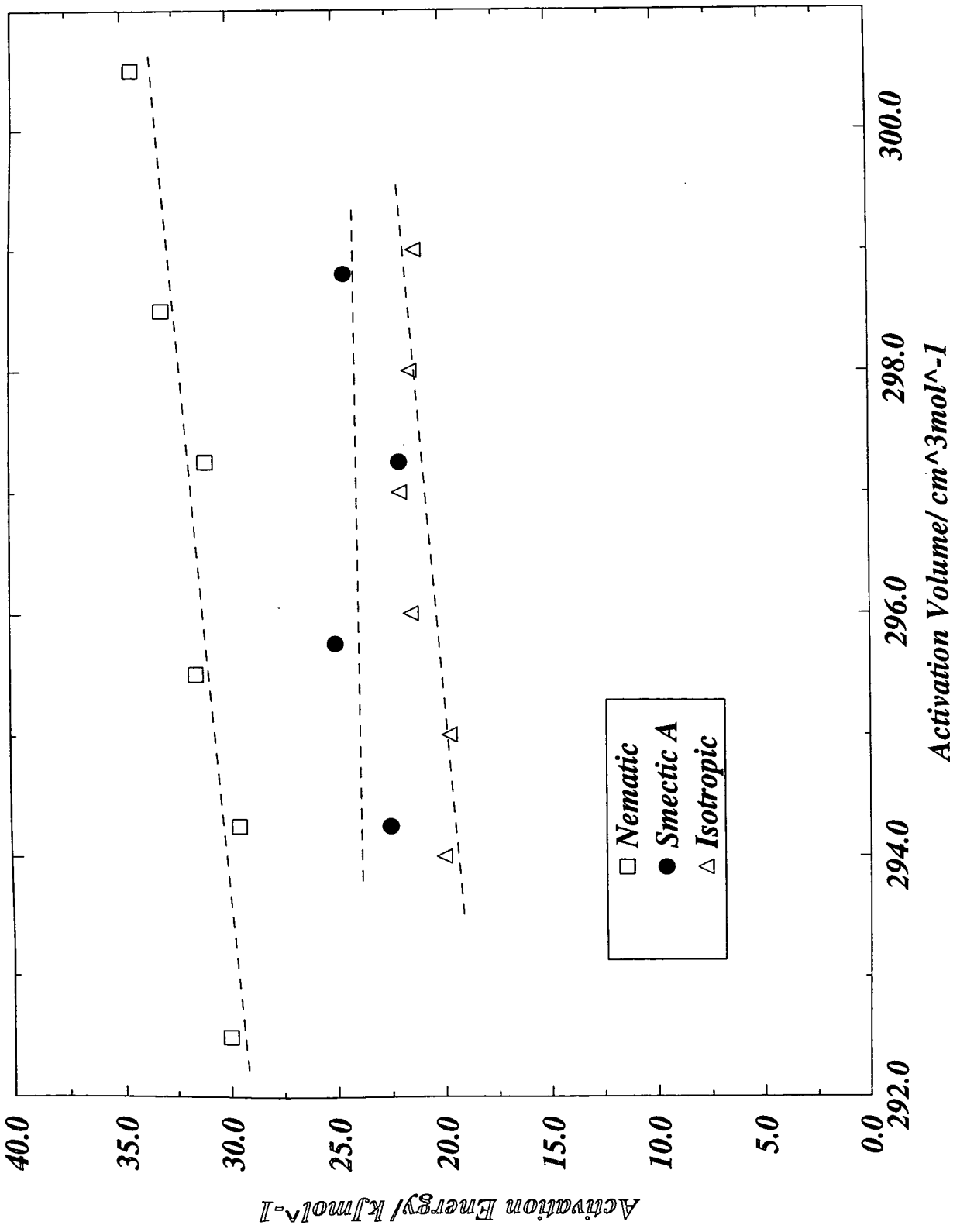

Fig. 40 8CB Order Parameter as a Function of Pressure

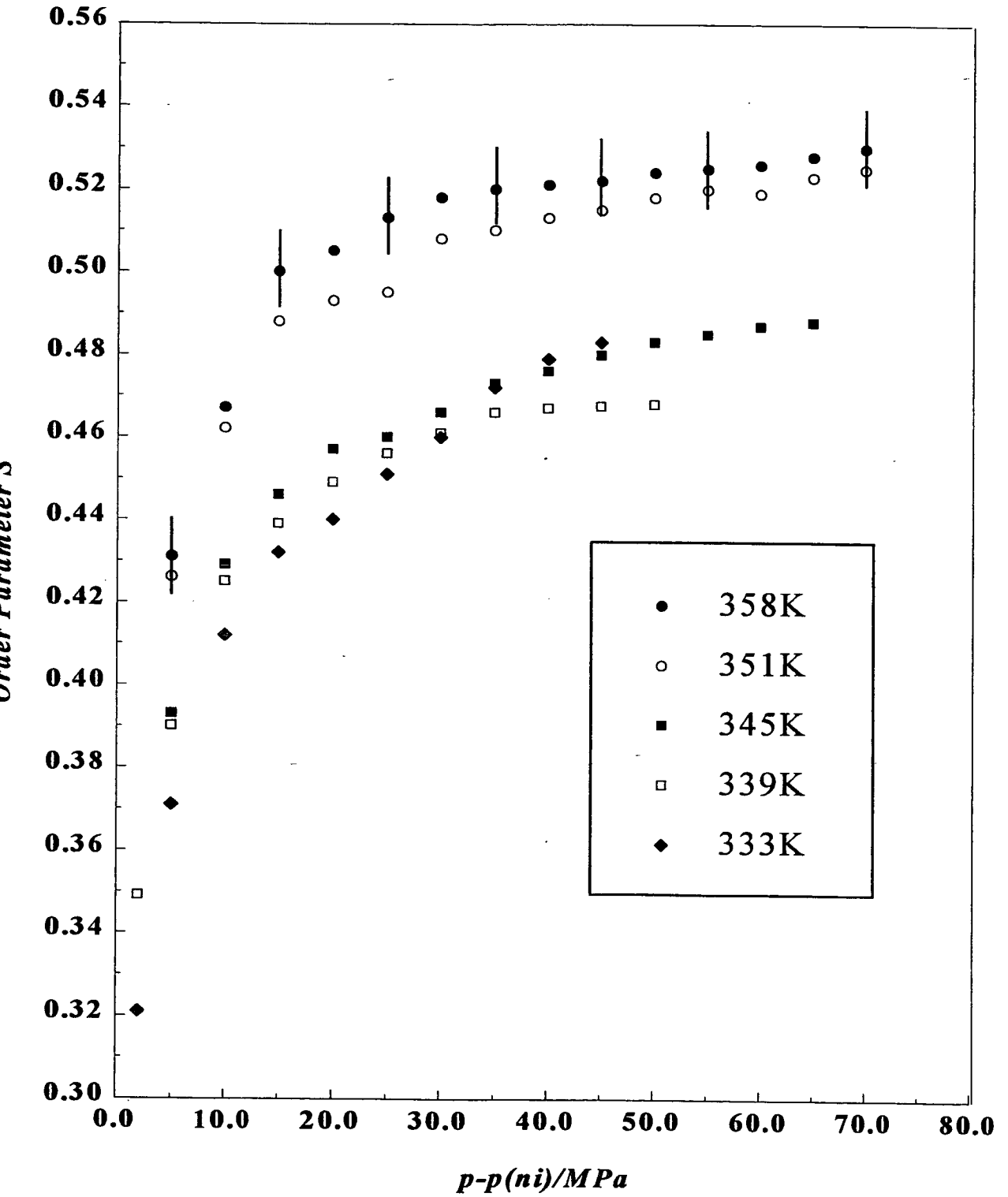

Chapter 10

Conclusions

The aim of this research project was to investigate the single molecule reorientation dynamics in partially disordered systems, in order to gain an understanding as to how the motion of constituent particles in such a system affects the local structuring and anisotropy of the system. The relationship that exists between single particle dynamics and macroscopic long-ranged orientational and positional ordering can be easily understood: on the one hand, the dynamics of a single particle is very much dependent on the particle's local environment, which determines the immediate potential energy surface. As the single particle relaxes, neighbouring molecules notice a change in their immediate environment, and react to this correspondingly. The intermolecular forces produce correlations that can propagate beyond the range of the forces themselves, and so these forces manifest themselves in the macroscopic properties of the system. However, the specific form of the intermolecular interaction potential is dependent on the physical and chemical properties of the individual molecules.On this basis, the work presented here is concerned with a much more general, fundamental area of contemporary science: the relationship between the macroscopic properties of a system given by statistical mechanics and the microscopic quantum mechanical properties of the constituent molecules, such as molecular size, shape, flexibility and even chemical make-up.

Results have been presented for a series of systems, each displaying a different degree of orientational and positional order. For each given system a summary has been provided highlighting the phenomena of interest. The purpose of this chapter is to provide a more general overview and to discuss possible future work. The single-particle reorientational correlation function is extremely sensitive to

changes in the local environment caused by varying the temperature or pressure of the system. This is in comparison to the single particle vibrational correlation function, which appears to be predominantly dependent on the molecular mass and the specific vibrational frequency.

The most important general observation in this research project is that none of the observed reorientational correlation functions decay as true exponentials with a single time exponent over all timescales. Despite the fact that initial experimental work on small molecular systems in the gas phase provided near perfect free-rotor correlation functions, early experimentalists working on Raman line-shape analysis in condensed matter phases in the 1960s and 1970s assumed that the single molecule reorientation dynamics would be stochastic. Their argument was that due to the enormous range of directional forces acting on the single molecule in a condensed phase, reorientational motion could only be rationalised by probabilistic statistical models dependent on a single characteristic relaxation time. Raman bands were fitted to Lorenzians, or in many cases no line shape analysis was carried out at all, and only the FWHH measurements were taken. In this work, high resolution Raman spectroscopy combined with precise and intensive baseline correction and line shape analysis techniques has shown that accurate reproducible correlation functions can be extracted from Raman line-shapes and the complexity of the functional form of these correlation functions is much greater than that previously assumed.

It is not surprising that stochastic behaviour is not observed in the systems studied here. Only a system which is truly isotropic will give an exponentially decaying reorientational correlation function. The fact that these systems are only partially disordered means that over some given distance scale the highly directional intermolecular interactions overcome thermal motion, thereby obtaining partial orientational and/or positional ordering, which breaks the isotropy. The value of accurate correlation functions is that they allow us to distinguish different means of reorientational relaxation that are occurring simultaneously, but on different timescales. Considering the results presented in this work we can assign, in general, the different types of reorientational relaxation to their given timescales. In the first $0.1ps$ we observe intra-molecular reorientation due to molecular flexibility. This process could be interpreted by a site-site model, whereby the relaxation rate would be determined by the height of the energy barrier between orientational sites given by the torsional bond potential. However, torsional bond potentials

are very small, and the relaxation process is complicated by intermolecular interactions such as dipole-induced-dipoles and Van-der-Waals interactions. Such behaviour was observed in the nCB homologous series. In the case of a rigid molecule, such as CS_2, the correlation function is that of the free-rotor in the first $0.1ps$. On the timescale $0.1ps - 0.5ps$ the reorientation process is dominated by the interaction between the molecule and its immediate local environment. In the case of CS_2, we observed the temperature dependence of the intermolecular torque on the damped free-rotational behaviour in this regime. Qualitatively, the correlation function on this time-scale provides an insight into what the molecule experiences from its local environment. It is in this time-scale that the effect of an increase in the free-volume is observed as the cyclohexane/CS_2 solution undergoes a liquid to plastic crystalline phase transition. At timescales greater than $0.5ps$ we observe that the reorientational relaxation is dominated by collisions and the functional form of the correlation function can best be described by the J- or M-extended diffusion models with a characteristic collision frequency. On progressing to increasingly longer timescales, the correlation functions enter the hydrodynamic regime and tend to exponential decay. Following the discussion on the relationship between time and distance, this observation can easily be explained by considering that partially disordered systems are isotropic over large distance scales.

The Raman lineshape analysis is not suited to the study of very slow dynamical behaviour. At such long timescales alternative techniques such as dielectric relaxation are more favourable. The fact that dielectric relaxation only gives the integrated correlation time is of no particular significance as at such long timescales the molecular motion is hydrodynamic. In such cases it is more profitable to look at the thermodynamic properties of the system as demonstrated for the chosen liquid crystals 6PCH and 8CB. However, Widom's argument, that partially disordered systems such as liquids reflect in their bulk properties the attractions and repulsions of their constituent particles, and Kubo's fluctuation-dissipation theory, which defines the relation between microscopic fluctuations and macroscopic dissipative coefficients, such as the rotation diffusion coefficient, both suggest that the ultra-fast, short-time processes instill the basis of the dynamics at longer timescales. The information concerning the ultra-fast dynamics is contained in the very far wings of the Raman band where, unfortunately, the S/N ratio is very small and much of this useful information is lost. Recent developments in the generation of stable ultra-short laser pulses have made possible the direct observation of dynamical behaviour on the femtosecond time scale and

in the last ten years a hierachy of time-resolved pump-probe non-linear optical experimental techniques [128-142] have been developed providing information complementary to that obtained *via* frequency domain inelastic light scattering techniques.

Ostensibly, all time-resolved pump-probe experiments follow the same basic idea. A high intensity ultra-short linearly polarised excitation pulse brings the system into a coherent vibrationally excited state and simultaneously creates some net alignment of the molecules giving rise to orientational anisotropy. The decay of this orientational anisotropy and vibrational coherence is measured directly by the non-linear response intensity from a secondary probe pulse incident on the system at some variable delay time. The response function is therefore a combination of the collective reorientational relaxation and various vibrational relaxations, such as libration. The probe pulse can be tuned into a given vibrational frequency. Particularly for low frequency vibrations, the vibrational dephasing can be classified into homogeneous and inhomogeneous contributions [143,144]. The homogeneous contribution arises from a rapid perturbation by neighbouring molecules of the oscillator of interest, whilst the inhomogeous contribution arises from differences in the environment around the oscillator. These two contributions can thought of as single-molecule self-vibrational dephasing, and collective vibrational dephasing respectively. The important point to notice in these experiments is that these collective relaxation processes occur on the same time-scales as the fast single-molecule dynamic processes reported in this work and there is therefore a coupling between single-particle and collective molecular motion in partially disordered phases.

At the moment no models have been developed for collective reorientational motion, though it is clear that there is a strong connection between single-particle and collective reorientational dynamics. More recent time-resolved non-linear spectroscopic experiments have concentrated on deconvoluting the homogeneous and inhomogeneous contributions to the vibrational dephasing using multiple excitation pulses and several time delays. In general the time-resolved non-linear experiments have two main advantages over frequency domain techniques. The use of multiple incident pulses allows the study of numerous possible polarisation components, in comparison to Raman spectroscopy where there are only two possible polarisation components (VV and VH). By comparing the response functions from different polarisation components more information as to the specific dynamics of the system can be deduced. Secondly, the direct observation of the

time-domain response functions preserve any inherent temporal ordering which may be compromised by a diffusive relaxation treatment of light scattering data in the frequency domain. However, time-resolved non-linear optical techniques are expensive. In particular, the collection optics must be extremely sensitive, as, in general, an increase by one order of non-linearity results in a one-hundred-fold decrease in signal intensity. Obviously, the non-linear signal intensity is largest at very short delay times (several tenths of picoseconds). At longer delay times the non-linear signal intensity decreases as the system of interest relaxes. Despite the use of lock-in amplifiers and heterodyne amplification techniques [145], the collection of accurate response functions at long time delays is not possible.

The fundamental problem with all experimental techniques is that the results are averages over all molecular conformations, orientations and positions in the system. There is no single experimental technique to date that allows the experimentalist to follow the specific motion of a given molecule in a macroscopic system. Furthermore there has also been no attempt as yet to look at the dynamics at different positions in a given molecule. Such experiments involve tagging a molecule. The author provides here a few ideas for future experiments.

Let us consider a liquid crystalline system, such as those studied here by dielectric relaxation. The model formulated suggests that the dynamics are dominated by steric effects (collisions). The immediate question is then : where in the molecule are most of these steric interactions occurring? By inserting an eximer (such as a pyrene molecule) at different positions along the length of the liquid crystalline molecule, it is possible to qualitatively determine as a function of the intensity of fluorescence where the steric interactions are most prominent: in the middle of the molecule, in the rigid rod, or at the end of the flexible molecular tail. This experiment provides information about the collisions between molecules. Another possible future experiment would be to chemically insert a specific Raman active chromophore, such as a silicon fluoride group, at different positions into a liquid crystalline molecule. Assuming that the vibration at this active chromophore is localised, correlation functions from this chromophore would give information about the difference between the dynamics of the rigid-rod section of the molecule and the flexible tail. For the case of a silicon fluoride chromophore, both tumbling and spinning correlation functions could be extracted. Both these examples involve the use of designer substances, specifically chemically synthesised for the study of reorientation dynamics and molecular interactions. In each case a particular position in the molecule is being tagged. This is not the only possible way

of tagging molecules. Let us consider an isotropic liquid system with an interface (either liquid-liquid or liquid-gas). It would be of interest here to compare the dynamics of molecules in the bulk liquid with those at the interface. It is well known that any form of second harmonic generation (hyper-Rayleigh, hyper-Raman) is only allowed in systems which do not possess an inversion centre. The bulk isotropic liquid possesses an inversion centre. However, the interface destroys this symmetry. The extension of the theory for extraction of correlation functions from hyper-Raman or hyper-Rayleigh bands is simple. In this example the molecules at the interface are being tagged by virtue of the symmetry of the system.

Computer simulation techniques play an increasingly important role in the study of dynamics in condensed phases. The level of computer simulation required depends on the time-scale of the dynamics of interest. Classical MD simulations generate very good results for the dynamics of systems at long time scales. However, due to the use of a static interaction potential, classical MD techniques are not suitable for the study of ultra-fast dynamics occurring at timescales similar to the fluctuations of the interaction potential due to changes in the molecular conformation and vibrations. It has been shown in this work that DFT *ab initio* computer simulation can successfully probe the dynamics of the system at ultra-fast time scales. However, *ab initio* techniques require a large amount of cpu time and simulations are restricted to a very small number of molecules in a periodically repeating super-cell. The author argues here that the *ab initio* simulation over very short time-scales (less than one picosecond) can be considered to be accurate. However, at longer timescales the DFT simulation is not realistic due to finite size effects and periodic boundary conditions. As computers become more and more powerful, *ab initio* simulation techniques can be extended to increasingly larger systems. In the meantime, results from present *ab initio* calculations could be used to formulate more accurate interaction potentials for classical MD simulations.

In summary, we conclude that there is an intrinsic relationship between the structure and dynamics of a macroscopic condensed matter system and the dynamics of a single constituent molecule in that system. The single molecule reorientational relaxation is complicated: numerous relaxation processes occur simultaneously at different timescales and the motion of the molecule and its interaction with its local environment are highly dependent on the particular physical and chemical molecular properties. The extraction of accurate correlation functions from

Raman lineshapes allows the separation and analysis of these different relaxation processes. In particular, the dynamics occurring at very fast timescales appears to play a significant role in determining the dynamics at longer timescales. These fast relaxation processes can be simulated using *ab initio* computer simulation techniques. Future work will involve combining frequency domain experiments with more recent time-domain experiments. In general, the research will progress along two paths:

1: Probing the relationship between homogeneous and inhomogeneous vibrational and reorientational relaxation, including in particular the development of models for collective reorientational relaxation.

2: Developing new experimental techniques to tag molecules in condensed matter systems, and combining this research with computer simulation techniques in order to probe the dynamics of a specific molecule in a system over a given time period.

This research will increase our understanding of the relationship between the macroscopic properties of a system and the microscopic physical and chemical properties of the constituent molecules. This will lead to the development of designer systems, whose constituent molecules are specifically chosen and synthesised such that the macroscopic properties of that system are best suited to a particular industrial application.

Appendix A

Quantisation of Angular Momentum

In order to establish a scientific representation of reorientation dynamics in condensed phases it is neccessary to formulate a quantum theory of angular momentum to describe the orientational motion of the individual constituent components of a given system. What follows here is a brief introduction to the basis concepts of quantisation of angular momentum including the definition and formulism of the mathematical identities, which are used to define explicit forms of the correlation function for different models of reorientational motion.

To define the angular momentum operators [146,147], we first consider the rotation of a coordinate system through an angle θ about an axis defined by the direction $\mathbf{n}$, a unit vector. The wavefunction ψ in the original system is then related to the wavefunction ψ' in the rotated system by a unitary transformation:

$$\psi' = R(\mathbf{n}, \theta)\psi \ . \tag{A.1}$$

$R(\mathbf{n}, \theta)$ depends on three angles, two to define the direction of $\mathbf{n}$ and θ which defines the magnitude of rotation. $R(\mathbf{n}, \theta)$ tends to 1 as θ tends to zero. In exponential form, we can now write:

$$R(\mathbf{n}, \theta) = \exp(-iS(\mathbf{n}, \theta)) \ . \tag{A.2}$$

As R is unitary, S is hermitian. Considering an infinitessimal unitary transformation, expanding $\exp(-iS(\mathbf{n},\theta))$ to the first power only:

$$R(\mathbf{n},\theta) = 1 - iS(\mathbf{n},\theta) \tag{A.3}$$

and

$$R\psi = (1 - iS)\psi \ . \tag{A.4}$$

Using the above formulae, and considering the case where the axis of rotation lies along one of the cartesian axes, x, y or z, we find:

$$R\psi - \psi = i\theta \hat{J}_x \psi \tag{A.5}$$

$$R\psi - \psi = i\theta \hat{J}_y \psi \tag{A.6}$$

$$R\psi - \psi = i\theta \hat{J}_z \psi \ . \tag{A.7}$$

$\hat{J}_x$, $\hat{J}_y$ and $\hat{J}_z$ are the three Hermitian operators for the three cartesian components of angular momentum. They are a complete set in so far that components formed in any other way are expressible as linear combinations of these three. The total angular momentum operator (three operators), $\hat{\mathbf{J}}$ is defined more generally for any axis of rotation $\mathbf{n}$ as:

$$R\psi - \psi = -i\theta(\mathbf{n} \cdot \hat{\mathbf{J}})\psi \tag{A.8}$$

for infinitessimal rotations. For finite rotations:

$$R\psi = \exp(-i\theta(\mathbf{n} \cdot \hat{\mathbf{J}}))\psi \ . \tag{A.9}$$

Similarly, the transformation of an arbitrary quantum operator $\hat{O}$ under an infinitessimal rotation has the the form:

$$R\hat{O} - \hat{O} = -i\theta \mathbf{n} \cdot [\hat{\mathbf{J}}, \hat{O}] \ . \tag{A.10}$$

The angular momentum thus determines the transformation properties of a system or quantum operator under rotations of the coordinate system. Conversely, the angular momentum operator $\hat{\mathbf{J}}$ (i.e the three operators $\hat{J}_x, \hat{J}_y, \hat{J}_z$) can be determined from the transformation properties of the system.

Of course the explicit form of the total angular momentum operator is defined by the transformation properties of the particular system under consideration. As a

simple example, we concentrate on a wavefunction or state vector $\psi(x, y, z)$ which transforms under rotation to a new wavefunction $\psi(x', y', z')$. For an infinitessimal rotation $d\theta$ about the z-axis:

$$x' = x + yd\theta \tag{A.11}$$

$$y' = y - xd\theta \tag{A.12}$$

$$z' = z \ . \tag{A.13}$$

Now

$$\psi(x', y', z') = \psi(x, y, z) - d\theta(y\partial/\partial x - x\partial/\partial y)\psi(x, y, z) \ . \tag{A.14}$$

However, from equation A.8

$$R\psi(x, y, z) = (1 - id\theta\hat{J}_z)\psi(x, y, z) \ . \tag{A.15}$$

Therefore

$$\hat{J}_z = -i(x\partial/\partial y - y\partial/\partial x) \equiv \hat{L}_z \ . \tag{A.16}$$

Similarly

$$\hat{J}_x = -i(y\partial/\partial z - z\partial/\partial y) \equiv \hat{L}_x \tag{A.17}$$

$$\hat{J}_y = -i(z\partial/\partial x - x\partial/\partial z) \equiv \hat{L}_y \ . \tag{A.18}$$

$\hat{L}_x, \hat{L}_y$ and $\hat{L}_z$ are the three Hermitian operators for the three cartesian components of orbital angular momentum. The total angular momentum is the sum of the orbital angular momentum operator $\hat{\mathbf{L}}$ and the spin angular momentum operator $\hat{\mathbf{S}}$,

$$\hat{\mathbf{J}} = \hat{\mathbf{L}} + \hat{\mathbf{S}} \ . \tag{A.19}$$

As the state vector ψ has no internal degrees of rotational freedom (no spinor index) there is no spin angular momentum and variation occurs only in the configuration space coordinates. For our purposes we will deal only with systems possessing no internal degrees of freedom and therefore spin angular momentum will not be discusssed any further here. Orbital angular momentum is well understood in terms of its classical analogue:

$$\mathbf{L} = \mathbf{r} \times \mathbf{p} \tag{A.20}$$

where $\mathbf{r}$ is the position vector of the particle and $\mathbf{p}$ is its linear momentum. In quantum mechanics we obtain the orbital angular momentum operator by substituting $\mathbf{r} \longrightarrow \hat{\mathbf{r}}$ and $\mathbf{p} \longrightarrow \hat{\mathbf{p}}$, where $\hat{\mathbf{r}}$ and $\hat{\mathbf{p}}$ are the position and momentum

operators respectively. In the coordinate representation $\hat{\mathbf{r}} = \mathbf{r}, \hat{\mathbf{p}} = -i\nabla$ and the orbital angular momentum operator is given by

$$\hat{\mathbf{L}} = -i[\mathbf{r} \times \nabla] \, . \tag{A.21}$$

We now consider two consecutive finite rotations. In the first case we rotate a system through an angle $d\theta_x$ about the x-axis, and then through an angle $d\theta_y$ about the y-axis. In the second case we rotate the system through an angle $d\theta_y$ about the y-axis, and then through an angle $d\theta_x$ about the x-axis. Comparison of these two rotation operators shows that they are indeed not the same. Subtracting one from the other we arrive at the result:

$$\exp(-id\theta_x\hat{J}_x)\exp(-id\theta_y\hat{J}_y) - \exp(-id\theta_y\hat{J}_y)\exp(-id\theta_x\hat{J}_x) = \exp(-id\theta_x d\theta_y\hat{J}_z) - 1 \, . \tag{A.22}$$

It follows that

$$d\theta_x d\theta_y(\hat{J}_x\hat{J}_y - \hat{J}_y\hat{J}_x) = id\theta_x d\theta_y\hat{J}_z \tag{A.23}$$

$$\hat{J}_x\hat{J}_y - \hat{J}_y\hat{J}_x = i\hat{J}_z \, . \tag{A.24}$$

This form of commutation is called cyclic commutation and similar commutation relations are obtained for combinations of the other components of the total angular momentum. Defining $[\hat{J}_i, \hat{J}_j] \equiv \hat{J}_i\hat{J}_j - \hat{J}_j\hat{J}_i; (i, j = x, y, z)$:

$$[\hat{J}_x, \hat{J}_z] = -[\hat{J}_z, \hat{J}_x] = i\hat{J}_y \tag{A.25}$$

$$[\hat{J}_y, \hat{J}_z] = -[\hat{J}_z, \hat{J}_y] = i\hat{J}_x \, . \tag{A.26}$$

All components commute directly with themselves and the square of the total angular momentum operator:

$$[\hat{J}_x, \hat{J}_x] = [\hat{J}_y, \hat{J}_y] = [\hat{J}_z, \hat{J}_z] = 0 \tag{A.27}$$

$$[\hat{\mathbf{J}}^2, \hat{J}_x] = [\hat{\mathbf{J}}^2, \hat{J}_y] = [\hat{\mathbf{J}}^2, \hat{J}_z] = 0 \, . \tag{A.28}$$

Such commutation relations mean that it is experimentally possible to measure or calculate both the square of the total angular momentum and a single cartesian component of the total angular momentum simultaneously. However it is not posssible to know simultaneously any more than one cartesian component of the total angular momentum. The cyclic commutation properties between components of the total angular momentum operator play an important role in the

formulation of irreducible tensors.

In order to describe the rotation of a system it is necessary to define two sets of coordinate axes, or frames. The first is a coordinate frame fixed in the system of interest, for example a molecule. The centre of this coordinate frame is found at the molecular centre of mass. This is called the body-fixed frame. The second coordinate frame is one fixed in space, and is called the laboratory frame, or space-fixed frame. Using the space-fixed frame as a reference, and rotating the body-fixed frame such that it coincides with the reference frame, it is possible to explicitly define a rotation of the system of interest. The representation of any property of the system with respect to the body fixed frame will remain constant under rotation due to the symmetry laws of rotation. However, the representation of a given property of a system, if non-spherical, will transform under rotation when measured in the space-fixed frame.

We will now define explicitly the representation of the rotation matrix R for rotation in three dimensions. We consider the rotation of the body-fixed frame associated with a coordinate system $S(x, y, z) \longrightarrow S(x', y', z')$. Any such rotation in three dimensions may be considered as three successive rotations about the coordinate axes: first we transform the axes to new positions by rotating through an angle $\alpha(0 \leq \alpha \leq 2\pi)$ about the z-axis. This is followed by a rotation about the new y-axis through an angle $\beta(0 \leq \beta \leq \pi)$. Finally we perform a third rotation about the new z-axis through an angle $\gamma(0 \leq \gamma \leq 2\pi)$. The same rotation may be performed by another succession of rotations: a rotation through an angle γ about the original z-axis, then a rotation through an angle β about the original y-axis and finally a rotation through an angle α about the original z-axis. The angles α, β, γ are called the Euler angles and completely define the rotation of the coordinate system. It should be noted that in the second approach, all three successive rotations are about the original axes in the body fixed frame. We may express the rotation operator $\hat{D}(\alpha, \beta, \gamma)$ as:

$$\hat{D}(\alpha, \beta, \gamma) = \exp(-i\alpha \hat{J}_z) \exp(-i\beta \hat{J}_y) \exp(-i\gamma \hat{J}_z) \ . \tag{A.29}$$

Rotation defined by the Euler angles is shown illustratively in figure A1.

Irreducible tensors occupy a central position in angular momentum theory [148,149]. Under rotations of coordinate systems these tensors transform in the same manner as eigenfunctions of the angular momentum operator. An irreducible tensor $\mathcal{M}_J$ of rank J is defined as a set of $2J + 1$ functions (components) $\mathcal{M}_{JM}$ (where

$M = -J, -J+1, ..., J-1, J$) which satisfy the following commutation rules with spherical components of the angular momentum operator:

$$[\hat{J}_{\pm 1}, \mathcal{M}_{JM}] = \mp 2^{-1/2} \exp(\pm i\delta) \times (J(J+1) - (M(M \pm 1)^{1/2} \mathcal{M}_{JM\pm 1} \quad \text{(A.30)}$$

$$[\hat{J}_0, \mathcal{M}_{JM}] = M\mathcal{M}_{JM} \ . \quad \text{(A.31)}$$

It follows that:

$$[\hat{\mathbf{J}}^2, \mathcal{M}_{JM}] = J(J+1)\mathcal{M}_{JM} \ . \quad \text{(A.32)}$$

The quantity δ which determines relative phases of different $\mathcal{M}_{JM}$ components is arbitrary. For our purposes and for simplicity we will define $\delta = 0, (\exp(i\delta) = 1)$, and choose the positive sign of the square root. The linear equations define the components of the irreducible tensor $\mathcal{M}_{JM}$ within an arbitrary scalar factor, which is the same for all of the components. This factor can be real or complex. In the case of an integer rank J, as we will be considering, the overall phase of the $\mathcal{M}_{JM}$ components is usually defined with the Condon-Shortley choice of phases [150], such that:

$$(\mathcal{M}_{JM})^* = (-1)^{-M} \mathcal{M}_{J-M} \quad \text{(A.33)}$$

which coincides with that for spherical harmonics as shall be seen later.

An irreducible tensor $\mathcal{M}_J$ of rank J can be expanded in a series based on a complex set of orthonormal irreducible tensors $\mathbf{e}_{JM}$ of rank J,

$$\mathbf{e}_J^M \cdot \mathbf{e}_{J'M'} = \delta_{JJ'}\delta_{MM'}, \quad \text{(A.34)}$$

composed of basis functions. The expansion of $\mathcal{M}_J$ is written as

$$\mathcal{M}_J = \sum_M \mathbf{e}_J^M \cdot \mathcal{M}_{JM} = \sum_M \cdot \mathcal{M}_J^M \quad \text{(A.35)}$$

where $\mathcal{M}_{JM}$ represents the covariant component of the tesnsor $\mathcal{M}_J$ and $\mathcal{M}_J^M$ denotes the contravariant component. These components are related by

$$\mathcal{M}_J^M = (\mathcal{M}_{JM})^* = (-1)^{-M} \mathcal{M}_{J-M} \ . \quad \text{(A.36)}$$

Under rotations of the coordinate system described by the Euler angles α, β, γ the components of irreducible tensors $\mathcal{M}_{JM}$ undergo linear transformation. The

coefficients of such transformations are the Wigner D-functions, defined by:

$$\mathcal{M}_{JM'} = \hat{D}(\alpha,\beta,\gamma)\mathcal{M}_{JM'}[\hat{D}(\alpha,\beta,\gamma)]^{-1} = \sum_M \mathcal{M}_{JM} D^J_{MM'}(\alpha,\beta,\gamma) \; . \qquad \text{(A.37)}$$

As seen above, the Wigner D-functions $D^J_{MM'}(\alpha,\beta,\gamma)$ may be defined as the matrix elements of the rotation operator in the JM-representation. Using the familiar Dirac bra-ket notation, we have

$$\langle JM \mid \hat{D}(\alpha,\beta,\gamma) \mid J'M' \rangle = \delta_{JJ'} D^J_{MM'}(\alpha,\beta,\gamma) \; . \qquad \text{(A.38)}$$

The D-functions realise transformations of covariant components of any irreducible tensor of rank J (e.g. the wavefunction ψ_{JM} of a quantum mechanical system with total angular momentum J and its projection M) under coordinate rotations. If the basis vectors of the representation are chosen to be the eigenfunctions of $\hat{J}_z$, the matrices simplify as follows:

$$D^J_{MN}(\alpha,\beta,\gamma) = \langle JM \mid \exp(-i\alpha\hat{J}_z)\exp(-i\beta\hat{J}_y)\exp(-i\gamma\hat{J}_z) \mid JN \rangle \qquad \text{(A.39)}$$

$$D^J_{MN}(\alpha,\beta,\gamma) = \exp(-i(\alpha M+\gamma N))\langle JM \mid \exp(-i\beta J_y) \mid JN \rangle \qquad \text{(A.40)}$$

$$D^J_{MN}(\alpha,\beta,\gamma) = \exp(-i(\alpha M+\gamma N)) d^J_{MN}(\beta) \; . \qquad \text{(A.41)}$$

Phases of the rotation matrices depend upon the convention adopted for the Euler angles and of the choice of phases of the matrix elements $\hat{\mathbf{J}}$. With the Condon and Shortly choice of phases, the small Wigner rotation matrices d^J_{MN} are real and can be expressed explicitly as [151]:

$$\begin{aligned} d^J_{MN}(\beta) = \quad & \textstyle\sum_t (-1)^t \frac{[(J+M)!(J-M)!(J+N)!(J-N)!]^{1/2}}{(J+M-t)!(J-N-t)!t!(t+N-M)!} \\ & \times (\cos\beta/2)^{2J+M-N-2t} (\sin\beta/2)^{2t+N-M} \end{aligned} \qquad \text{(A.42)}$$

where the sum is taken over all values of t which lead to non-negative factorials.

The Wigner D-functions represent wavefunctions of a rigid symmetric top. They are eigenfunctions of three operators; $\hat{J}_z = -i\partial/\partial\alpha$, $\hat{J}_{z'} = -i\partial/\partial\gamma$ and $\hat{\mathbf{J}}^2 = -[\partial^2/\partial\beta^2 + cot\beta\partial/\partial\beta + 1/\sin^2\beta(\partial^2/\partial\alpha^2 - 2\cos\beta\partial/\alpha\partial\gamma + \partial^2/\partial\gamma^2)]$. $\hat{\mathbf{J}}$ is the total angular momentum operator of the top; $\hat{J}_z$ and $\hat{J}_{z'}$ are projections of $\hat{\mathbf{J}}$ onto the z-axis of the rotating (body-fixed) and non-rotating (space-fixed) coordinate

systems respectively. The eigenvalues of these operators are defined by

$$\hat{J}_z D^J_{MM'}(\alpha_{bf}, \beta_{bf}, \gamma_{bf}) = -M D^J_{MM'}(\alpha_{bf}, \beta_{bf}, \gamma_{bf}) \tag{A.43}$$

$${}_{bf}\hat{J}_{z'} D^J_{MM'}(\alpha_{bf}, \beta_{bf}, \gamma_{bf}) = -M' D^J_{MM'}(\alpha_{bf}, \beta_{bf}, \gamma_{bf}) \tag{A.44}$$

$$\hat{\mathbf{J}}^2 D^J_{MM'}(\alpha_{bf}, \beta_{bf}, \gamma_{bf}) = J(J+1) D^J_{MM'}(\alpha_{bf}, \beta_{bf}, \gamma_{bf}) \tag{A.45}$$

where the angles $\alpha_{bf}, \beta_{bf}, \gamma_{bf}$ now represent the orientation of the set of body-fixed axes relative to the set of space fixed axes. For the sake of completeness, the symmetry and properties of Wigner D-functions are summarised below.

Orthogonality:

$$(2j+1) \int D^j_{mn}{}^* D^J_{MN} \sin\beta d\beta d\alpha d\gamma = \delta_{jJ}\delta_{mM}\delta_{nN} 8\pi^2 \ . \tag{A.46}$$

Summation:

$$\sum_M \mid D^J_{MN} \mid^2 = 1 \ . \tag{A.47}$$

Closure:

$$\sum_N D^J_{MN}(\alpha 2, \beta 2, \gamma 2) D^J_{NP}(\alpha 1, \beta 1, \gamma 1) = D^J_{MP}(\alpha, \beta, \gamma) \tag{A.48}$$

where (α, β, γ) represent the total orientation of first $(\alpha 1, \beta 1, \gamma 1)$ followed by $(\alpha 2, \beta 2, \gamma 2)$.

Symmetry:

$$D^J_{MN}(\alpha, \beta, \gamma)^* = (-)^{M-N} D^J_{-M-N}(\alpha, \beta, \gamma) = D^J_{NM}(-\gamma, -\beta, -\alpha) \ . \tag{A.49}$$

Additionally there are several special cases, most notably for D^J_{M0}. Defining the spherical harmonics as:

$$Y_{kq} = [(2k+1)/4\pi]^{1/2} C_{kq} \tag{A.50}$$

where

$$C_{kq}(\theta, \phi) = (-)^q [(k-q)!/(k+q)!]^{-1/2} P^q_k(\theta) \exp(iq\phi) \tag{A.51}$$

then

$$D^J_{M0}(\alpha, \beta, \gamma) = C^*_{jm}(\beta\alpha) \ . \tag{A.52}$$

Therefore

$$D^J_{M0}(\beta) = (-)^M[(J-M)!/(J+M)!]^{-1/2} P^M_J(\beta) \tag{A.53}$$

for $M \geq 0$. In its simplest form:

$$D^J_{00}(\beta) = P_J(\cos\beta) \ . \tag{A.54}$$

In the above discussion we have outlined the general features of the quantum theory of angular momentum. It is however useful to summarise the topics discussed within the framework of reorientation dynamics. The transformation properties of physical quantities with respect to rotations reveal themselves either through rotations of the given physical system relative to some fixed reference frame or through rotations of the coordinate axes relative to the physical system. Many of these physical quantities are invariants under coordinate rotations. In particular the properties of any closed system should be independent of rotations, as follows from the isotropy of space. As a consequence of this fundamental property of space, the total angular momentum of such a system is an integral of the motion.

A quantum mechanical wavefunction $\psi(\mathbf{r})$ of any closed physical system may be characterised by the eigenvalues of the four commuting operators: the Hamiltonian, the parity operator, the operator $\hat{\mathbf{J}}^2$ of the square of the angular momentum and the operator $\hat{J}_z$ of the projection of this momentum onto a quantisation axis. For any given eigenvalue j of the total angular momentum, there exist $2j+1$ wave functions which correspond to different m, where m is the eigenvalue of the azimuthal angular momentum (the projection of this momentum onto a quantisation axis). These functions describe the quantum states of the system which differ only by the orientation of the angular momentum in space. Under coordinate rotations these functions undergo linear mutual transformations whose transformation coefficients are called the Wigner D-functions. These are elements of the finite rotation matrix in the j-representation and depend on the Euler angles α, β, γ which describe the rotation.

These wavefunctions with fixed j but different m constitute an irreducible tensor of rank j. Irreducible tensors can also be constructed from various physical quantities: the dipole moment is a tensor of first rank (vector), whilst the polarisability is a tensor of second rank. All irreducible tensors transform under rotations of coordinate systems in the same manner as eigenfunctions of the angular momentum operator, whereby the transformation coefficients are once again the Wigner D-functions. These physical properties, such as the polarisability tensor, are fixed

relative to the body-fixed frame. As the system of interest rotates, the transformations of these properties relative to the coordinate frame may be analysed, allowing the formulation of models of reorientation and extraction of correlation functions from spectroscopic experiments.

Fig. 1A The Euler Angles

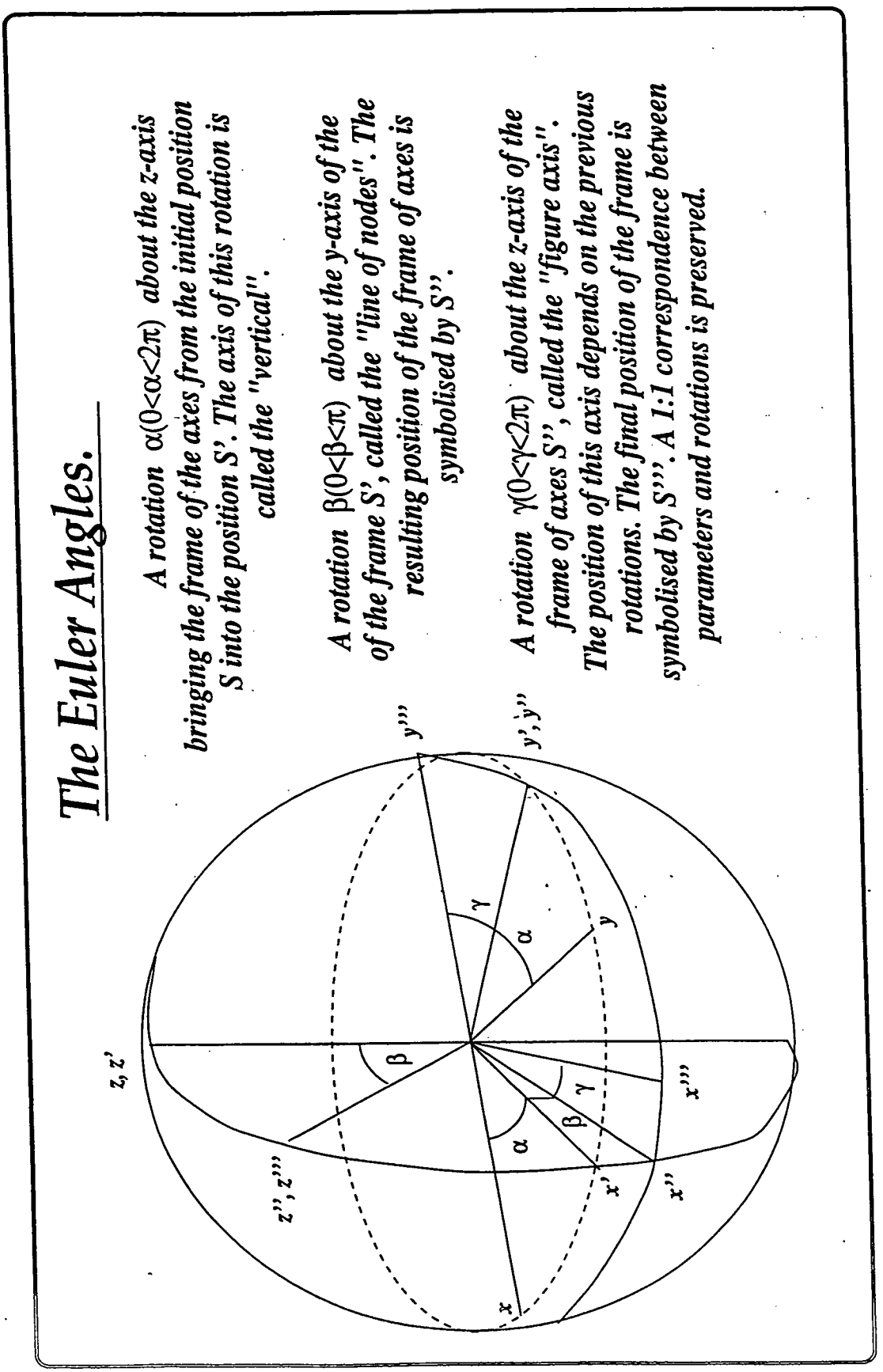

Bibliography

[1] J.Sherwood, *The Plastically Crystalline State* (Interscience, Chichester, 1979)

[2] P.J. Collings, *Liquid Crystals: Nature's Delicate Phase of Matter* (Hilger, Bristol 1990)

[3] W.A.Steele, *Transport Phenomena in Fluids* (New York, 1969)

[4] F.J.Bartoli, T.A.Litovitz, *J. Chem. Phys.* **56** 404 (1972)

[5] R.G.Gordon, *Advances in Magnetic Resonance* **3** 1 (1968)

[6] L.A.Nafie, W.L.Peticolas, *J. Chem. Phys.* **57** 3145 (1972)

[7] G. Placzek, *Z. Physik* **70** 84 (1931)

[8] P.M.Mathews and K.Venkatesan, *A Textbook of Quantum Mechanics* (McGraw-Hill, 1977)

[9] F.J.Bartoli, T.A.Litovitz, *J. Chem. Phys.* **56** 413 (1972)

[10] R.Loudon, *Advan. Phys.* **13** 423 (1964)

[11] H.Goldstein, *Classical Mechanics* (Addison-Wesley, Reading, Mass. 1950)

[12] W.A.Steele, *Advances in Chemical Physics* **34** (1976)

[13] A.G.St.Pierre and W.A.Steele, *Phys. Rev.* **184** 172 (1969)

[14] R.G.Gordon, *J. Chem. Phys.* **43**(4) 1307 (1965)

[15] R.G.Gordon, *J. Chem. Phys.* **44** 1830 (1966)

[16] W. Feller, *An Introduction to Probability Theory and Its Applications*, Wiley, NY, 1950)

[17] A.K Agrawal and S.Yip, *Phys. Rev.* **171** 263 (1968)

[18] R.E.D.McClung, *J. Chem. Phys.* **51** 3842 (1969)

[19] R.E.D.McClung, *J. Chem. Phys.* **57** 5478 (1972)

[20] M. Fixman and K.Rider, *J. Chem. Phys.* **51** 2425 (1969)

[21] A.G.St.Pierre and W.A.Steele, *J. Chem. Phys.* **57** 4638 (1972)

[22] F.Perrin, *J. Phys. Radium* **7** 1 (1936)

[23] L.D.Favro, Phys. Rev. **119** 53 (1960)

[24] K.A.Valiev and M.M.Zapirov, *Sov. Phys. J.E.T.P* **15** 353 (1962) Translation

[25] P.Debye, *Polar Molecules* (Reinhold, NY. 1929)

[26] R.Kubo, *Adv. Chem. Phys.* **16** 101 (1969)

[27] W.G.Rothschild, *Dynamics in Molecular Liquids* (Wiley, 1984)

[28] D.E.Woessner, *J. Chem. Phys.* **37** 647 (1962)

[29] H.Shimizu, *J. Chem. Phys.* **37** 765 (1962)

[30] C.M.Hu and R.Zwanzig, *J. Chem. Phys.* **60** 4354 (1974)

[31] J.T.Hynes, R.Kapral, M.Weinberg, *J. Chem. Phys.* **69** 2725 (1978)

[32] R.G.Gordon, *J. Chem. Phys.* **38** 2788 (1963)

[33] R.G.Gordon, *J. Chem. Phys.* **41** 1819 (1964)

[34] R.G.Gordon, *J. Chem. Phys.* **43** 1307 (1965)

[35] M.P.Allen, D.J.Tildesley, *Computer Simulation of Liquids* (Clarendon Press 1993)

[36] P.W.Atkins, *Physical Chemistry* (Ed. 6, Oxford Univ. Press 1998)

[37] M.C.Payne, M.P.Teter, D.C.Allan, T.A.Arias and J.D.Joannopoulos, *Rev. Mod. Phys.* **64** 1045 (1992)

[38] A.L.Fetter and J.D.Walecker, *Quantum Theory of many-Particle Systems* (McGraw-Hill, NY 1971)

[39] P.Hohenberg and W.Kohn, *Phys. Rev.* **136** B864 (1964)

[40] W.Kohn and L.J.Sham, *Phys. Rev.* **140** A1133 (1965)

[41] P.P.Ewald, *Ann. Phys. (Leipzig)* **54** 519 (1917a), **54** 557 (1917b) and **64** 253 (1921)

[42] N.W.Ashcroft and N.D.Mermin, *Solid State Physics* (Holt Saunders, Phil. 1976)

[43] L.Hedin and B.Lundqvist, *J. Phys. C* **4** 2064 (1971)

[44] J.P.Perdew and A.Zunger, *Phys. Rev. B* **23** 5048 (1981)

[45] S.H.Vosko, L.Wilk and M.Nusair, *can. J. Phys.* **58** 1200 (1980)

[46] J.C.Phillips, *Phys. Rev.* **112** 685 (1958)

[47] M.L.Cohen and V.Heine, *Solid State Physics* **24** 37 (1970)

[48] M.T.Yin and M.L.Cohen, *Phys. Rev. B* **26** 5668 (1982b)

[49] J.D.Joannopoulos, T.Starkloff, and M.A.Kastner, *Phys. Rev. Letts.* **38** 660 (1977)

[50] T.Starkloff and J.D.Joannopoulos, *Phys. Rev. B* **16** 5212 (1977)

[51] A.W.Redondo, A.Goddard III and T.C.McGill, *Phys. Rev. B* **15** 5038 (1977)

[52] D.R.Hamann, M.Schlueter and C.Chiang, *Phys. Rev. Letts.* **43** 1494 (1979)

[53] A.Zunger and M.L.Cohen, *Phys. Rev. B* **20** 4082 (1979)

[54] G.Kerker, *J. Phys. C* **13** L189 (1980)

[55] E.L.Shirley, D.C.Allan, R.M.Martin and J.D.Joannopoulos, *Phys. Rev. B* **40** 3652 (1989)

[56] R.Car and M.Parinnello, *Phys. Rev. Letts.* **55** 2471 (1985)

[57] H.Hellmann, *Einfuehrung in die Quantum Chemie* (Deuticke, Leipzig 1937)

[58] R.P.Feynman, *Phys. Rev.* **56** 340 (1939)

[59] J.C.Tully in *Classical and Quantum Dynamics in Condensed Phase Simulations*, Chap. 21, eds. B.J. Berne *et. al.* (World Scientific, Singapore, 1998).Here Ehrenfest Dynamics is discussed using a mean-field approximation to the electronic structure.

[60] C.Leforestier, *J.Chem. Phys.* **68** 4406 (1978).

[61] B.P.Asthana and W.Kiefer, *Vibrational Spectra and Structure* **20** 67 (1992)

[62] E.O.Brigham, *The Fast Fourier Transform and its Aplications* (Prentice Hall Int. 1998)

[63] D.Goettges, *Mikro-Raman Spektroskopische Untersuchungen an Orientierten Multi- und Monoschichten* (Dissertation, Wuerzburg 1993)

[64] D.W.N.Edington, P.R.L.Markwick, W.C.K.Poon, H.Vass and J.Crain, *Phys. Rev. Letts.* **82**(19) 3827 (1999)

[65] S.Wallen, L.Nikiel, J.Yi and J.Jonas, *J. Phys. Chem.* **99** 15421 (1995)

[66] C.C.Lin and L.A.Segel, *Mathematics Apllied to Deterministic Problems in the Natural Sciences* (Macmillan, NY 1974)

[67] L.Kleinman and D.M.Bylander, *Phys. Rev. Letts.* **4** 1425 (1982)

[68] H.J.Bohm, C.Meissner and R.Ahlrichs, *Mol. Phys.* **53**(3) 651 (1984)

[69] T.Dorfmuller and J.Samios, *Mol. Phys.* **53**(5) 1167 (1984)

[70] H.Stassen and T.Dorfmuller, *Berichte der Bunsengesellschaft fuer Physik und Chemie* **95** No. 9 995 (1991)

[71] H.Stassen, T.Dorfmuller and B.M.Ladanyi, *J. Chem. Phys.* **100**(9) 6318 (1994)

[72] M.C.C.Ribeiro and P.S.Santos, *J. Mol. Structure* **372**(2-3) 267 (1995)

[73] C.Kalpouzos, W.T.Lotshaw, D.McMorrow and G.A.Kenney-Wallace, *Chem. Phys. Letts.* **150**(1-2) 138 (1998)

[74] N.Wilding, J.Crain, P.Hatton and G.Bushnell-Wye, *Acta Crys.* Sec.B **49** 320 (1993)

[75] J.Crain, W.C.-K.Poon, A.Cairns-Smith and P.Hatton, *J. Chem. Phys.* **96** 8168 (1992)

[76] D.O'Reilly, E.Peterson and D.Hogenboom, *J. Chem. Phys.* **57** 3969 (1972)

[77] M.Bansal and A.Roy, *Mol.Phys.* **38** 1419 (1979)

[78] B.Widom, *Science* **157** 375 (1967)

[79] J.D.Bernal, *Nature* (London) **183** 68 (1959)

[80] H.Reiss and A.D.Hammerlich *J. Phys. Chem.* **90** 6252 (1986)

[81] F.A.Lindemann, *Phys. Z.* **11** 375 (1910)

[82] P.G.Debenedetti, *Metastable Liquids: Concepts and Principles* (Princeton University Press, NJ, 1996)

[83] J.O'Dell and B.J.Berne, *J. Chem. Phys.* **63** 2376 (1975)

[84] A.V.Komolkin, A.Laaksonen and A.Maliniak, *J. Chem. Phys.* **101** 4103 (1994)

[85] M.P.Allen and M.R.Wilson, *J. Comp. Aid. Mol. Des.* **3** 335 (1989)

[86] M.R.Wilson and M.P.Allen, *Mol. Cryst. Liq. Cryst.* **198** 465 (1991)

[87] E.de Miguel, L.F.Rull and K.E.Gubbins, *Phys. Rev. A* **45**(6) 3813 (1992)

[88] S.J.Clark, C.J.Adam, G.J.Ackland, J.White and J.Crain, *Liq. Cryst.* **22** 469 (1997)

[89] M.P.Allen, *Philos. Trans. R. Soc. London* SERIES A **344**(1672) 323 (1993)

[90] A.Samborski, G.T.Evans, C.P.Mason and M.P.Allen, *Mol. Phys.* **81** 263 (1994)

[91] M.R.Wilson and M.P.Allen, *Mol. Phys.* **80** 227 (1993)

[92] B.J.Bulkin and K.Brezinsky, *J. Chem. Phys.* **69**(1) 15 (1978)

[93] N.Kirov, I.Dozov and M.P.Fontana, *J. Chem. Phys.* **83**(10) 5267 (1985)

[94] B.Rosi, M.P.Fontana, I.Dozov, N.Kirov, *Phys. Rev. A* **36**(6) 2870 and 2879 (1987)

[95] S.Ye.Yakovenko, A.A.Minko, B.Arnscheidt and J.Pelzl, *Liq. Cryst.* **19**(4) 449 (1995), and all references therein.

[96] A.Sengupta and M.D.Fayer, *J. Chem. Phys.* **102**(10) 4193 (1995), and all references therein.

[97] D.McMorrow, W.T.Lotshaw and G.A.Kenney-Wallace, *IEEE J. Quant. Elec.* **24**(2) 443 (1988)

[98] T.Keyes and D.Kivelson, *J. Chem. Phys.* **56** 1057 (1972)

[99] A.J.Leadbetter, F.P.Temme, A.Heidemann and W.S.Howells, *Chem. Phys. Lett.* **34** 363 (1975)

[100] J.Y.Liu, M.G.Robinson, K.M.Johnson and D.Doroski, *Optics Letts.* **15**(5) 267 (1990)

[101] S.Ye.Yakovenko, A.A.Muravski, F.Eikelschulte and A.Geiger, *J. Chem. Phys.* **105**(24) 10766 (1996)

[102] C.J.F. Boettcher, *The Theory of Electric Polarisation* (Elsevier, Amsterdam 1973)

[103] L.Onsager, *J. Am. Chem. Soc.* **58** 1486 (1936)

[104] A.Chelkowski, *Dielectric Physics* (PWN, Warsaw, 1980)

[105] W.Maier and G.Meier, *Z. Naturforsch. A* **16** 262 1200 (1961)

[106] G.Meier, *Dielectric and Related Molecular Processes* (Vol. 2 Specialist Periodical Reports, The Chemical Society, London 1975)

[107] W.H. de Jeu, *Physical Properties of Liquid Crystalline Materials* (Gordon and Breach, London 1980)

[108] G.Vertogen and W.H. de Jeu, *Thermotropic Liquid Crystals, Fundamentals* (Springer, Berlin 1988)

[109] J.G.Kirkwood, *J. Chem. Phys.* **7** 911 (1939)

[110] S.R. Sharma, *Mol. Phys.* **78** 733 (1993)

[111] S.Urban and A.Wuerflinger, *Adv. Chem. Phys.* XCVIII (Wiley, NY 1997)

[112] N.E.Hill, W.E.Vaughan, A.H.Price and M.Davies, *Dielectric Properties and Molecular Behaviour* (ed. T.M.Sugden, van Nostrand, London 1969)

[113] A.Wuerflinger, *Ber. Bunsenges. Phys. Chem.* **95** 1040 (1991)

[114] N.Pingel, U.Poser and A.Wuerflinger, J. Chem Soc. Fara. Trans. I **80** 3221 (1984)

[115] G.Williams, *Trans. Fara. Soc.* **60** 1548 (1964)

[116] G.Meier and A.Saupe, *Mol. Cryst.* **1** 515 (1966)

[117] W.T.Coffey, Yu. P. Kalmykov, E.S.Massawe and J.T.Waldron, *J. Chem. Phys.* **99** 4011 (1993)

[118] W.T.Coffey, Yu. P. Kalmykov and E.S.Massawe, *Liq. Cryst.* **18** 677 (1995)

[119] W.T.Coffey and Yu. P. Kalmykov, *Liq. Cryst.* **14** 1227 (1993)

[120] Private Communication, M.Sandmann, Ruhr-Univeritaet-Bochum, Germany.

[121] P.R.L.Markwick, S.Urban and A.Wuerflinger, *Z. Naturforsch.* **54a** 275 (1999)

[122] A.Wuerflinger *et. al.*, *Z. Naturforsch.* **49a** 522 (1994)

[123] M.Sandmann and A.Wuerflinger, *Z. Naturforsch.* **53a** 787 (1998)

[124] S.Urban, D.Buesing, A.Wuerflinger and B.Gestblom, *Liq. Cryst.* **25** 253 (1998)

[125] T.Brueckert, S.Urban and A.Wuerflinger, *Ber. Bunsenges. Phys. Chem.* **100** 1133 (1998)

[126] T.Brueckert, D.Buesing, A.Wuerflinger and S.Urban, *Z. Naturforsch.* **50a** 977 (1995)

[127] T.Brueckert and A.Wuerflinger, *Z. Naturforsch.* **51a** 306 (1996)

[128] Y.-X.Yan, L.-T.Cheng and K.A.Nelson, *Advances in Non-Linear Spectroscopy* (eds. R.J.H.Clark and R.E.Hester, Wiley, NY 1987)

[129] S.Ruhman, B.Kohler, A.G.Joly and K.A.Nelson, *IEEE J. Quantum Electron* **24** 470 (1988)

[130] T.Hattori and T.Kobayashi, *J. Chem. Phys.* **94** 3332 (1991)

[131] Y.J.Chang and E.W.Castner Jr., *J. Chem. Phys.* **99** 113 (1993)

[132] M.Cho, M.Du, N.F.Schere, G.R.Fleming and S.Mukamel, *J. Chem. Phys.* **99** 2410 (1993)

[133] S.Palese, L.Schilling, R.D.J.Miller, P.R.Staver and W.T.Lotshaw, *J. Phys. Chem.* **98** 6308 (1994)

[134] E.T.J.Nibbering, D.A.Wiersma and K.Duppen, Chem. Phys. **183** 1647 (1994)

[135] C.J.Bardeen and C.V.Shank, *Chem. Phys. Letts.* **226** 310 (1994)

[136] D.Vanden Bout, L.J.Muller, and M.Berg, *Phys. Rev. Letts.* **67** 3700 (1991)

[137] L.J.Muller, D.Vanden Bout and M.Berg, *J. Chem. Phys.* **99** 810 (1993)

[138] R.Inaba, K.Tominaga, M.Tasumi, K.A.Nelson and K.Yoshihara, *Chem. Phys. Letts.* **211** 183 (1993)

[139] D.Zimdars, A.Tomakoff, S.Chen, S.R.Greenfield, M.D.Fayer, T.I.Smith and H.A.Schwettman, *Phys. Rev. Letts.* **70** 2718 (1993)

[140] A.Tomakoff, D.Zimdars, B.Sauter, R.S.Francis, A.S.Kwok and M.D.Fayer, *J. Chem. Phys.* **101** 1741 (1994)

[141] K.Tominaga, Y.Naitoh, T.J.Kang and K.Yoshihara, *Ultrafast Phenomena IX* (eds. G.Mourou, A.H.Zweil, W.H.Knox and P.F.Barbara, Springer, Berlin, 1994)

[142] K.Tominaga and K.Yoshihara, *Phys. Rev. Letts.* **74** 3061 (1995)

[143] D.W.Oxtoby, *Advan. Chem. Phys.* **40** 1 (1979)

[144] J.Jonas, *Acc. Chem. Res.* **17** 74 (1984)

[145] D.McMorrow, W.T.Lotshaw and G.A.Kenney-Wallace, *IEEE J. Quantum Electron.* QE-24 443 (1988)

[146] D.M.Brink and G.R.Satchler, *Angular Momentum* (Oxford University Press 1962)

[147] M.E.Rose, *Elementary Theory of Angular Momentum* (Wiley, NY 1957)

[148] E.P.Wigner, *Group Theory and its Application to the Quantum Mechanics of Atomic Spectra* (Academic Press, NY 1959)

[149] A.R.Edmonds, *Angular Momentum in Quantum Mechanics* (Princeton University Press 1957)

[150] E.U.Condon and G.H.Shortley, *Theory of Atomic Spectra* (Cambridge University Press 1935)

[151] U.Fano and G.Racah, *Irreducible Tensorial Sets* (Academic Press, NY 1959)